NUMERICAL ANALYSIS OF CONVECTIVE HEAT TRANSFER AND FLOW CHARACTERISTICS WITH NANOFLUIDS FLOWING OVER A MICROSCALE BACKWARD-FACING STEP

2016
M. Sc. Thesis
Mechanical Engineering

Recep EKİCİLER

NUMERICAL ANALYSIS OF CONVECTIVE HEAT TRANSFER AND FLOW CHARACTERISTICS WITH NANOFLUIDS FLOWING OVER A MICROSCALE BACKWARD-FACING STEP

A THESIS SUBMITTED TO
THE GRADUATE SCHOOL OF NATURAL AND APPLIED SCIENCES OF
KARABUK UNIVERSITY

BY

RECEP EKİCİLER

IN PARTIAL FULFILLMENT OF THE REQUIREMENTS FOR
THE DEGREE OF MASTER OF SCIENCE IN
DEPARTMENT OF
MECHANICAL ENGINEERING

June 2016

I certify that in my opinion the thesis submitted by Recep EKİCİLER titled "NUMERICAL ANALYSIS OF CONVECTIVE HEAT TRANSFER AND FLOW CHARACTERISTICS WITH NANOFLUIDS FLOWING OVER A MICROSCALE BACKWARD-FACING STEP" is fully adequate in scope and in quality as a thesis for the degree of Master of Science.

Assoc. Prof. Dr. Kamil ARSLAN
Thesis Advisor, Department of Mechanical Engineering

This thesis is accepted by the examining committee with a unanimous vote in the Department of Mechanical Engineering as a master thesis. June 30, 2016

Examining Committee Members (Institutions)	Signature
Chairman : Prof. Dr. Nevzat ONUR (ÇU)	.....
Member : Assoc. Prof. Dr. Kamil ARSLAN (KBU)	.....
Member : Assoc. Prof. Dr. Oğuz TURGUT (GU)	.....
Member : Assist. Prof. Dr. Hasan ÖZCAN (KBU)	.....
Member : Assist. Prof. Dr. Atilla ALTINTAŞ (KBU)	.....

..... / ..... / 2016

The degree of Master of Science by the thesis submitted is approved by the Administrative Board of the Graduate School of Natural and Applied Sciences, Karabük University.

Prof. Dr. Nevin AYTEMİZ
Head of Graduate School of Natural and Applied Sciences

"I hereby declare that all information in this document has been obtained and presented in accordance with academic rules and ethical conduct. I also declare that, as required by these rules and conduct, I have fully cited and referenced all material and results that are not original to this work."

Recep EKİCİLER

ABSTRACT

M. Sc. Thesis

NUMERICAL ANALYSIS OF CONVECTIVE HEAT TRANSFER AND FLOW CHARACTERISTICS WITH NANOFLUIDS FLOWING OVER A MICROSCALE BACKWARD-FACING STEP

Recep EKİCİLER

Karabük University
Graduate School of Natural and Applied Sciences
Department of Mechanical Engineering

Thesis Advisor:
Assoc. Prof. Dr. Kamil ARSLAN
June 2016, 83 pages

In this thesis, the forced convective heat transfer and fluid flow of ZnO/water, CuO/water, TiO_2/water, SiO_2/water and Al_2O_3/water nanofluids over the microscale backward-facing step were numerically investigated. The diameters of nanoparticles were changed between 45 nm and 80 nm. The flow was considered as three-dimensional, steady-state and laminar flow condition ($100 \leq Re \leq 1000$). The downward stepped wall was applied for constant heat flux and the other walls were insulated. The length of downstream and upstream wall was taken 0.15 m and 0.1 m, respectively. The total duct height was 1000 μm and width of duct was 1200 μm. Numerical analyses were performed for different nanoparticle volume concentrations (φ = 1.0- 4.0%) of each nanofluid and different expansion ratios (ER=1.25, 1.67 and 2.50). The Nusselt number and the Darcy friction factor values were obtained from numerical calculations. Moreover, the velocity and temperature profiles were also

analysed. Finally, it was observed that the Nusselt number increases with increasing Reynolds number and nanoparticle volume concentration. 4.0% volume fraction of Al_2O_3/water nanofluid has the highest Nusselt number for all expansion ratios. The Nusselt number increases with decreasing expansion ratios. The Darcy friction factor decreases with increasing expansion ratios. However, the Darcy friction factor does not affected by the increasing in nanoparticles volume concentration and the types of nanofluids.

Key Word : Laminar flow, ZnO/water, CuO/water, TiO_2/water, SiO_2/water, Al_2O_3/water, nanofluids, microscale backward-facing step, forced convection, expansion ratio, heat transfer.

Science Code : 914.1.065

ÖZET

Yüksek Lisans Tezi

BİR MİKRO BOYUTTAKİ GERİ BASAMAK ÜZERİNDEN NANOAKIŞKANLARIN AKIŞININ TAŞINIM ISI TRANSFER VE AKIŞ KARAKTERİSTİKLİRİNİN SAYISAL İNCELENMESİ

Recep EKİCİLER

Karabük Üniversitesi
Fen Bilimleri Enstitüsü
Makine Mühendisliği Anabilim Dalı

Tez Danışmanı:
Doç. Dr. Kamil ARSLAN

Haziran 2016, 83 sayfa

Bu tezde, mikro boyutta geri basamak üzerinden ZnO/su, CuO/su, TiO_2/su, SiO_2/su ve Al_2O_3/su nanoakışkanlarının akışının zorlanmış taşınım ısı transfer ve akış karakteristikleri sayısal olarak incelenmiştir. Nanopartiküllerin çapı 45 nm ile 80 nm arasında değiştirilmiştir. Akışın, üç boyutlu, kararlı ve laminer şartlarda olduğu gözönüne alınmıştır ($100 \leq Re \leq 1000$). Kanalın basamaktan sonraki alt duvarına sabit ısı akısı uygulanmış ve diğer duvarları yalıtılmıştır. Kanalın basamaktan sonraki ve önceki uzunlukları sırasıyla 0.15 m ve 0.10 m olarak ele alınmıştır. Toplam kanal yüksekliği 1000 μm ve genişliği ise 1200 μm'dir. Sayısal analizler, her bir nanoakışkanın farklı nanopartikül hacimsel oranı (φ = 1.0- 4.0%) ve farklı genişleme oranları (ER=1.25, 1.67 ve 2.50) için uygulanmıştır. Sayısal hesaplamalardan, Nusselt sayısı ve Darcy sürtünme faktörü değerleri elde edilmiştir. Bunlara ek olarak, hız ve sıcaklık profilleri analiz edilmiştir. Sonuç olarak, Nusselt sayısının artan

nanopartikül hacimsel oranı ve Reynolds sayısı ile arttığı gözlenmiştir. Bütün genişleme oranlarında, %4.0 nanopartikül hacimsel oranına sahip Al_2O_3/su nanoakışkanın en yüksek Nusselt sayısına sahip olduğu tespit edilmiştir. Nusselt sayısının, azalan genişleme oranı ile birlikte arttığı görülmüştür. Darcy sürtünme faktörünün, artan genişleme oranı ile beraber düştüğü görülmüştür. Bununla birlikte, Darcy sürtünme faktörünün artan nanopartikül hacimsel oranından ve nanoakışkanların çeşidinden etkilenmediği anlaşılmıştır.

Anahtar Sözcükler : Laminer akış, ZnO/su, TiO_2/su, CuO/su, SiO_2/su, Al_2O_3/su, nanoakışkanlar, mikro boyutta geri basamak, zorlanmış taşının, genişleme oranı, ısı transferi.

Bilim Kodu : 914.1.065

ACKNOWLEDGEMENTS

Firstly, I would like to express my sincere gratitude to my supervisor Assoc. Prof. Dr. Kamil Arslan for his guidance and encouragement throughout my thesis study. I have experienced an excellent academic study under his supervision and his invaluable suggestions and support helped me to plan my further academic studies in the best way.

I would like to thank to Karabük University of Scientific Research Project (KBU-BAP-15/2-YL-034) for its financial support during my academic study.

Lastly, this thesis would not have been possible without the support of my wife. I am grateful to her for her never-ending love, patience and encouragement.

CONTENTS

Page

APPROVAL ii
ABSTRACT iv
ÖZET vi
ACKNOWLEDGEMENTS viii
CONTENTS ix
LIST OF FIGURES xi
LIST OF TABLES xv
SYMBOLS AND ABBREVITIONS INDEX xvi

PART 1 1
INTRODUCTION 1
1.1. CONVECTIVE HEAT TRANSFER 1
1.1.1. Mean Velocity 4
1.1.2. Mean Temperature 4
1.1.3. Pressure Drop 5
1.2. DIMENSIONLESS NUMBERS AND THEIR PHYSICAL MEANINGS 5
1.2.1. Reynolds Number (Re) 6
1.2.2. Nusselt Number (Nu) 6
1.2.3. Darcy Friction Factor 6
1.3. BACKGROUND OF NANOFLUIDS 7
1.4. GENERAL INFORMATION FOR FLOW SEPARATION AND GENERAL STRUCTURE OF BACKWARD-FACING STEP (BFS) 8
1.5. LITERATURE SURVEY 12
1.5.1. Literature Survey on BFS 12
1.5.2. Literature Survey on BFS Using Nanofluids 16
1.6. OBJECTIVES 18

PART 2 20

METHODOLOGY 20
2.1. THERMOPHYSICAL PROPERTIES OF NANOFLUIDS 20
2.2. PROBLEM DESCRIPTION AND GOVERNING EQUATIONS 22
2.3. BOUNDARY CONDITIONS 24
2.4. NUMERICAL PROCEDURES 24
2.5. MESH DEPENDENCY ANALYSIS 25
2.6. COMPARISON WITH EXPERIMENTAL RESULTS 26

PART 3 28
RESULTS AND DISCUSSIONS 28
3.1. HEAT TRANSFER CHARACTERISTICS 28
3.2. FLOW CHARACTERISTICS 47
3.3. COMPARISION OF TYPES OF NANOFLUIDS, NANOPARTICLE VOLUME FRACTIONS AND EXPANSION RATIOS DUE TO HEAT TRANSFER PERFORMANCE 67

PART 4 71
CONCLUSIONS 71

PART 5 73
SUGGESTIONS FOR FUTURE WORK 73
REFERENCES 74

APPENDIX A. 78
SAMPLE CALCULATIONS 78

RESUME 83

LIST OF FIGURES

Page

Figure 1.1. Schematic view of convective heat transfer [1]..... 1

Figure 1.2. Some examples including convective heat transfer [1]..... 2

Figure 1.3. Developing of boundary layer due to convective heat transfer..... 2

Figure 1.4. Comparison of thermal conductivities of conventional fluids, metal oxide and metalic materials [17]..... 8

Figure 1.5. Nanofluids applications in some fields..... 9

Figure 1.6. Flow separation over smooth surface [19]..... 9

Figure 1.7. Flow separation over discontinuous surfaces [19]..... 10

Figure 1.8. Effect of viscosity on a body in a moving fluid; shear stress and separated flow [20]..... 10

Figure 1.9. Separated flow caused by adverse pressure gradient [20]..... 11

Figure 1.10. Flowfield of backward-facing step [21]..... 12

Figure 1.11. Definition of pitch angle (θ_1) and rolling angle (θ_2)..... 15

Figure 2.1. Schematic view of three-dimensional microscale backward-facing step..... 22

Figure 2.2. Boundary conditions of 2D duct having MBFS..... 24

Figure 2.3. Sample mesh distribution of the duct having MBFS geometry..... 26

Figure 2.4. Changing of average heat transfer coefficient and average Darcy friction factor with mesh number for pure water at Re=1000..... 26

Figure 2.5. Comparison of average Darcy friction factor of the present result for pure water with the result of Kherbeet et al. [38]..... 27

Figure 3.1. The average Nusselt number variation with Reynolds number for different nanoparticle volume fractions of different nanofluids at ER=1.25..... 29

Figure 3.2. The average Nusselt number variation with Reynolds number for different nanoparticle volume fractions of different nanofluids at ER=1.67..... 30

Figure 3.3. The average Nusselt number variation with Reynolds number for different nanoparticle volume fractions of different nanofluids at ER=2.50..... 31

Figure 3.4. The average Nusselt number variation with Reynolds number for 4.0% nanoparticle volume fractions and different types of nanofluids at ER=1.25..... 32

Page

Figure 3.5. The average Nusselt number variation with Reynolds number for 4.0% nanoparticle volume fractions and different types of nanofluids at ER=1.67. 33

Figure 3.6. The average Nusselt number variation with Reynolds number for 4.0% nanoparticle volume fractions and different types of nanofluids at ER=2.50. 33

Figure 3.7. The average Nusselt number distributions for different expansion ratios and Al_2O_3/water nanofluid with 4.0% volume fraction. 34

Figure 3.8. The local Nusselt number distributions along the dimensionless length for different expansion ratios and Al_2O_3/water nanofluid with 4.0% volume fraction. 35

Figure 3.9. The local Nusselt number distributions along the dimensionless length for different Reynolds number and Al_2O_3/water nanofluid with 4.0% volume fraction at ER=1.25. 36

Figure 3.10. The local Nusselt number distributions along the dimensionless length for different nanofluids with 4.0% volume fraction at Re=500 and ER=1.25. 36

Figure 3.11. Isothermal contours of temperature at the duct outlet for different nanoparticle volume fraction using Al_2O_3/water nanofluid at ER=1.25 and Re=500 a) 1.0%, b) 2.0%, c) 3.0%, d) 4.0%. 38

Figure 3.12. Isothermal contours of temperature at the duct outlet for different Reynolds number using Al_2O_3/water nanofluid with 4.0% volume fraction at ER=1.25 a) 100, b) 500, c) 1000. 39

Figure 3.13. Isothermal contours of temperature at the duct outlet for different expansion ratios using Al_2O_3/water nanofluid with 4.0% volume fraction at ER=1.25 a) 1.25, b) 1.67, c) 2.50. 40

Figure 3.14. Isothermal contours of temperature at the duct outlet for different distances from the step wall using Al_2O_3/water nanofluid with 4.0% volume fraction at ER=1.25 a) x/s=500.5, b) x/s=502.5, c) x/s=504.5, d) x/s=525, e) x/s=550, f) x/s=750, g) x/s=1000, h) x/s=1250. 41

Figure 3.15. Contours of temperature for different expansion ratios using Al_2O_3/water nanofluid with 4.0% volume fraction at Re=500 a) ER=1.25, b) ER=1.67, c) ER=2.50. 43

Figure 3.16. Contours of temperature for different nanoparticle volume fractions using Al_2O_3/water nanofluid at ER=1.25 and Re=500 a) 1.0%, b) 2.0%, c) 3.0%, d) 4.0%. 44

Figure 3.17. Contours of temperature for different Reynolds numbers using Al_2O_3/water nanofluid with 4.0% volume fraction at ER=2.50 a) Re=100, b) Re=500, c) Re=1000. 45

Figure 3.18. Contours of temperature for different nanofluids with 4.0% volume fraction at ER=2.50 and Re=500 a) Al_2O_3/water, b) SiO_2/water, c) TiO_2/water, d) CuO/water, e) ZnO/water. 46

Figure 3.19. Average Darcy friction factor variation with Reynolds number for different nanoparticle volume fractions of different nanofluids at ER=1.25. 48

Figure 3.20. Average Darcy friction factor variation with Reynolds number for different types of nanofluids and nanoparticles volume fractions at ER=1.67 49

Figure 3.21. Average Darcy friction factor variation with Reynolds number for different types of nanofluids and nanoparticles volume fractions at ER=2.50. 49

Figure 3.22. Average Darcy friction factor variation with Reynolds number for Al_2O_3/water, SiO_2/water, CuO/water, ZnO/water and TiO_2/water nanofluids having 4.0% nanoparticle volume fractions at ER=1.25..... 50

Figure 3.23. Average Darcy friction factor variation with Reynolds number for Al_2O_3/water, SiO_2/water, CuO/water, ZnO/water and TiO_2/water nanofluids having 4.0% nanoparticle volume fractions at ER=1.67..... 50

Figure 3.24. Average Darcy friction factor variation with Reynolds number for Al_2O_3/water, SiO_2/water, CuO/water, ZnO/water and TiO_2/water nanofluids having 4.0% nanoparticle volume fractions at ER=2.50..... 51

Figure 3.25. Average Darcy friction factor variation with Reynolds number for different expansion ratios using Al_2O_3/water nanofluid having 4.0% nanoparticles volume fractions. 52

Figure 3.26. Variation of local Darcy friction factor for different Reynolds numbers using Al_2O_3/water, SiO_2/water, CuO/water, ZnO/water and TiO_2/water nanofluids having 4.0% nanoparticle volume fractions and pure water at Re=500. 53

Figure 3.27. Variation of local Darcy friction factor for different expansion ratios using Al_2O_3/water nanofluid having 4.0% nanoparticle volume fractions at Re=500. 54

Figure 3.28. Variation of local Darcy friction factor for different Reynolds numbers using Al_2O_3/water nanofluid having 4.0% nanoparticle volume fractions at ER=1.25. 54

Figure 3.29. Velocity contours at the duct outlet for different nanoparticle volume fraction using Al_2O_3/water nanofluid at ER=1.25 and Re=500 a) 1.0%, b) 2.0%, c) 3.0%, d) 4.0%. 56

Figure 3.30. Velocity contours at the duct outlet for different Reynols number using Al_2O_3/water nanofluid with 4.0% volume fraction at ER=1.25 a) Re=100, b) Re= 500, c) Re=1000. 57

Figure 3.31. Velocity contours at the duct outlet for different expansion ratios using Al_2O_3/water nanofluid with 4.0% volume fraction at Re=500 a) 1.25, b) 1.67, c) 2.50. 58

Figure 3.32. Velocity contours at the duct outlet for different distances from the step wall using Al_2O_3/water nanofluid with 4.0% volume fraction at ER=1.25 a) x/s=500.5, b) x/s=502.5, c) x/s=504.5, d) x/s=525, e) x/s=550, f) x/s=750, g) x/s=1000, h) x/s=1250..... 59

Figure 3.33. Streamlines of velocity for different expansion ratios using Al_2O_3/water nanofluid with 4.0% volume fraction at Re=500 a) ER=1.25, b) ER=1.67, c) ER=2.50. 61

Figure 3.34. Streamlines of velocity for different nanoparticle volume fractions using Al_2O_3/water nanofluid at ER=1.25 and Re=500 a) 1.0%, b) 2.0%, c) 3.0%, d) 4.0%. 62

Figure 3.35. Streamlines of velocity for different Reynolds numbers using Al_2O_3/water nanofluid with 4.0% volume fraction at ER=2.50 a) Re=100, b) Re=500, c) Re=1000. 62

Figure 3.36. Streamlines of velocity for different nanofluids with 4.0% volume fraction at ER=2.50 and Re=500 a) Al_2O_3/water, b) SiO_2/water, c) TiO_2/water, d) CuO/water, e) ZnO/water..... 63

Figure 3.37. Velocity vectors for different expansion ratios using Al_2O_3/water nanofluid with 4.0% volume fraction at Re=500 a) ER=1.25, b) ER=1.67, c) ER=2.50..... 64

Figure 3.38. Velocity vectors for different nanoparticle volume fractions using Al_2O_3/water nanofluid at ER=1.25 and Re=500 a) 1.0%, b) 2.0%, c) 3.0%, d) 4.0%..... 65

Figure 3.39. Velocity vectors of for different Reynolds numbers using Al_2O_3/water nanofluid with 4.0% volume fraction at ER=2.50 a) Re=100, b) Re=500, c) Re=1000. 66

Figure 3.40. Velocity vectors of for different nanofluids with 4.0% volume fraction at ER=2.50 and Re=500 a) Al_2O_3/water, b) SiO_2/water, c) TiO_2/water, d) CuO/water e) ZnO/water..... 67

Figure 3.41. Comparision of performance evaluation criterion for different nanofluids at 4.0% nanoparticle volume fraction and ER=1.25. 69

Figure 3.42. Comparision of performance evaluation criterion for different nanoparticles volume fractions of Al_2O_3/water nanofluid at ER=1.25. 69

Figure 3.43. Comparision of performance evaluation criterion for the MBFS having different expansion ratios for Al_2O_3/water nanofluid having 4.0% nanoparticle volume fraction. 70

LIST OF TABLES

Page

Table 2.1. β values of different nanoparticles and their boundary conditions 22

Table 2.2. Geometrical dimensions of horizontal three-dimensional microscale backward-facing step 23

Table 2.3. Thermophysical properties of nanoparticles and pure water 23

SYMBOLS AND ABBREVITIONS INDEX

SYMBOLS

Cp : specific heat, J/kg K

D_h : hydraulic diameter, m

dp : nanoparticles diameter, nm

f : Darcy friction factor, (-)

g : gravitational acceleration, m/s^2

h : convective heat transfer coefficient, W/m^2 K

h : inlet channel height, m

H : total channel height, m

h_x : local convective heat transfer coefficient, W/m^2 K

K : Boltzman constant

k : thermal conductivity, W/m K

L : length of the heated section, m

L_t : total length of the duct, m

L_S : the length of step, m

M : base fluid's moleculer weight

N : Avogadro number

Nu : average Nusselt number, (-)

Nu_x : local Nusselt number, (-)

q'' : heat flux, W/m^2

Re : Reynolds number, (-)

s : step height, m

T : fluid temperature, K

T_b : fluid bulk temperature, K

T_0 : reference temperature, K

V_m : average velocity for inlet flow, m/s

w : duct width, nm

φ : nanoparticles volume fraction

β : thermal expansion coefficient, 1/K

ρ_f : density of fluid, kg/m^3

ρ_s : density of solid, kg/m^3

μ : dynamic viscosity, $N\ s/m^2$

τ_w : wall shear stress, N/m^2

υ : kinematic viscosity, m^2/s

ABBREVITIONS

eff : effective

f : fluid

s : solid

nf : nanofluid

w : wall

m : mean

∞ : inlet condition

PART 1

INTRODUCTION

1.1. CONVECTIVE HEAT TRANSFER

The process involved when energy is transferred from a surface to a fluid which flows over it as a result of a temperature difference between the surface and the fluid as shown Figure 1.1 is named heat convection. In convection heat transfer, there must be always a surface, a moving fluid and a temperature difference between the fluid and the surface and the attention is with the rate of heat transfer between the fluid and the surface [1].

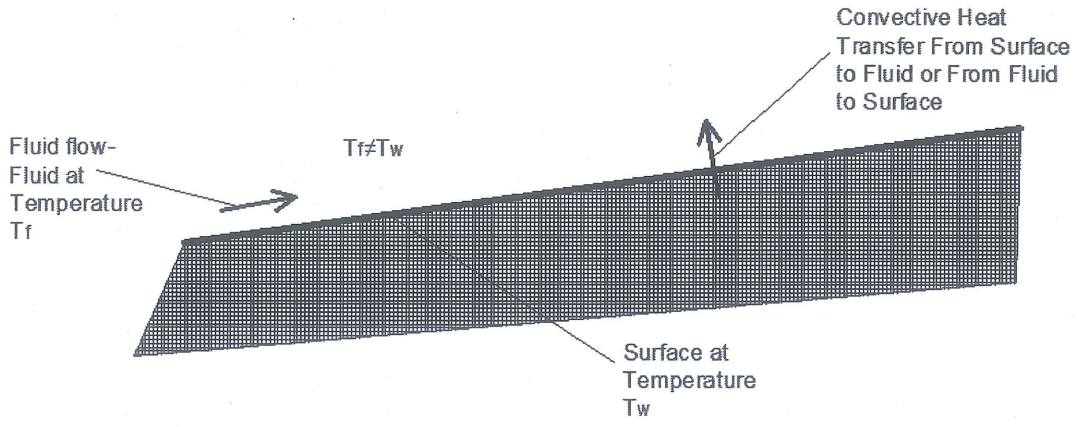

Figure 1.1. Schematic view of convective heat transfer [1].

In practice, convective heat transfer takes place broadly. The cutting tool's cooling during a machining, the electronic components' cooling in a computer, the generation and condensation of steam in thermal power plant, the heating and buildings' cooling, cooking, and the thermal control of re-entering spacecraft. Some examples of situations in which convective heat transfer is substantial are presented in Figure 1.2 [1].

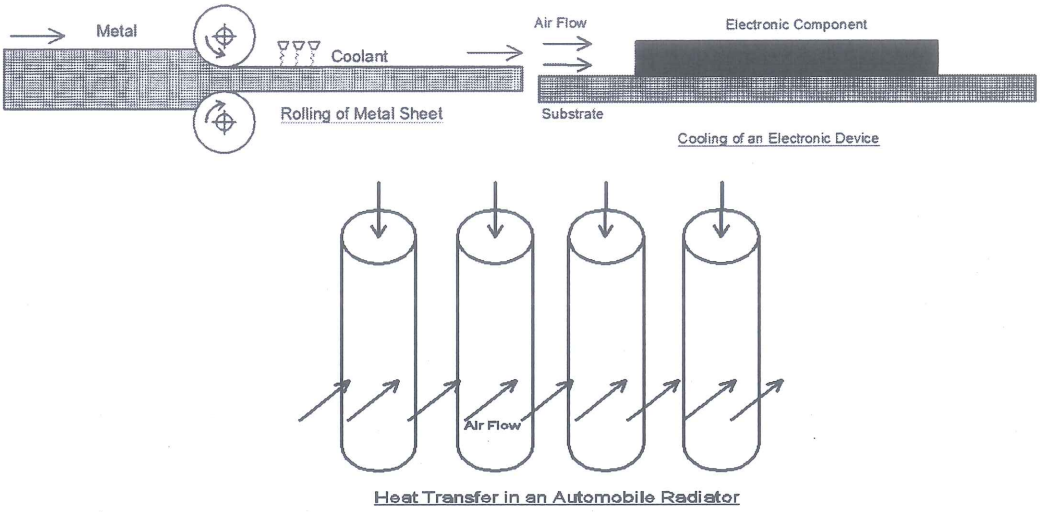

Figure 1.2. Some examples including convective heat transfer [1].

The fluid flow on the heated surface is shown in Figure 1.3. Close to the surface of a wall in contact with a moving fluid that the flow velocity changes from zero at the wall (where the flow "sticks" to the surface due to its viscosity) up to free stream velocity u_∞ at the region defined as velocity boundary layer. Also, the effect of thermal interaction is confined to a thin region near the surface called the thermal boundary layer and it can be smaller, greater and equal as compared to velocity boundary layer.

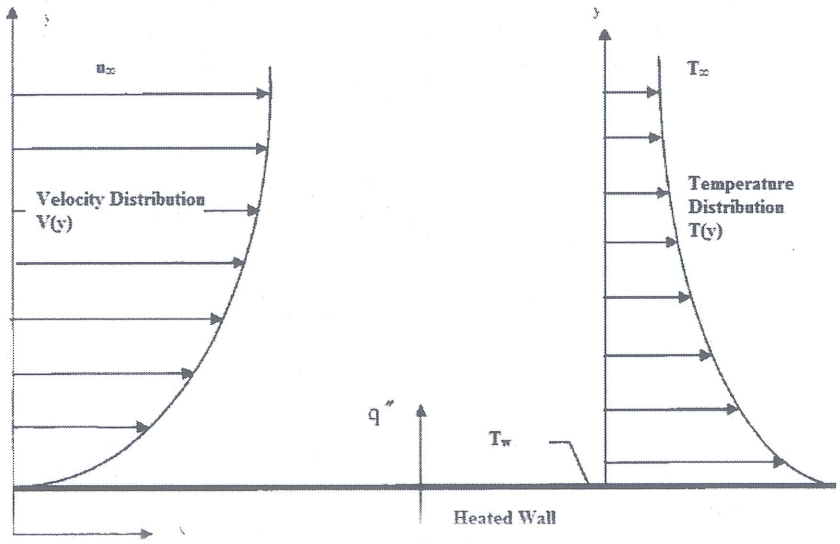

Figure 1.3. Developing of boundary layer due to convective heat transfer.

Convection heat transfer is stated by Newton's law of colling as [1]:

$$q''_x = h_x(T_w - T_\infty) \tag{1.1}$$

Flow conditions changes at the every point of the surface, so values of convection heat transfer coefficient and heat flux change along the surface of the wall. If average convection heat transfer coefficient is defined for the whole surface, total heat transfer may be stated as:

$$Q=h_{avg}A_s(T_w-T_\infty) \tag{1.2}$$

Average convection heat transfer coefficient is stated as:

$$h_{avg} = \frac{1}{A_s}\int_{A_s} h_x dA_s \tag{1.3}$$

In order to give the right desicion if the flow is turbulent or laminar, the Reynolds number must be calculated. For internal flow in ducts Reynolds number can be expressed as:

$$Re = \frac{\rho V D_h}{\mu} \tag{1.4}$$

where D_h (m) is hydraulic diameter of duct.

The critical Reynolds number for flow in duct:

$$Re_{cr}=2300 \tag{1.5}$$

For laminar flow Reynolds number can be expressed as:

$$Re \leq 2300 \tag{1.6}$$

For turbulent flow [2] :

$$Re>10000 \tag{1.7}$$

1.1.1. Mean Velocity

The velocity of fluid in a duct varies from zero at the surface due to the no-slip condition, to the highest value at the center of the duct. Therefore, it is suitable to utilize using an average or mean velocity V_m, which remains stable for incompressible fluid flow when considered the cross sectional area of the duct is fixed. The value of the mean velocity V_m in a duct is determined from conservation of mass principle, as follows:

$$\dot{m} = \rho V_m A_c \tag{1.8}$$

where $\dot{m}$ is the mass flow rate. The mean velocity for incompressible fluid flow in a duct of can be expressed as,

$$V_m = \frac{\dot{m}}{\rho A_c} \tag{1.9}$$

1.1.2. Mean Temperature

Since free stream velocity is unknown, mean or average velocity is needed to describe the internal flow and since the free stream temperature is unknown, mean temperature is needed. The value of mean temperature T_m is determined from the conservation of energy equation. This may be stated mathematically as, [3]

$$\dot{E}_{fluid} = \dot{m} CpT_m = \int_{A_c} \rho V_m CpTdA_c \tag{1.10}$$

where $\dot{E}_{fluid}$ is at any cross section throughout the duct represents the energy flow with the fluid at the cross section. Finally, the mean temperature of a fluid with constant specific heat and density flowing in a duct can be expressed as:

$$T_m = \frac{\int_{A_c} \rho V_m C_p T dA_c}{\dot{m} C_p} \tag{1.11}$$

1.1.3. Pressure Drop

A quantity of concern in the study of duct flow is the pressure drop because it is directly relevant to the power requirements of the pump or fan to continue fluid flow. So, viscous slip on the surface of the duct and pressure loss occuring along the duct is equalized. This equation is expressed as:

$$\frac{\Delta P}{\Delta x} = \frac{4\tau_w}{D_h} \quad \left(\tau_w = f \frac{1}{2} \rho V_m^{\,2} \right) \tag{1.12}$$

where τ_w (N/m^2) is wall shear stress and f is Darcy friction factor.

Pressure loss in duct having lenght of L (m) is expressed as,

$$\Delta P = f \frac{L}{D_h} \frac{\rho V_m^{\,2}}{2} \tag{1.13}$$

$$D_h = \frac{4 A_c}{P} \tag{1.14}$$

1.2. DIMENSIONLESS NUMBERS AND THEIR PHYSICAL MEANINGS

Dimensionless numbers are often correlated with some performance parameters and greatly assist engineering analysis and design. Some of the dimensionless numbers

operated in forced convective heat transfer are the Reynolds number (Re), the Nusselt number (Nu) and Darcy friction factor (f).

1.2.1. Reynolds Number (Re)

The Reynolds number is defined as the ratio of inertia forces to viscous forces.

$$Re = \frac{\rho V_m D_h}{\mu} = \frac{V_m D_h}{\upsilon} \tag{1.15}$$

where υ (m^2/s) is kinematic viscosity.

1.2.2. Nusselt Number (Nu)

The Nusselt number (Nu) is the ratio of convective to conductive heat transfer across surface.

$$Nu = \frac{\dot{q}_{convection}}{\dot{q}_{conduction}} = \frac{h\Delta T}{k\Delta T / L_c} = \frac{hL_c}{k} \tag{1.16}$$

where L_c is the characteristic length and $L_c = D_h$ for fluid flow in ducts.

1.2.3. Darcy Friction Factor

Darcy friction factor associates with either the head or the pressure loss depending on friction along a stated length of duct to the mean velocity of the fluid flow for an incompressible fluid. It is stated as,

$$f = \frac{\Delta P(D_h / L)}{(\rho V_m^{\ 2} / 2)} \tag{1.17}$$

1.3. BACKGROUND OF NANOFLUIDS

Nowadays, more and more energy is needed to supply energy of the World due to the developing technologies. Therefore, diversified heat transfer technologies have been set out to be developed. One of them is initiated by using nanofluids that are used for increasing heat transfer. Nanofluids have become top of the topic for researchers because of the following advantages [4]:

1. Reduced pumping power when considered compared to pure liquid to achieve equivalent heat transfer intensification.
2. Adjustable properties.
3. High dispersion stability with predominant Brownian motion of particles.
4. High specific surface area and thus more heat transfer surface between fluids and particles.
5. Reduced particle clogging as compared to conventional slurries, thus promoting system miniaturization.

Nanofluids are novel heat transfer fluids having nanoparticles whose sizes change from 1 nm to 100 nm suspended in the base fluids. In recent years nanofluids have been progressively studied. The studies have generally proved that nanofluids enhance heat transfer but there are some studies claming opposite state. Namely, it is contradictory issue whether heat transfer is enhanced by nanofluids. Many years ago, Maxwell [5] presented his theoretical model by predicting increased thermal conductivity of fluids by composing particles in liquids. After Maxwell, scientists have striven to enhance heat transfer adding solid particles in liquid. However, their efforts have not provided useful results due to particle size. Particle size was in micrometer or milimeter. So, settling problem was occured in liquids. Currently, modern nanotechnology is suitable for the production of nanoparticles havig sizes under 100 nm. Thus, existing problems have been achieved with modern nanotechnology. The first scientist who used nanofluid was Choi [4].

Nanofluids include broadly one kind of base fluid and one kind of nanoparticle. Nanofluids are used for increasing thermal conductivity to enchance heat transfer.

Due to this, nanoparticles are chosen as either metalic or metal oxide materials which have high thermal conductivity [6-10] as illustrated in Figure 1.4. Nanoparticles are not restricted only as metalic or metal oxide. They also include carbon, diamond and graphite materials [11-16].

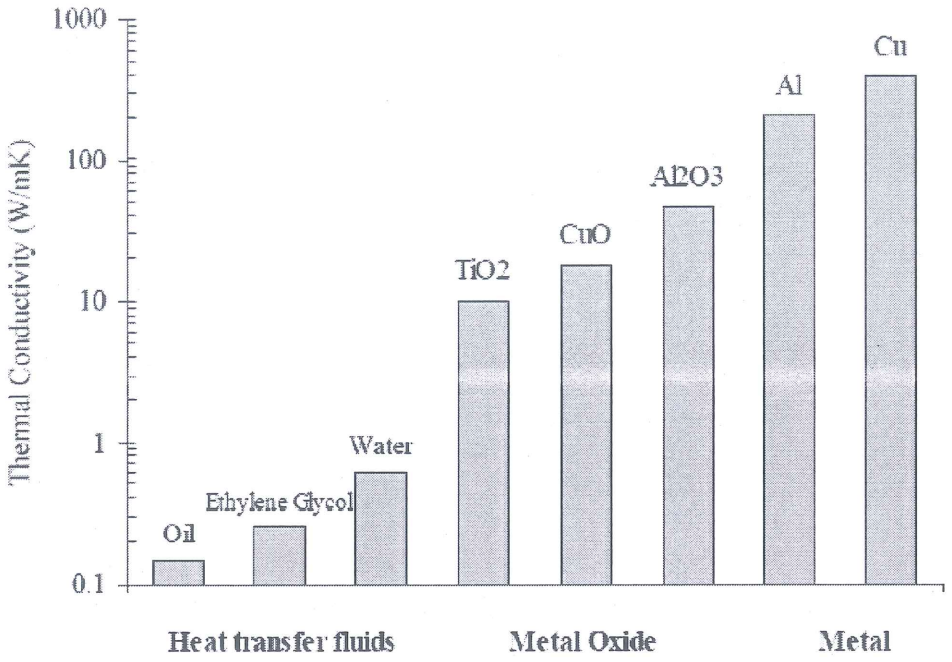

Figure 1.4. Comparison of thermal conductivities of conventional fluids, metal oxide and metalic materials [17].

Nanaofluids are used for various fields from engineering to medical applications since they are admitted as new generation fluids. Some of the applications of using nanofluids are represented in Figure 1.5 [18].

1.4. GENERAL INFORMATION FOR FLOW SEPARATION AND GENERAL STRUCTURE OF BACKWARD-FACING STEP (BFS)

Flow separation is crucial for engineering devices. It is one of the troublous forms of a viscous flow. It is significant for both science and engineering applications. Since flow separation occurs, energy losses and pressure drops occur. If energy losses can be gone over for fluid flow, flow separation will be controlled. This may be coped with perceiving effects, physical mechanisms and characteristics of flow separation.

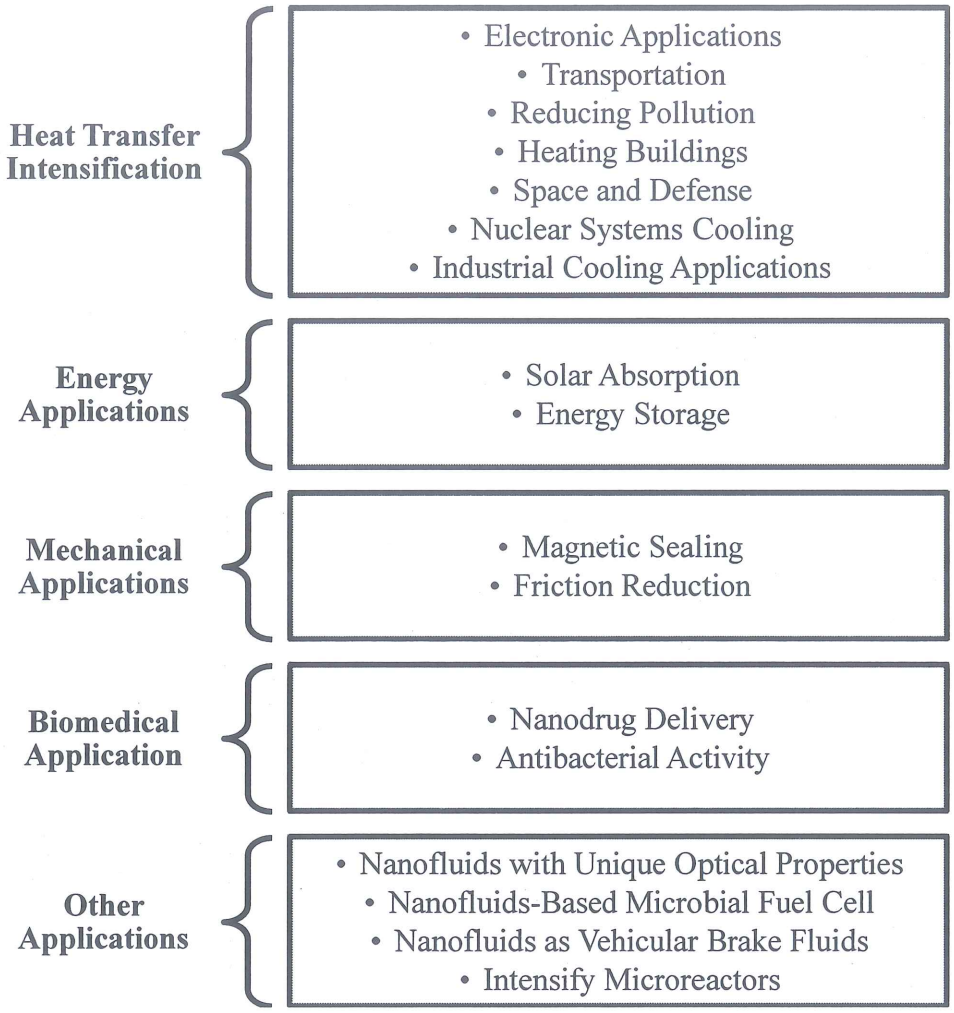

Figure 1.5. Nanofluids applications in some fields.

As Chang depicted, there are two basic flow separation categories [19]:

a- Flow separation over a smooth surface

b- Flow separation over discontinous surfaces

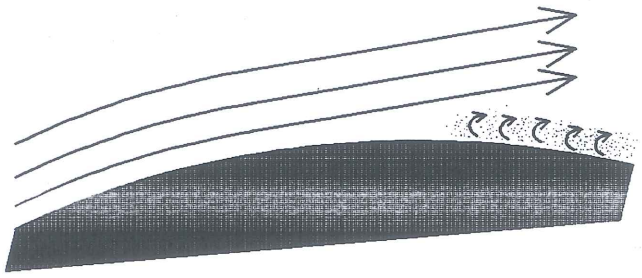

Figure 1.6. Flow separation over smooth surface [19].

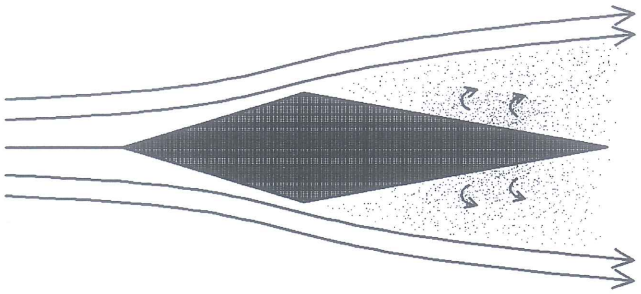

Figure 1.7. Flow separation over discontinuous surfaces [19].

Flow separation generally occurs under adverse pressure gradient and viscosity. If one of these two factors is missing, then the flow does not separate [19]. On the surface of the body, velocity is zero for viscous flow due to the friction. This is defined as no-slip condition. Above the surface of the body, velocity increases but it is restricted as seen in Figure 1.8 by insert (a). Assuming *n* stands for normal to the surface of the body, velocity increases with increasing *n*.

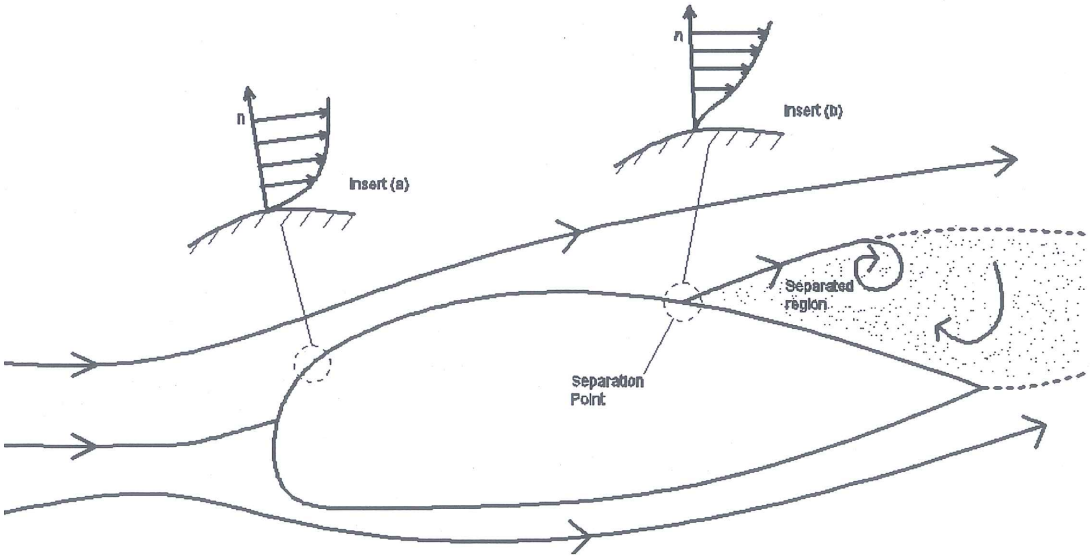

Figure 1.8. Effect of viscosity on a body in a moving fluid; shear stress and separated flow [20].

As shown in Figure 1.9, the fluid element is moving near surface of a body. At the point s_1, fluid element velocity is V_1. Pressure distribution increases through the flow direction. With increasing pressure, adverse pressure gradient is occured. Adverse pressure gradient reduces the velocity of the flow. For instance as given in Figure 1.9 at point s_2, V_2 is smaller than V_1. At a definite point in the flow, velocity of fluid

element is zero. Then velocity of fluid element is reversed its flow direction. '*Reversed flow*' is sketched at the point of s_3. Separation point takes place where velocity gradient ($\frac{\partial V}{\partial n}$) is zero as illustrated in insert (b) of Figure 1.8.

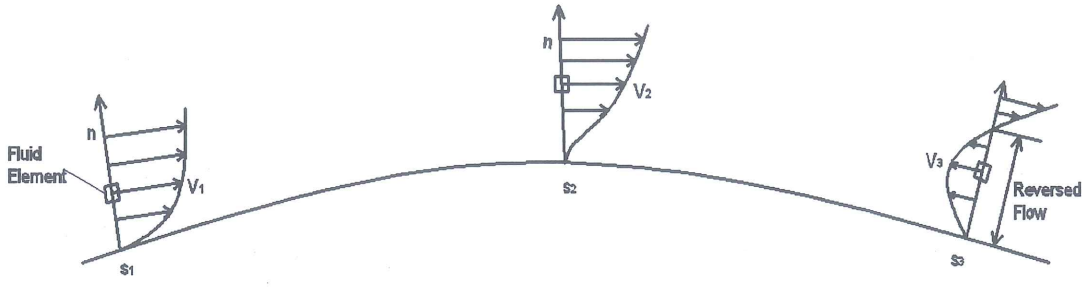

Figure 1.9. Separated flow caused by adverse pressure gradient [20].

A flow separation phenomenon is useful in many various engineering discipline. Some examples of advantages of flow separation are given below:

1. At combustors, the presence of the turbulence and recirculation depending on separation may assist enhance the mixing of fuel and air.

2. A thin airfoil which is suitable for high-speed flight may be made suitable for low speeds by separation of the flow. If the flow is allowed to separate over a portion of the upper surface and then reattaches and remains attached, a very thick pseudo-airfoil results. This thick airfoil is better suited for low speed flight [19].

3. For external flow at subsonic speeds such as airborn vehicles, the streamline deviates, the drag increases, the lift decreases, and reverse flow and stalling take place. In the transonic speed range, control and structure problems occur by flow separations. For cases of internal flow, separation can cause reduction in efficiencies of fluid handling devices such as engines, turbines and compressors [19].

Backward-facing step is a simple geometry in terms of separating and reattaching flow, but its flowfield is still entangeled. As shown in Figure 1.10, the flow separates

as of the step and then develops as a shear layer. After the shear layer, the flow reattaches to the wall.

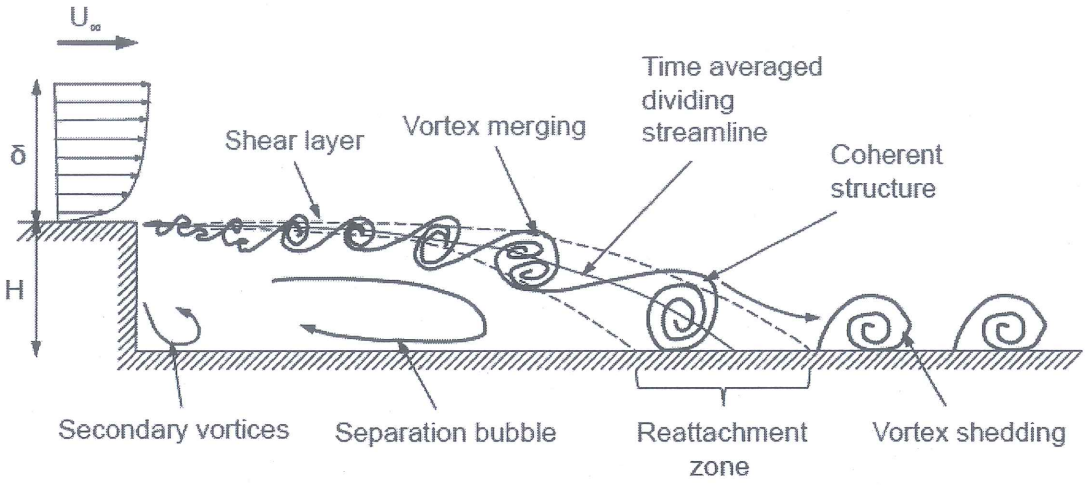

Figure 1.10. Flowfield of backward-facing step [21].

Flow characteristics of the BFS originate with upsteam boundary layer which separates at the edge of step because of the increasing pressure distribution that is called *adverse pressure gradient*. Due to the adverse pressure gradient and viscosity, velocity of flow reduces with time, and eventually stops. Conclusion of that case, secondary vortices and separation bubbles occur. This region composes of secondary vortices and separation bubble and it is called recirculation zone. Depending on adverse pressure gradient, the shear layer curves downward to the wall and finally impinges on the wall. This is defined as reattachment point. The length between reattachment point and the step is known as reattachment length. The flow characteristic in the reattachment region, which occurs separating and reattachment flow, influences the heat transfer characteristics.

1.5. LITERATURE SURVEY

1.5.1. Literature Survey on BFS

Using backward-facing step geomerty, which is simpler in terms of understanding the flow separation and reattachment, has been extensively researched with numerically and experimentally since 1950s.

Goldstein et al. [22] performed an experimental study to investigate the reattacment point under laminar and subsonic flow conditions over a step. They noticed that the reattachment point and boundary displacement thickness change with Reynolds number.

Denham and Patrick [23] investigated 2D laminar flow over the BFS. Water was used as working fluid. The channel's expansion and aspect ratios are equal to 3 and 20, respectively. The Reynolds number was varied between 50-250. They observed that flow characteristics of BFS approximates to other 2D geometries having sudden expansion. Yet, both recirculation length and mass flow rate circulating were smaller. At Re=229, they noticed a fluctation, which shows the beginning of transition to turbulent separated boundary layer.

Armaly et al. [24] analysed the effect of Reynolds number on velocity distributions and length of reattachment. The work was numerically done as two-dimensional under laminar, transitional and turbulent flow conditions. Air was flowed in the channel having aspect ratio of AR=36. They observed that length of reattachment strongly depends on Reynolds number. Reattachment length increases to Re=1200 and then velocity fluctations occur. At higher Reynolds numbers 3D effects was dominant near the sidewalls. Numerical predictions were compared with the experimental results. They realized that numerical and experimental results were in good agreement.

Chen et al. [25] investigated the influence of the step height on flow and heat transfer characteristics in 2D BFS channel under turbulent forced convection flow conditions, with the Reynolds number was 28000. Constant and uniform heat flux (q''_w=270 W/m^2) was exposed to the stepped wall downstream from the step and the other walls were adiabatic. Step heights were 0.019, 0.038 and 0.076 m. They observed that bulk temperature, maximum turbulent kinetic energy, primary and secondary recirculation regions increase while the step height increases.

Pulat and Diner [26] researched numerically effects of Reynolds number and expansion ratio on reattachment point in a 2D channel. Working fluid was air to be

assumed incompressible. Flow was under steady state and laminar conditions. The numerical results were obtained for Re=50 and Re=150. Expansion ratios were 1.5 and 2. They concluded that reattachment length increases with increasing Reynolds number and decreases with increasing channel expansion ratio.

Mahdi et al. [27] studied to explore heat transfer mechanism and flow behavior due to expansion ratio and Reynolds number over 2D BFS. The study was conducted on laminar incompressible flow conditions. They found that separation zone size and reattachment length increases with increasing expansion ratio and Reynolds number. As long as Reynolds number increases, Nusselt number increases, also.

As known, engineering practical applications are mostly on three-dimensional. 3D backward-facing step studies have been accelarated to clarify heat and fluid flow charactarictics and obtain more realistic results.

Rinoie et al. [28] experimentally investigated turbulent flow over the backward-facing step to clarify behaviour of turbulent flow inside the reattachment shear layer using turbulent energy balance assisting in understanding of turbulent flow of BFS. Step height and aspect ratio were 0.02 m and 10, respectively. They observed that turbulent structures can be classified in three categories (the dead air, reversed flow and separated shear layer zone). In the turbulent energy balance, transverse diffusion assisting to balance the dissipation term was positive.

Iwai et al. [29] conducted a three dimensional numerical simulation in a channel for laminar mixed convection to examine the influence of duct inclination angle (θ_1 and θ_2). As shown Figure 1.11, θ_1, pitch angle was define between the vertical upward direction and stream-wise direction. θ_2, rolling angle was between the vertical upward direction and normal direction.Values of Reynolds number, aspect ratios and expansion ratios were constant at Re=125, AR=16 and ER=2, respectively. Uniform and constant heat flux was applied to downstream of the step but other walls were insulated. They noticed that pitch and rolling angle influence flow and heat transfer.

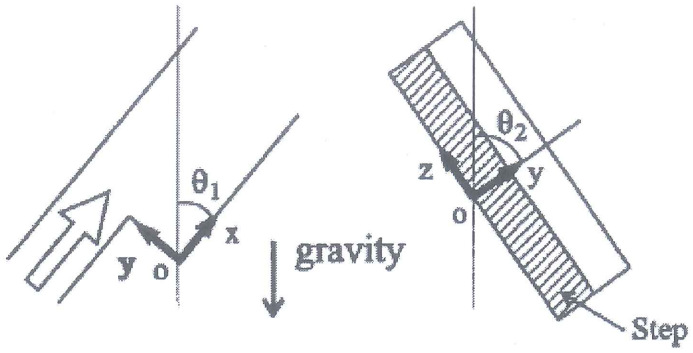

Figure 1.11. Definition of pitch angle (θ_1) and rolling angle (θ_2).

Nie and Armally [30] examined numerically the effects of step height on heat transfer and flow characteristics in a three dimensional BFS channel. Flow was thought as laminar and forced convection conditions. Air was passed through the channel as working fluid. Thermophysical properties of air was assumed constant along the channel. The study was performed at constant Reynold number (Re=343). Constant and uniform heat flux (q''_w=50 W/m^2) was subjected to downward of the step wall while the other walls were insulated. Three different step height was performed in this study. They observed at the end of the study that Nusselt number, general three dimensional flow characteristic features, gradient locating in recirculation region increases with increasing step height. Also, they noticed that step height effects the friction coefficient distribution.

Chen et al. [31] aimed to explore the effects of step inclination on heat transfer and flow features in a BSF duct using numerical prediction. The study was performed as three dimensional and laminar forced convection conditions. Range of angle of the step was changed from 15° to 90°. Air was the working fluid and its physical properties were assumed to be constant. Constant heat flux was applied to downward bottom wall and the rest of walls were adiabatic. The Nusselt number, temperature, velocity and friction coefficient distribution with changing step inclination were examined. They realized that maximum Nusselt number is placed near the sidewall when inclination angle is grater than 30°. Friction coefficient occuring in recirculation zone increases with increasing step inclination angle increases. They additionally observed that velocity and tempetature distributions change with inclination angle.

Lan et al. [32] conducted numerical simulation of 3D turbulent forced convection flow in backward-facing step channel. Range of Reynolds number was at 20000-50000. The channel's step height and expansion ratio was 4.8 and 1.48 mm, respectively. This study was done to understand the effects of Reynolds number and aspect ratio on heat transfer and fluid flow features. The Nusselt number, temperature, and general flow features distributions were presented. They concluded that Reynolds number and aspect ratio influence slightly flow separation and reattachment point but heat transfer is substantially influenced.

1.5.2. Literature Survey on BFS Using Nanofluids

As mentioned in the literature survey, studies carried out regarding heat transfer represent minority. In ducts with backward-facing step, heat transfer applications have been increased by using nanofluids. However, studies should be enhanced regarding flow and heat transfer characteristics in BFS using nanofluids

Abu-Nada [33] is the first researcher who conducted a numerical study concerning heat tranfer by using nanofluids in ducts with backward-facing step. In this study, five different nanoparticles (CuO, Cu, TiO_2 , Ag, and Al_2O_3) were used with volume fractions between 0.05% to 2.0%. Water was the base fluid. Duct was thougth 2D and its expansion ratio was 2. The range of Reynolds number was 200-600. He reported that Nusselt number increases with increasing volume fractions.

Al-aswadi et al. [34] studied numerically 2D laminar forced convection flow of nanofluids in channel with BFS. The base fluid was water. They conducted this study by using Al_2O_3, Au, Ag, CuO, TiO_2, Cu, , SiO_2 and diamond nanoparticles with 0.05 volume fraction. The study was performed for Re=50, 100 and 175. Expansion ratio and step height and of the devised channel were 2 mm and 4.8 mm, respectively. All the walls were insulated. They presented the effects of Reynolds number and nanofluids types on pressure drop, velocity distribution and friction coefficient. They noticed that the highest wall shear stress is observed for SiO_2/water nanofluid. They found that nanofluids prepared nanoparticle with low density increase velocity much more compared to nanofluids prepared nanoparticle with high density. Also, they

obtained that Reynolds number and skin friction coeffcient are inversely proportional.

Heshmati et al. [35] investigated a numerical simulation of a two dimensional duct having backward-facing step devised slotted baffles on the top wall. Flow was performed for laminar mixed convection condition. Working fluids were SiO_2/water, Al_2O_3/water, CuO/water and ZnO/water nanofluids. Nanoparticles were added obvious volume fraction (φ =1.0-4.0%) and their diameters range were at 20–50 nm. Also, constant and uniform heat flux (q''_w=10000 W/m^2) was applied to downward of the step wall while the other walls and slotted baffle were insulated. The main goal of the study was to investigate the effects of the slotted baffle's positions (with a vertical solid baffle, with a solid inclined baffle, with two inclined slotted baffle), nanofluid's volume fractions and diameters on heat transfer. They observed that SiO_2/water nanofluid having 4.0% nanoparticle volume fraction and 20 nm nanoparticle diameter enhances heat transfer much more amoung the other nanofluids. In addition, they found that maximum Nusselt number is obtained in duct with inclined slotted baffle.

Togun et al. [36] numerically investigated a study of heat transfer characterictics in laminar and turbulent flow conditions by using two dimensional duct having BFS. Working fluid was Cu/water nanofluid whose volume fractions were 0%, 2.0% and 4.0%. Reynolds number were changed from 50 to 200 for laminar flow condition and 5000 to 20000 for turbulent flow condition. The duct was only heated at downstream of stepped wall with constant heat flux at 4000 W/m^2 and its expansion ratio was 2. They obtained that Nusselt number increases with increasing volume fraction of nanoparticle for laminar and turbulent conditions. They presented that maximum Nusselt number occurs at 4.0% volume fractions and Reynolds number of 20000. In additon, they observed that turbulent flow enchances the Nusselt number amount of 10% compared to laminar flow.

Kherbeet et al. [37] conducted a numerical simulation for flow and heat transfer characteristics in 2D duct with microscale backward-facing step (MBFS). Flow was considered at laminar mixed convection condition. Four different nanoparticles types

which were ZnO, Al_2O_3, SiO_2 and CuO with volume fraction of 1.0%, 2.0%, 3.0%, and 4.0% were dispersed in ethylene glycol. The range of Reynolds number and diameter of nanoparticles were at 0.05-0.5 and 25-75 nm, respectively. Duct having expansion ratio of 2 and step height of 96 μm was heated downstream of stepped wall with uniform heat flux. Main aim of the study was the effect of nanofluids on heat transfer. They noticed that the increase of Reynolds number causes increase the skin friction coefficient and Nusselt number. They also revealed that the smallest diameter of nanoparticles have the highest Nusselt number.

Kherbeet et al. [38] carried out numerical and experimental studies under laminar forced convection nanofluids flow over MBFS to observe the effects of nanofluid on heat transfer. The duct's step height was 600 μm and its downstream of wall was exposed uniform heat flux. The experiment was studied at Reynolds number was changed from 280 to 470. In the experimental studies, SiO_2/water and Al_2O_3/water nanofluids were used as working fluids. Diameter of nanoparticles was 30 nm and volume fractions were varied from 0 to 0.01. They compared the experimental results with numerical simulation. They obtained that the numerical and experiment results were in good agreement. They also found that maximum Nusselt number is obtained by using SiO_2/water nanofluid.

Kherbeet et al. [39] aimed to clarify the effect of step height on heat and flow characteristics in three dimensional duct having microscale backward-facing step. The flow was considered as laminar mixed convection condition. Reynolds number was 35. While downstream stepped wall was heated with constant heat flux of 12 W/m^2, straight wall temperature was 323 K. The base fluid was ethylene glycol. SiO_2 nanoparticle with volume fraction of 4.0% was added to base fluid. Step heights were 350, 450 and 550 μm. They found that the increasing step height of duct increases both Nusselt number and skin friction coefficient.

1.6. OBJECTIVES

In light of relatively literature survey of fluid flow and heat transfer in a duct having microscale backward-facing step summarized above and the studies regarding flow

over microscale backward-facing step are not adequate to understand the flow and heat transfer characteristics in ducts having MBFS. The present study attempts to develop the knowledge of nanofluid flow and heat transfer characteristics of flow over microscale backward-facing step.

The objectives of the study are:

1. To conduct laminar forced convection flow of nanofluids in a 3D duct having microscale backward-facing step.
2. To investigate the effects of expansion ratio (ER) on heat and fluid flow characteristics by designing three different expansion ratios of ER=1.25, 1.67 and 2.50.
3. To investigate the effects of nanofluids on heat and fluid flow characteristics by using five different nanoparticles (Al_2O_3, SiO_2, CuO, ZnO and TiO_2).
4. To investigate the effects of volume fraction ($\varphi = 1.0\%$, 2.0%, 3.0% and 4.0%) of nanofluids on heat and fluid flow characteristics.
5. To investigate the effects of the Reynolds number on heat and fluid flow characteristics by changing from 100 to 1000.
6. To investigate the effects of velocity and temparature distributions to understand the structure of flow separation in ducts having microscale backward-facing step.
7. The most efficient expansion ratio and nanofluid are proposed at the end of the study.

PART 2

METHODOLOGY

2.1. THERMOPHYSICAL PROPERTIES OF NANOFLUIDS

The necessary thermophysical properties of nanofluids in this study are thermal conductivity, viscosity, density, and specific heat.

The effective thermal conductivity of nanofluid was present as [40]:

$$k_{eff} = k_{static} + k_{brownian} \tag{2.1}$$

The k_{static} was presented as [41]:

$$k_{static} = k_f \left[\frac{(k_s + 2k_f) - 2\varphi(k_f - k_s)}{(k_s + 2k_f) + \varphi(k_f - k_s)} \right] \tag{2.2}$$

Thermal conductivity resulting from Brownian motion is offered as [40]:

$$k_{brownian} = 5x10^4 \beta\varphi\rho_f Cp_f \sqrt{\frac{KT}{\rho_s d_p}} f(T,\varphi) \tag{2.3}$$

where

$$f(T,\varphi)=(2.8217x10^{-2}\varphi+3.917x10^{-3})\left(\frac{T}{T_0}\right)+(-3.0669x10^{-2}\varphi-3.91123x10^{-3})$$

where K is the Boltzman constant.

Corcione [42] presented viscosity of nanofluid equation as:

$$\frac{\mu_{eff}}{\mu_f}=\frac{1}{1-34.87(d_p/d_f)^{-0.3}\varphi^{1.03}} \tag{2.4}$$

$$d_f=\left[\frac{6M}{N\pi\rho_{fo}}\right]^{1/3}$$

The effective density of nanofluid was presented as [42]:

$$\rho_{eff}=(1-\varphi)\rho_f+\varphi\rho_s \tag{2.5}$$

The effective specific heat of nanofluid was presented as [42]:

$$(Cp)_{eff}=\frac{(1-\varphi)(\rho Cp)_f+\varphi(\rho Cp)_s}{(1-\varphi)\rho_f+\varphi\rho_s} \tag{2.6}$$

The effective thermal expansion of nanofluid was presented as [42]:

$$\beta_{eff}=\frac{(1-\varphi)(\rho\beta)_f+\varphi(\rho\beta)_s}{(1-\varphi)\rho_f+\varphi\rho_s} \tag{2.7}$$

β values of different nanoparticles are given in Table 2.1.

Table 2.1. β values of different nanoparticles and their boundary conditions.

Type of particles	β		Concentration	Temperature
Al_2O_3	$8.4407(100\varphi)^{-1.07304}$	[40]	$1\% \leq \varphi \leq 10\%$	298 K≤T≤363 K
CuO	$9.881(100\varphi)^{-0.9446}$	[40]	$1\% \leq \varphi \leq 6\%$	298 K≤T≤363 K
SiO_2	$1.9526(100\varphi)^{-1.4594}$	[40]	$1\% \leq \varphi \leq 10\%$	298 K≤T≤363 K
ZnO	$8.4407(100\varphi)^{-1.07304}$	[40]	$1\% \leq \varphi \leq 7\%$	298 K≤T≤363 K
TiO_2	$6.6E\text{-}4(100\varphi)^{0.121}$	[43]	$1\% \leq \varphi \leq 4\%$	298 K≤T≤363 K

2.2. PROBLEM DESCRIPTION AND GOVERNING EQUATIONS

Laminar forced heat transfer and flow of nanofluids in a 3D duct having microscale backward-facing step is numerically investigated. Since the flow field is symmetric, only one half of the duct is considered in the numerical calculations for reducing the computational time. The shematic diagram and the geometrical dimensions of duct for different expansion ratios are presented in Figure 2.1 and Table 2.2, respectively.

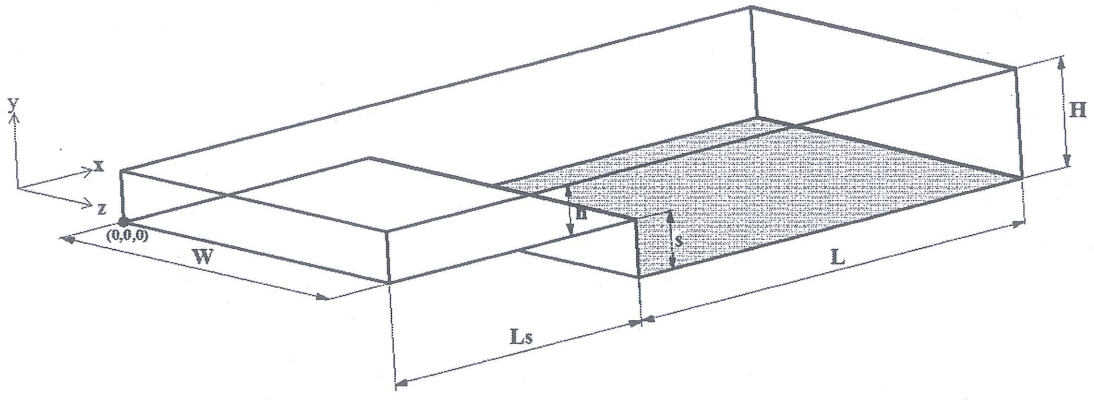

Figure 2.1. Schematic view of three-dimensional microscale backward-facing step

Table 2.2. Geometrical dimensions of duct having microscale backward-facing step.

Expansion Ratio [ER= H/(H-s)]	s *(μm)*	L *(m)*	Ls *(m)*	H *(μm)*	W *(μm)*
1.25	200	0.15	0.10	1000	1200
1.67	400				
2.50	600				

The length of downstream and upstream wall was 0.15 m and 0.1 m, respectively. Total duct height was 1000 μm and width of duct was 1200 μm. While downstream stepped wall was heated with uniform and constant heat flux of 10000 W/m^2, other walls were insulated. Solid particles with size under 100 nm were considered to be able to use single phase approach, thus single phase approach was practiced for nanofluid modeling and the phase of nanofluid was assumed to be as a continuous. The following assumptions were adopted for this numerical study: (i) Both heat transfer and fluid flow in duct were in three dimensional and steady-state; (ii) fluid flow was incompressible and laminar flow; (iii) the physical properties of nanofluid, such as specific heat, density, thermal conductivity were taken as temperature independent; (iv) negligible viscous dissipation and radiation heat transfer; and (v) the base fluid and the nanoparticles were in thermal equilibrium. The thermophysical properties of nanoparticles and pure water are presented in Table 2.3.

Table 2.3. Thermophysical properties of nanoparticles and pure water.

Property	Water	Al_2O_3 [44]	CuO [44]	SiO_2 [44]	ZnO [44]	TiO_2 [45]
ρ(kg/m^3)	997	3970	6500	2200	5600	4175
μ(N/ms)	0.000855	-	-	-	-	-
k(W/mK)	0.613	40	20	1.2	13	8.4
Cp(kJ/kgK)	4179	765	535.6	703	495.2	692

With mentioned above assumptions, governing equations; continuity, momentum and energy were given, respectively:

$$\vec{\nabla} \cdot \vec{V} = 0 \tag{2.8}$$

$$\rho \frac{D\vec{V}}{Dt} = -\nabla p + \mu \nabla^2 \vec{V} \tag{2.9}$$

$$\rho Cp \frac{DT}{Dt} = k \nabla^2 T \tag{2.10}$$

2.3. BOUNDARY CONDITIONS

The boundary conditions are used for solving the continuity, momentum and energy equations. They are treated as no slip conditions and thermally adiabatic at all the walls with the exception of the downstream stepped wall which is heated with uniform and constant at 10000 W/m^2 as shown Figure 2.2. Fluid enters the duct at uniform temperature and velocity. Velocity inlet and pressure outlet boundary conditions are used at the inlet and exit of the duct, respectively.

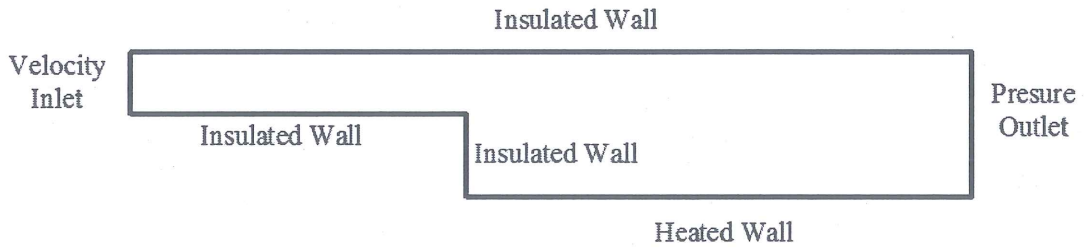

Figure 2.2. Boundary conditions of 2D duct having MBFS.

2.4. NUMERICAL PROCEDURES

In the computations, the finite-volume method based commercial CFD software Ansys Fluent 15.0 is used to perform the numerical calculations by solving the governing equations along with the boundary conditions. The convection terms in mass, momentum and energy equations are discretized using a second order upwind scheme, respectively. The standard scheme is employed for discretization of pressure and the SIMPLEC algorithm, which gives more accurate results, is used to resolve

the coupling between velocity and pressure. The Green-Gauss cell based method is applied for discretization of the momentum and energy equations. To obtain convergence, each equation for mass, momentum, and energy is iterated until the residual falls below $1x10^{-6}$. No convergence problems are observed during the calculations.

2.5. MESH DEPENDENCY ANALYSIS

Mesh is used to discretize the geometry of the model for numerical simulations. Meshing can be generated either in 2-D or in 3-D, depending on the dimensions of the analyses. The hexahedral mesh distribution is used for the duct having microscale backward-facing step. The numbers of mesh points or control volumes are increased close to wall of the duct and near to the backward-facing step to enhance the resolution and accuracy as given in Figure 2.3.

The mesh independence study is performed for the duct having expansion ratio of 2.5 by refining the mesh number until the variation in both average heat transfer coefficient and average Darcy friction factor are less than 0.06%. To obtain the optimum mesh number, a grid independence study is conducted using twenty different mesh numbers changing from $5x10^4$ to $8.5 x10^5$ for Re=1000. Changing the average heat transfer coefficient and average Darcy friction factor values with mesh number for pure water flow is given in Figure 2.4 as an illustration. It is observed that a further refinement of mesh number from $4x10^5$ to $8.5x10^5$, the changing of average heat transfer coefficient and average Darcy friction is negligible. If Figure 2.4 is observed, optimum mesh number with minimum computational time and maximum accuracy approximately can be seen at $3.2x10^5$. To obtain optimum mesh number, same procedure is used for other expansion ratios of 1.25 and 1.67 for pure water.

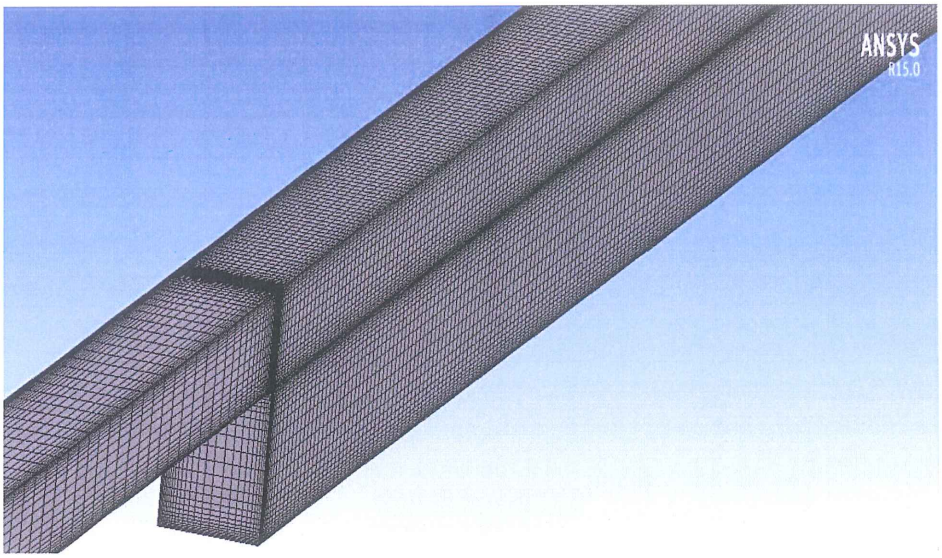

Figure 2.3. Sample mesh distribution of the duct having MBFS geometry.

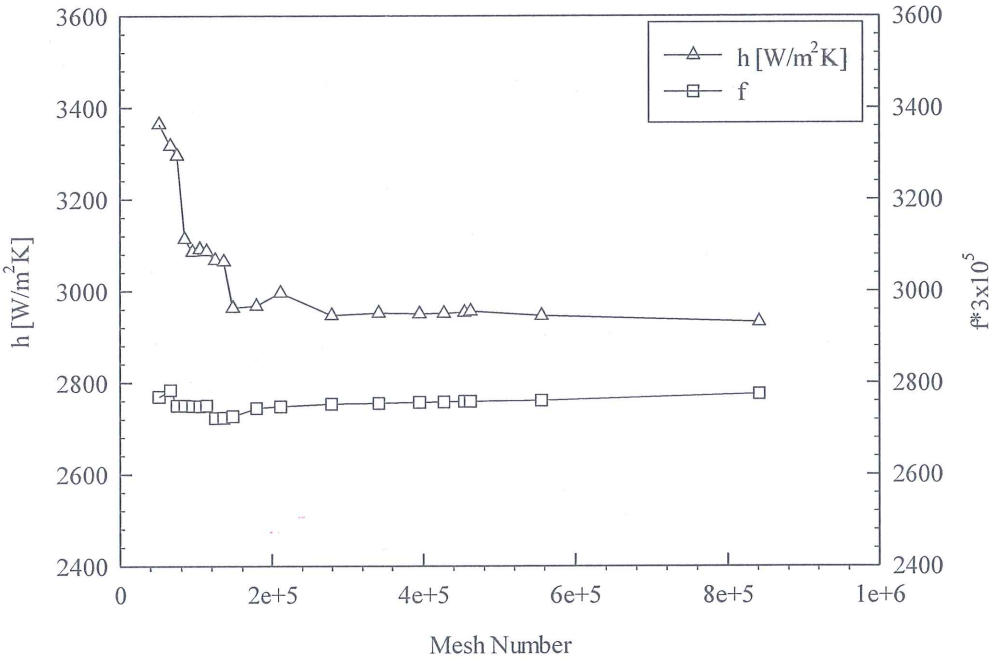

Figure 2.4. Changing of average heat transfer coefficient and average Darcy friction factor with mesh number for pure water at Re=1000.

2.6. COMPARISON WITH EXPERIMENTAL RESULTS

At the beginning of the study, the numerical code is validated by comparing the present result of average Darcy friction factor with the experimental result of average

Darcy friction factor of Kherbeet et al. [38] for the duct having MBFS as shown in Figure 2.5. The results obtained by present study are good agreement with the correlation proposed by Kherbeet et al. [38]. Error of numerical simulation results compared to experimental results is nearly below 5%.

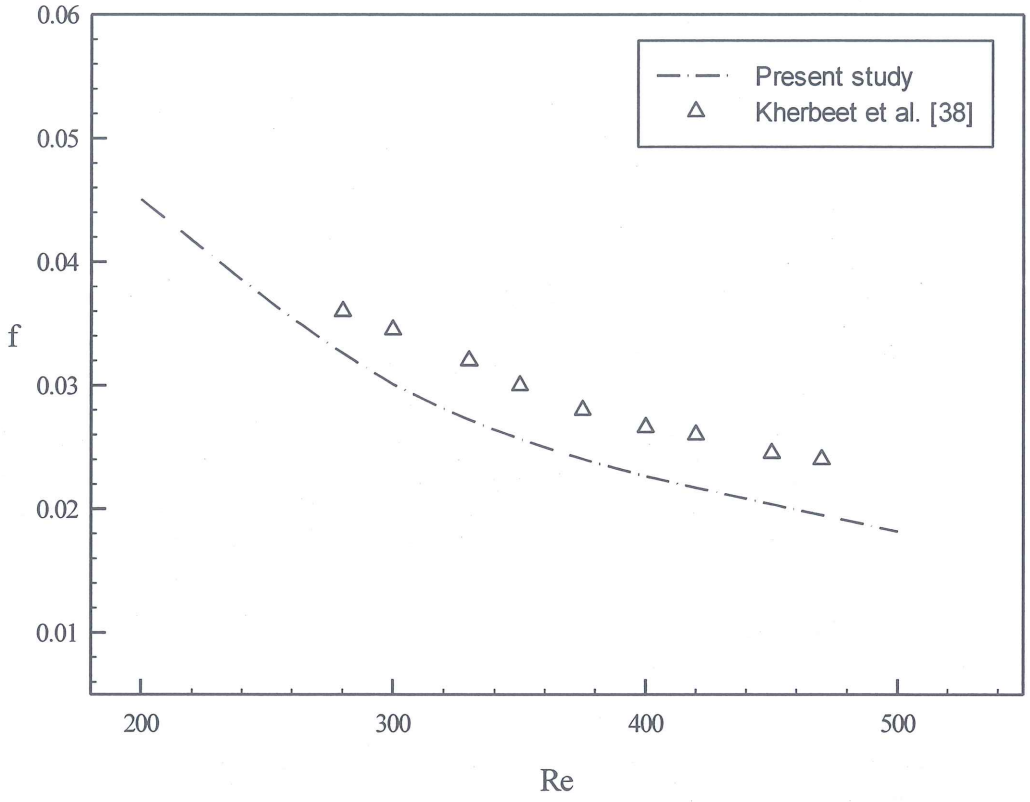

Figure 2.5. Comparison of average Darcy friction factor of the present result for pure water with the result of Kherbeet et al. [38].

PART 3

RESULTS AND DISCUSSIONS

Laminar forced convection flow and heat transfer characteristics of nanofluids over a three-dimensional horizontal microscale backward-facing step located in a rectangular cross-sectional duct is numerically investigated. Four different volume fractions ($\varphi = 1.0\% - 4.0\%$) of nanoparticles are dispersed in pure water and five different nanoparticles (Al_2O_3, SiO_2, CuO, ZnO and TiO_2) are used. The Reynolds number is in the range of $100 \leq Re \leq 1000$. The duct has three different expansion ratio (ER=1.25, 1.67 and 2.50). Numerical results are presented in nondimensional average and local Nusselt number and Darcy friction factor.

3.1. HEAT TRANSFER CHARACTERISTICS

Predictions of the Nusselt number from the numerical simulation are presented for different nanoparticle volume fractions and different nanofluids in this section. Figure 3.1 is presented to obtain the effects of different nanoparticle volume fractions on average Nusselt number for expansion ratio of 1.25. The numerical results show that the average Nusselt number increases with increasing all volume fractions for Al_2O_3/water, SiO_2/water and TiO_2/water nanofluids due to increase of thermal conductivity of fluid by dispersed nanoparticles. That is because while the nanoparticles volume fraction increases, random and irregular movements of nanoparticles increase the rates of the energy change in the fluid with penalty on the wall shear stress and eventually improve the thermal dispersion of the fluid flow [46]. Pure water has higher value of Nusselt number than 1.0% and 2.0% volume fractions of ZnO/water and CuO/water nanofluids. This occurs due to the effect of dynamic viscosity and density on the specific weight gravity [34]. The variation of average Nusselt number with nanoparticles volume fractions for ZnO/water and CuO/water nanofluids is very low. In addition, average Nusselt number increases

with increasing Reynolds number. Maximum Nusselt number is obtained at 4.0% nanoparticle volume fraction for all types of nanofluids.

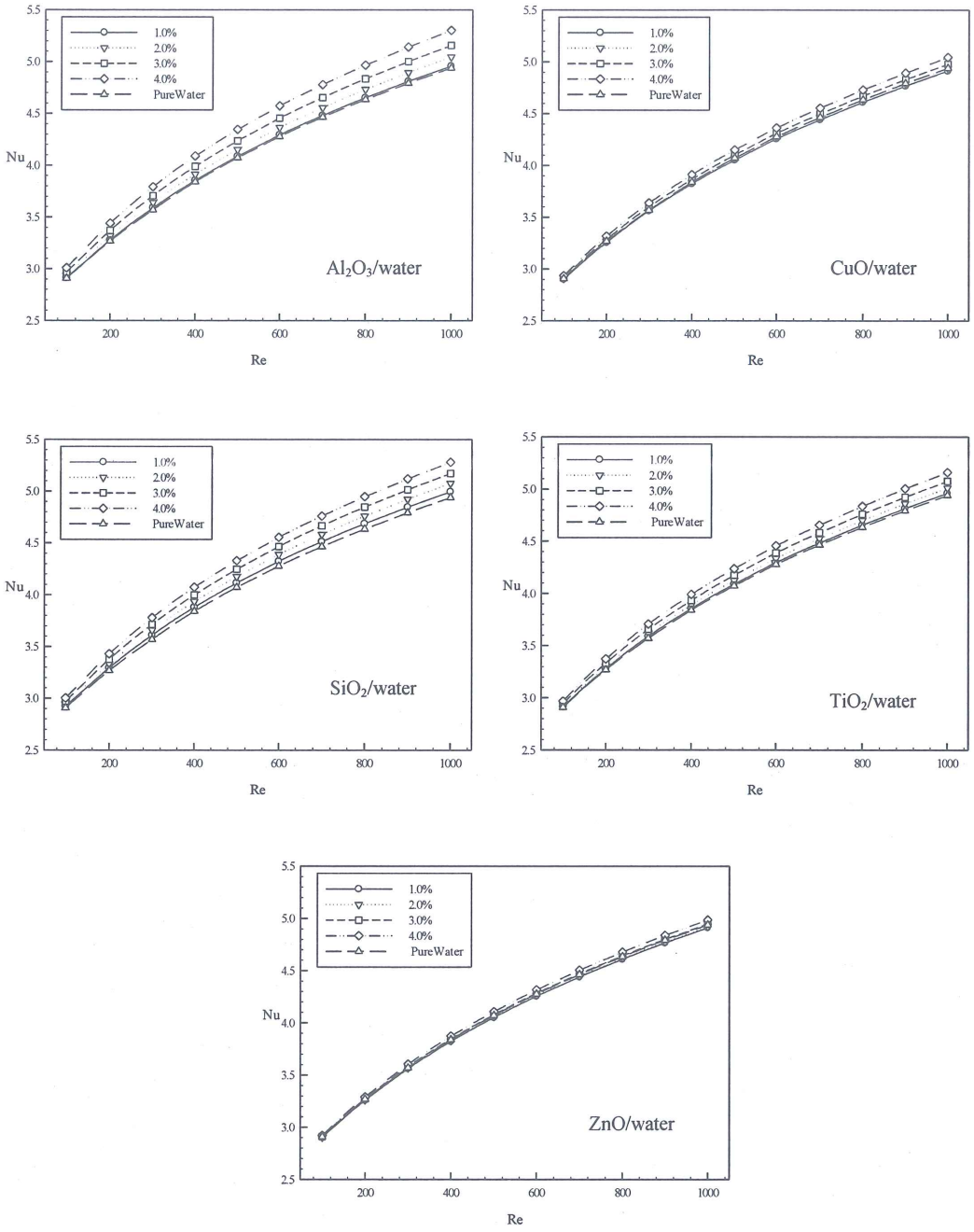

Figure 3.1. The average Nusselt number variation with Reynolds number for different nanoparticle volume fractions of different nanofluids at ER=1.25.

Figure 3.2 presents to evaluate the effects of different Reynolds numbers and nanoparticle volume fractions for expansion ratio of 1.67 on average Nusselt number. As seen in Figure 3.2, the numerical results of ER=1.67 have the same trend with numerical results of ER=1.25.

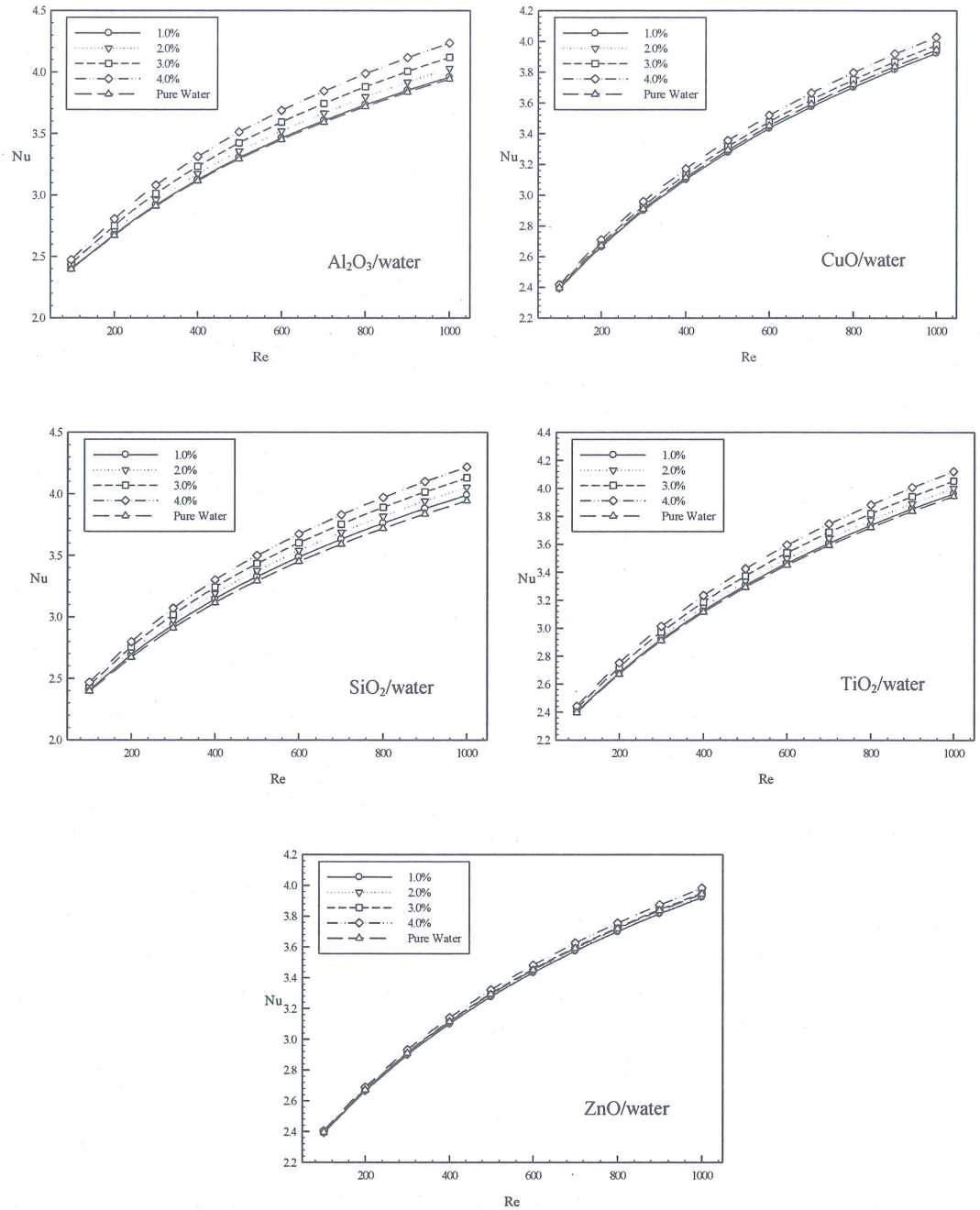

Figure 3.2. The average Nusselt number variation with Reynolds number for different nanoparticle volume fractions of different nanofluids at ER=1.67.

Effects of changing Reynolds numbers and nanoparticle volume fractions for expansion ratio of 2.50 on average Nusselt number is given in Figure 3.3. As can be seen in Figure 3.3, average Nusselt number increases with Reynolds number and nanoparticle volume fraction. The highest Nusselt number is obtained at ER=1.25.

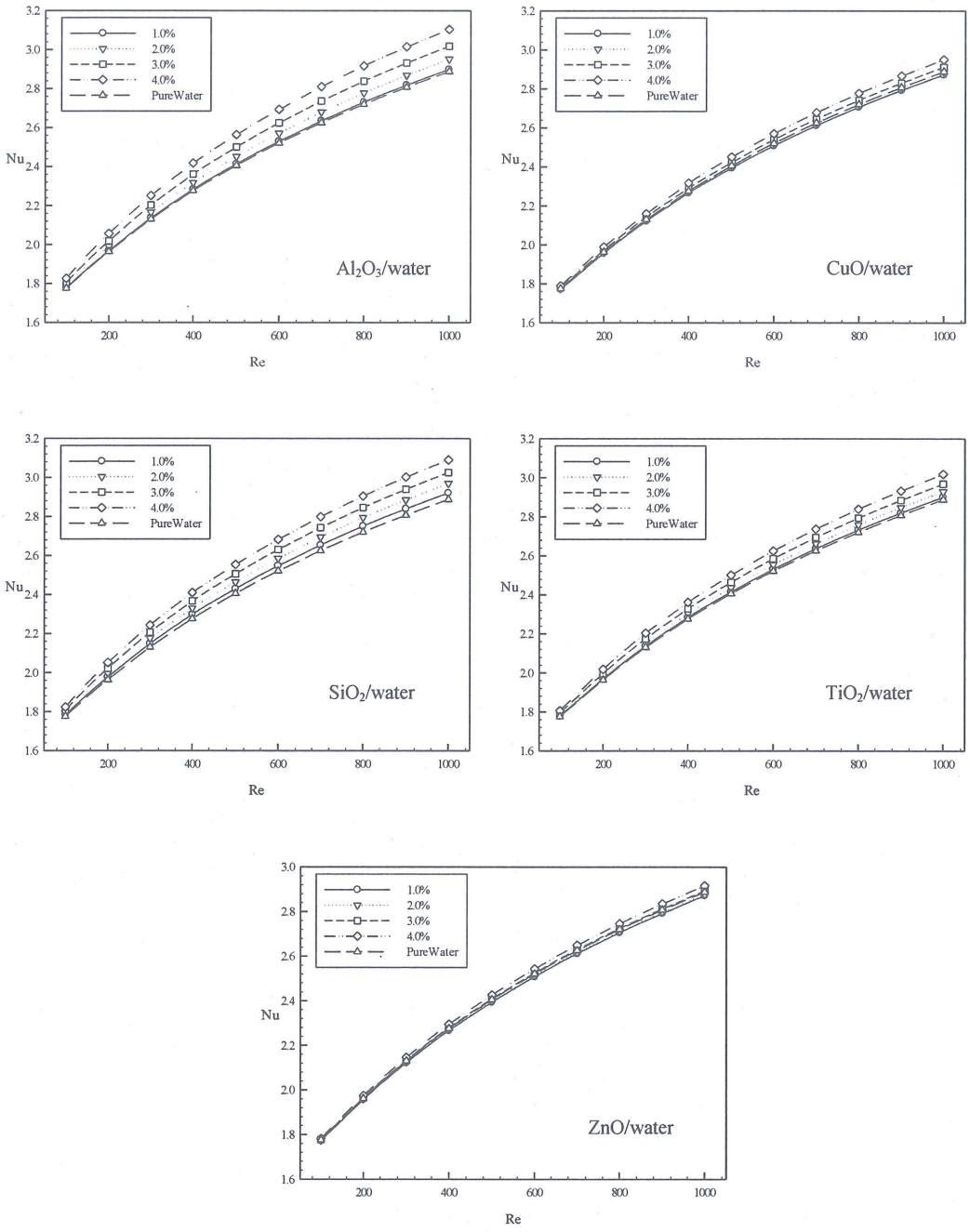

Figure 3.3. The average Nusselt number variation with Reynolds number for different nanoparticle volume fractions of different nanofluids at ER=2.50.

As seen above, the average Nusselt number of nanofluids is generally higher than the pure water. This may be related that the nanofluids with a high Prandtl number having a higher Nusselt number [38]. The maximum average Nusselt number is obtained at volume fraction of 4.0% for all types of nanofluid.

Figure 3.4, Figure 3.5 and Figure 3.6 are given to obtain the effect of nanofluid types on heat transfer for ER=1.25, ER=1.67 and ER=2.50, respectively. As can be seen from these figures, the average Nusselt number increases gradually with increasing Reynolds number for all cases. It was revealed that Al_2O_3/water nanofluid has the highest average Nusselt number at maximum Reynolds number and ZnO/water nanofluid has the lowest average Nusselt number for all expansion ratios. As expransion ratio increases, the average Nusselt number decreases.

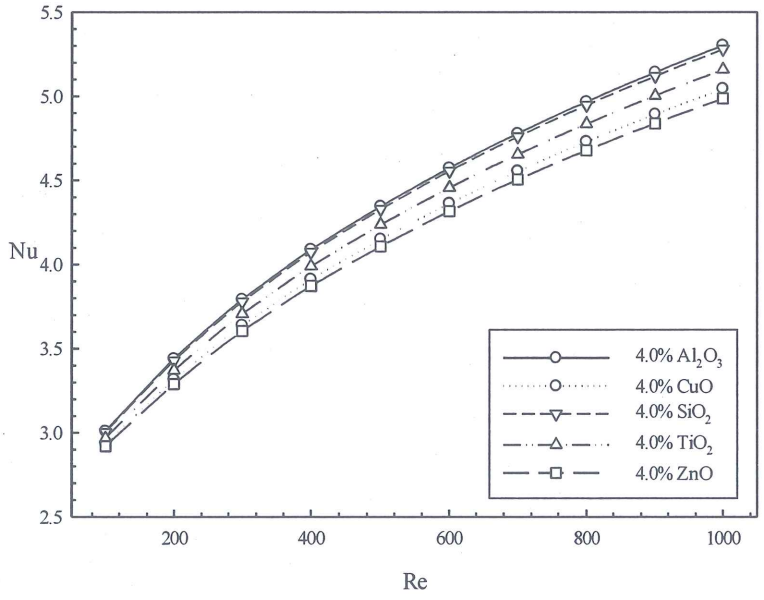

Figure 3.4. The average Nusselt number variation with Reynolds number for 4.0% nanoparticle volume fractions and different types of nanofluids at ER=1.25.

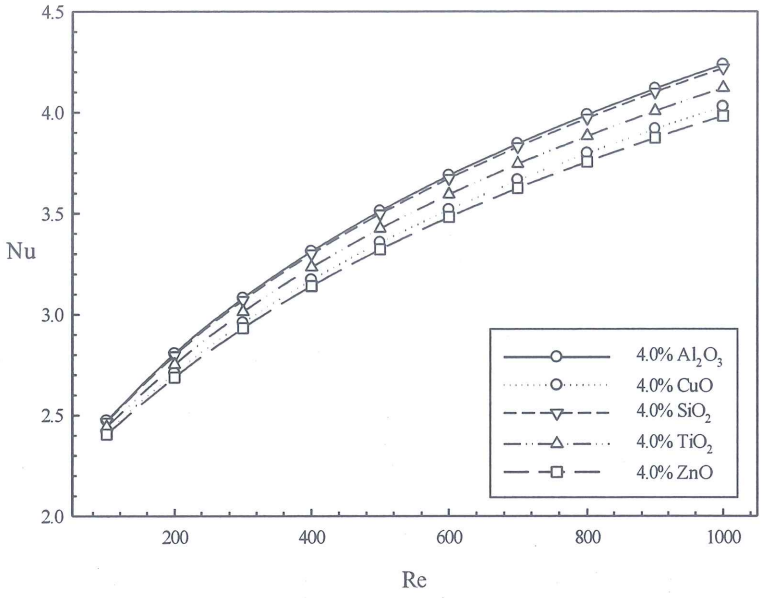

Figure 3.5. The average Nusselt number variation with Reynolds number for 4.0% nanoparticle volume fractions and different types of nanofluids at ER=1.67.

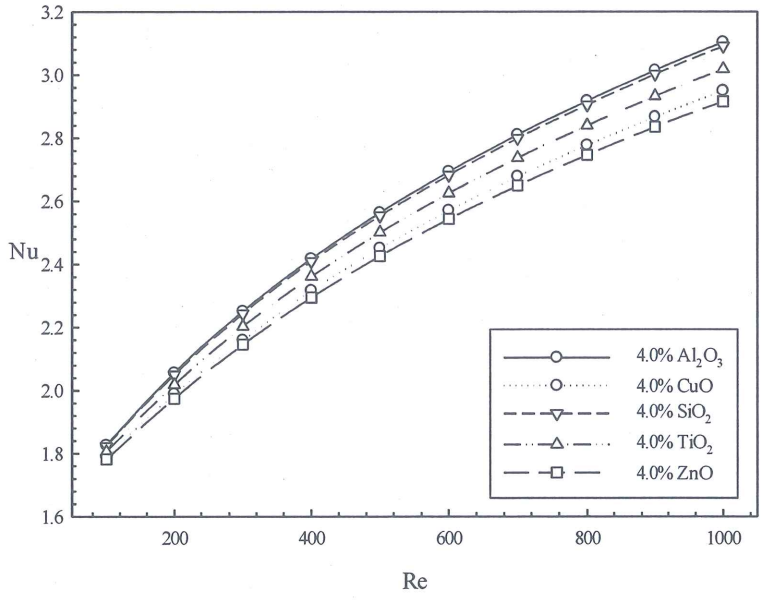

Figure 3.6. The average Nusselt number variation with Reynolds number for 4.0% nanoparticle volume fractions and different types of nanofluids at ER=2.50.

Figure 3.7 shows the effect of expansion ratios on average Nusselt number for Al_2O_3/water nanofluid having 4.0% nanoparticles volume fraction. It can be obtained that the average Nusselt number increases with decreasing expansion ratio of MBFS.

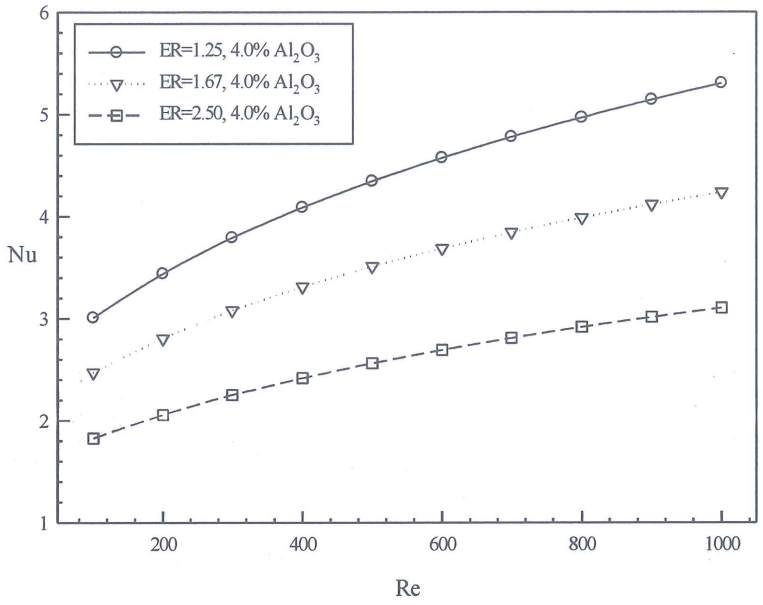

Figure 3.7. The average Nusselt number distributions for different expansion ratios and Al_2O_3/water nanofluid with 4.0% volume fraction.

Figure 3.8 illustrates the change of local Nusselt number along the downstream stepped wall (heated wall). The local Nusselt number is considered to increase uprightly to its maximum value at the separation point and then decreases with moving away from the step of the duct having MBFS until the reattachment point and then it takes a stable form when the nanofluid flow is being fully developed condition. This is due to the fluid flow separation which leads to heat transfer enhancement [47]. It is noticed that the local Nusselt number increases with decreasing the expansion ratio.

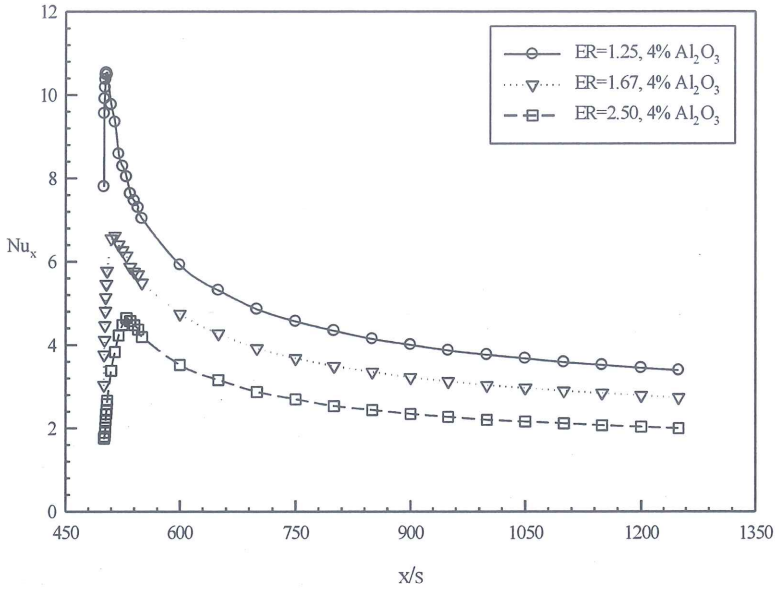

Figure 3.8. The local Nusselt number distributions along the dimensionless length for different expansion ratios and Al_2O_3/water nanofluid with 4.0% volume fraction.

The effects of the Reynolds number on the local Nusselt number for Al_2O_3/water nanofluid with 4.0% volume fraction rate is given in Figure 3.9. It is noticed that the Reynolds number affects the local Nusselt number and the highest Reynolds number has the highest local Nusselt number.

The effect of nanoparticle type dispersed in pure water on the local Nusselt number distribution is shown in Figure 3.10. Five different nanoparticles were used at constant Reynolds number of 500. It is noticed that Al_2O_3 nanoparticle has the highest local Nusselt number while the pure water has the lowest local Nusselt number.

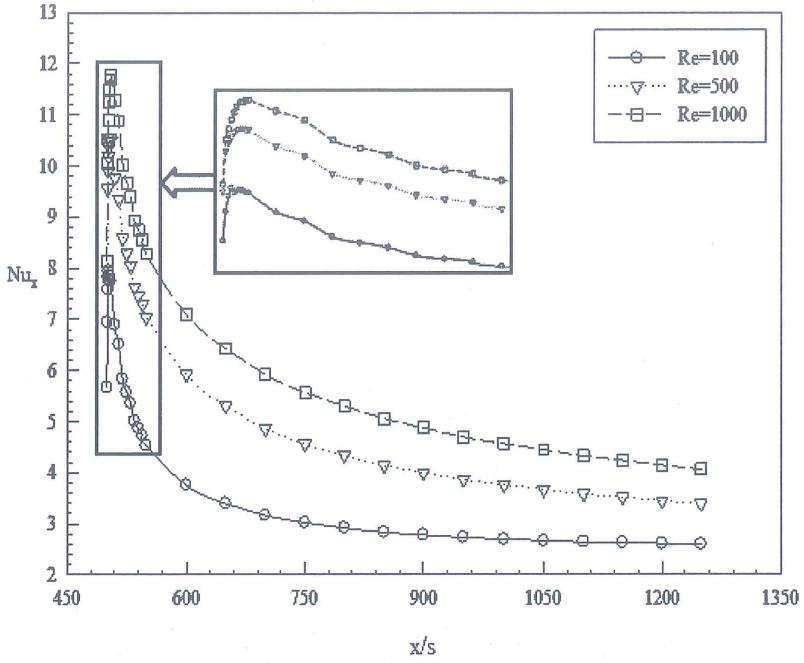

Figure 3.9. The local Nusselt number distributions along the dimensionless length for different Reynolds number and Al_2O_3/water nanofluid with 4.0% volume fraction at ER=1.25.

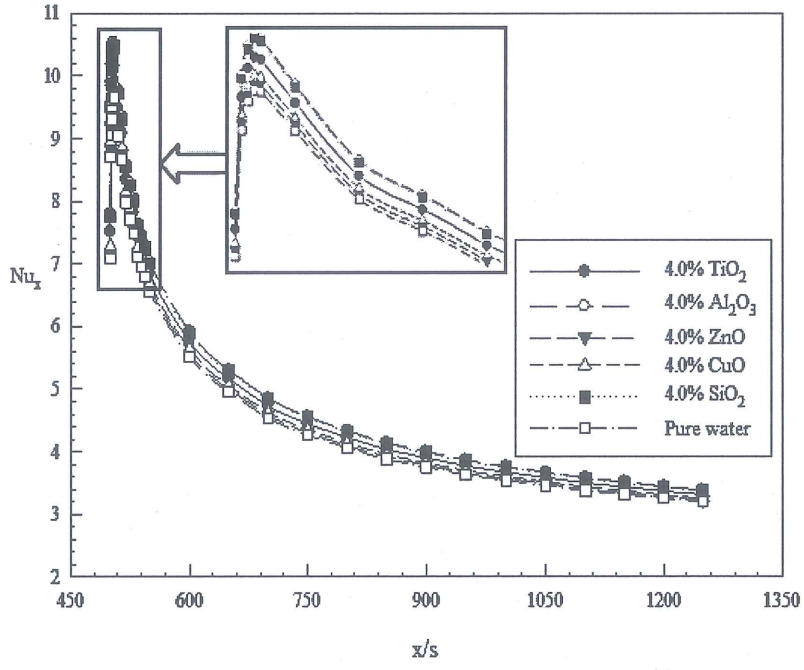

Figure 3.10. The local Nusselt number distributions along the dimensionless length for different nanofluids with 4.0% volume fraction at Re=500 and ER=1.25.

Figure 3.11 is drawn to understand effects of nanoparticle volume fraction on temperature distribution of duct outlet. It was revealed that temperature distributions have same distributions for all nanoparticle volume fractions. It is obtained that nanoparticle volume fraction does not significantly affect duct's the outlet temperature.

Figure 3.12 explains the effects of Reynolds number on temperature distributions at the duct outlet. It can be seen that Reynolds number significantly affects the temperature distribution. As Reynolds number increases, temperature value at the duct outlet decreases.

Figure 3.13 is drawn to understand effects of expansion ratio on temperature distributions at duct outlet. It can be obtained that temperature distribution of duct outlet is not affected by changing of expansion ratio.

Figure 3.14 is drawn to show the changing of local temperature distributions from stepped wall to outlet of the duct. It was revealed that the temperature distribution repeats itself at the exit of the duct outlet. This means that the flow reaches thermally fully developed condition.

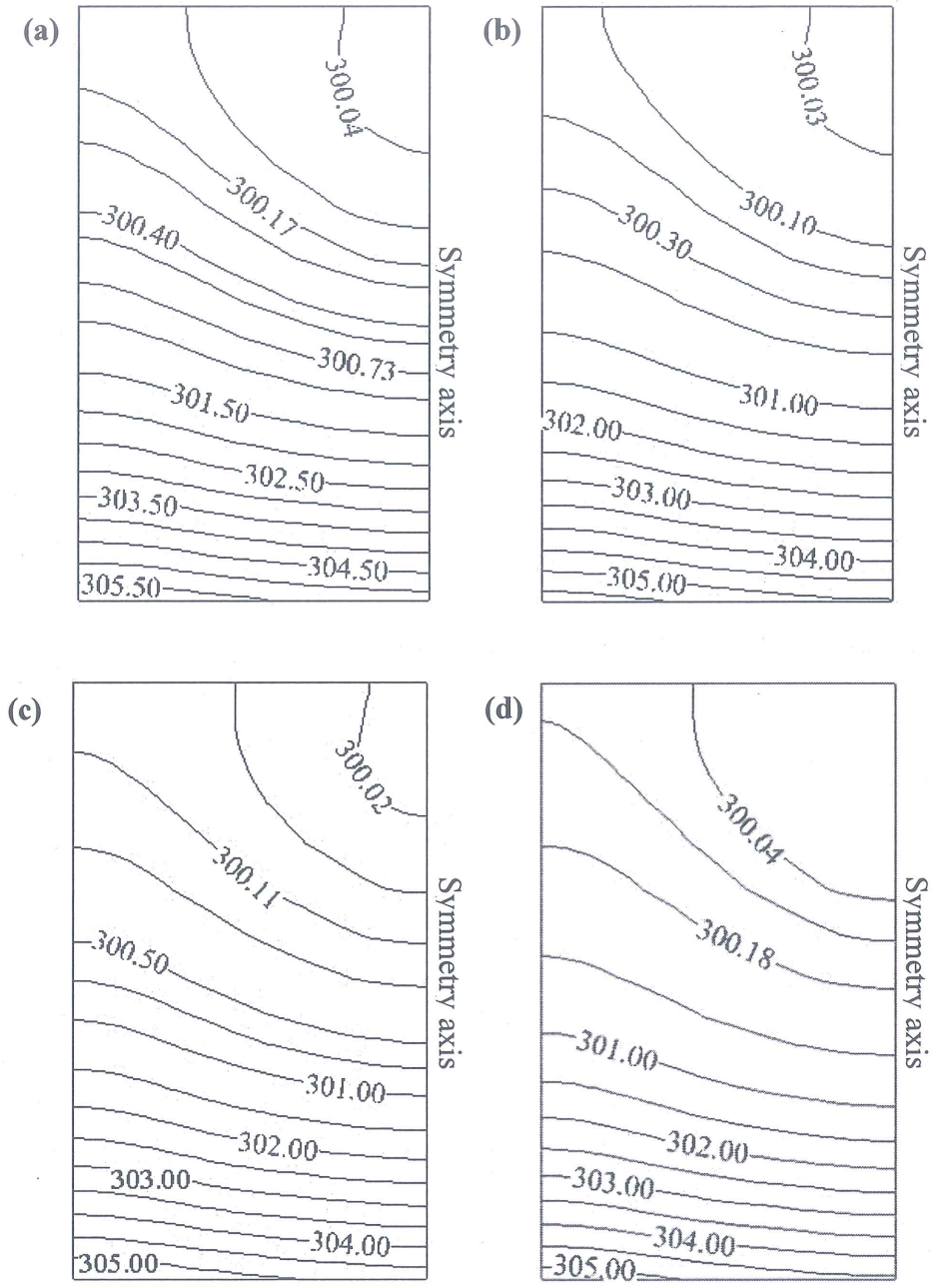

Figure 3.11. Isothermal contours of temperature at the duct outlet for different nanoparticle volume fraction using Al_2O_3/water nanofluid at ER=1.25 and Re=500 a) 1.0%, b) 2.0%, c) 3.0%, d) 4.0%.

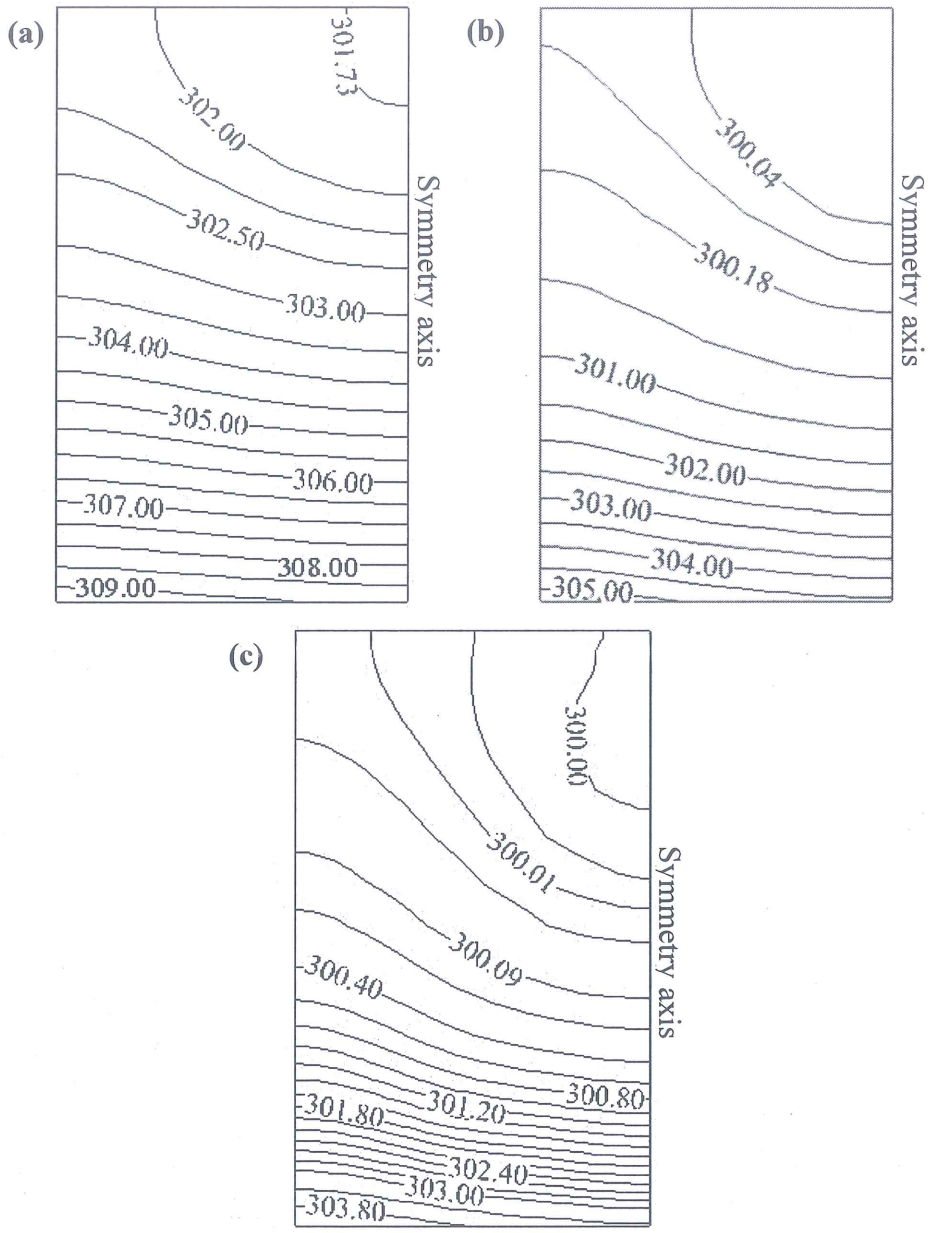

Figure 3.12. Isothermal contours of temperature at the duct outlet for different Reynolds number using Al_2O_3/water nanofluid with 4.0% volume fraction at ER=1.25 a) 100, b) 500, c) 1000.

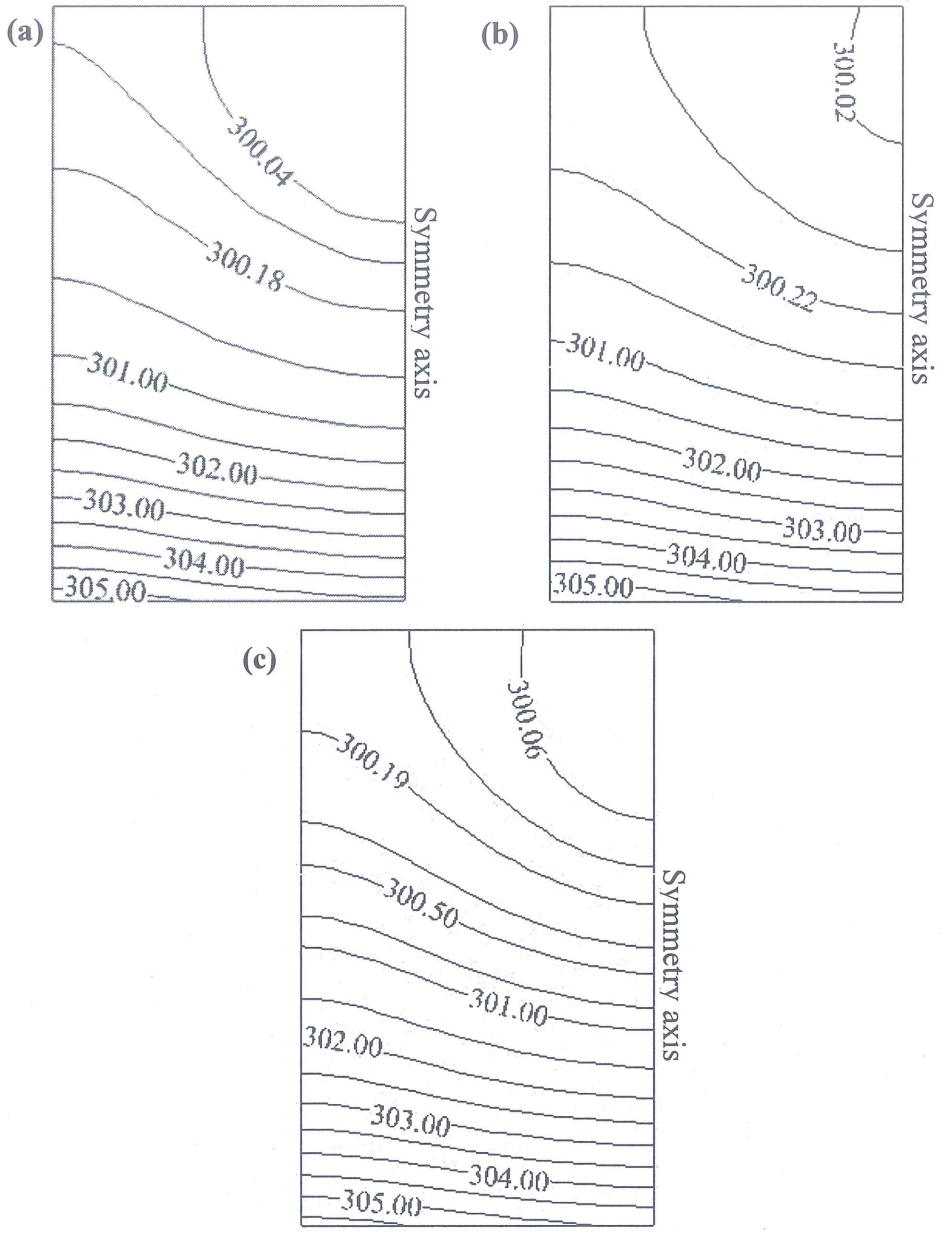

Figure 3.13. Isothermal contours of temperature at the duct outlet for different expansion ratios using Al_2O_3/water nanofluid with 4.0% volume fraction at ER=1.25 a) 1.25, b) 1.67, c) 2.50.

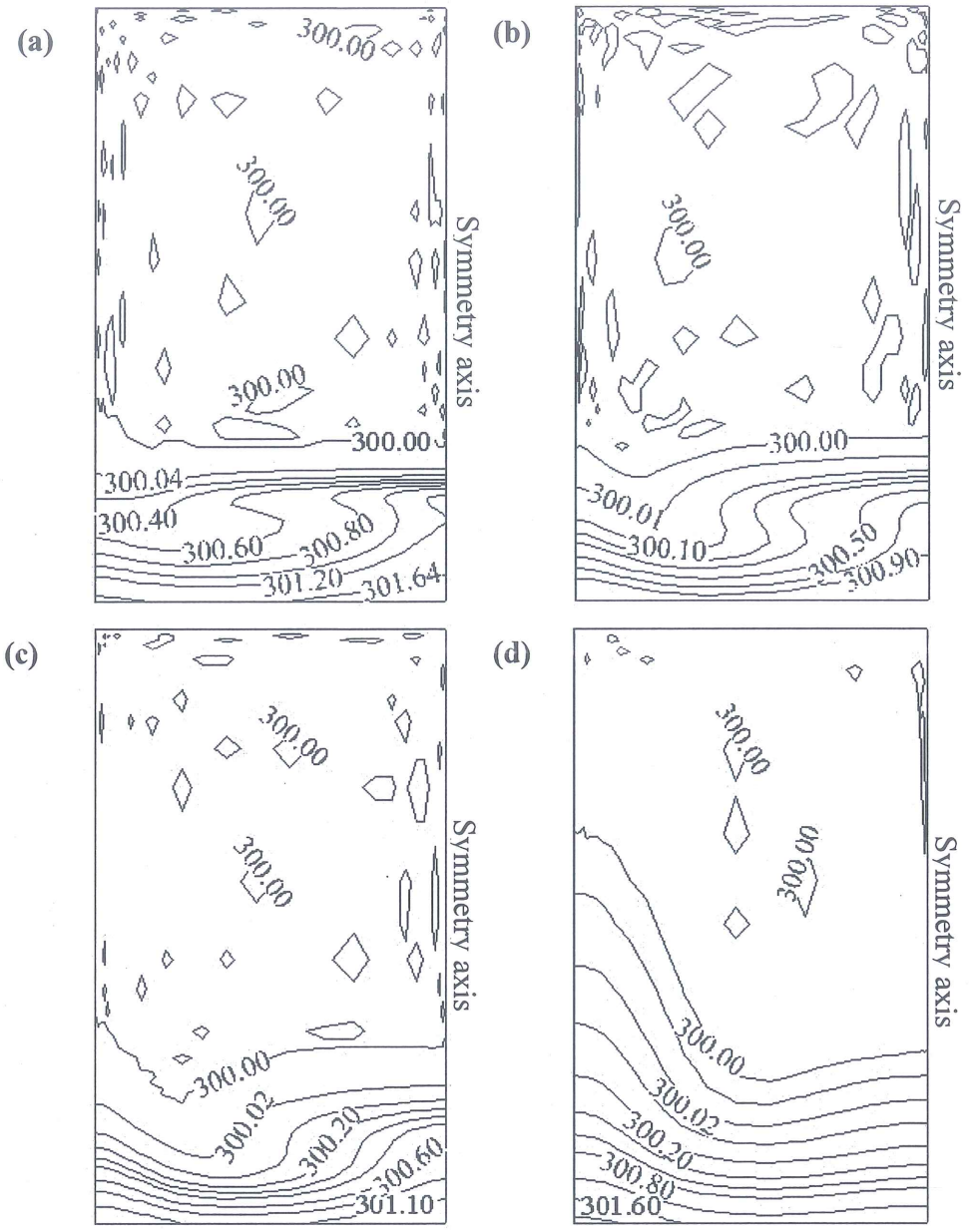

Figure 3.14. Isothermal contours of temperature at the duct outlet for different distances from the step wall using Al_2O_3/water nanofluid with 4.0% volume fraction at ER=1.25 a) x/s=500.5, b) x/s=502.5, c) x/s=504.5, d) x/s=525, e) x/s=550, f) x/s=750, g) x/s=1000, h) x/s=1250.

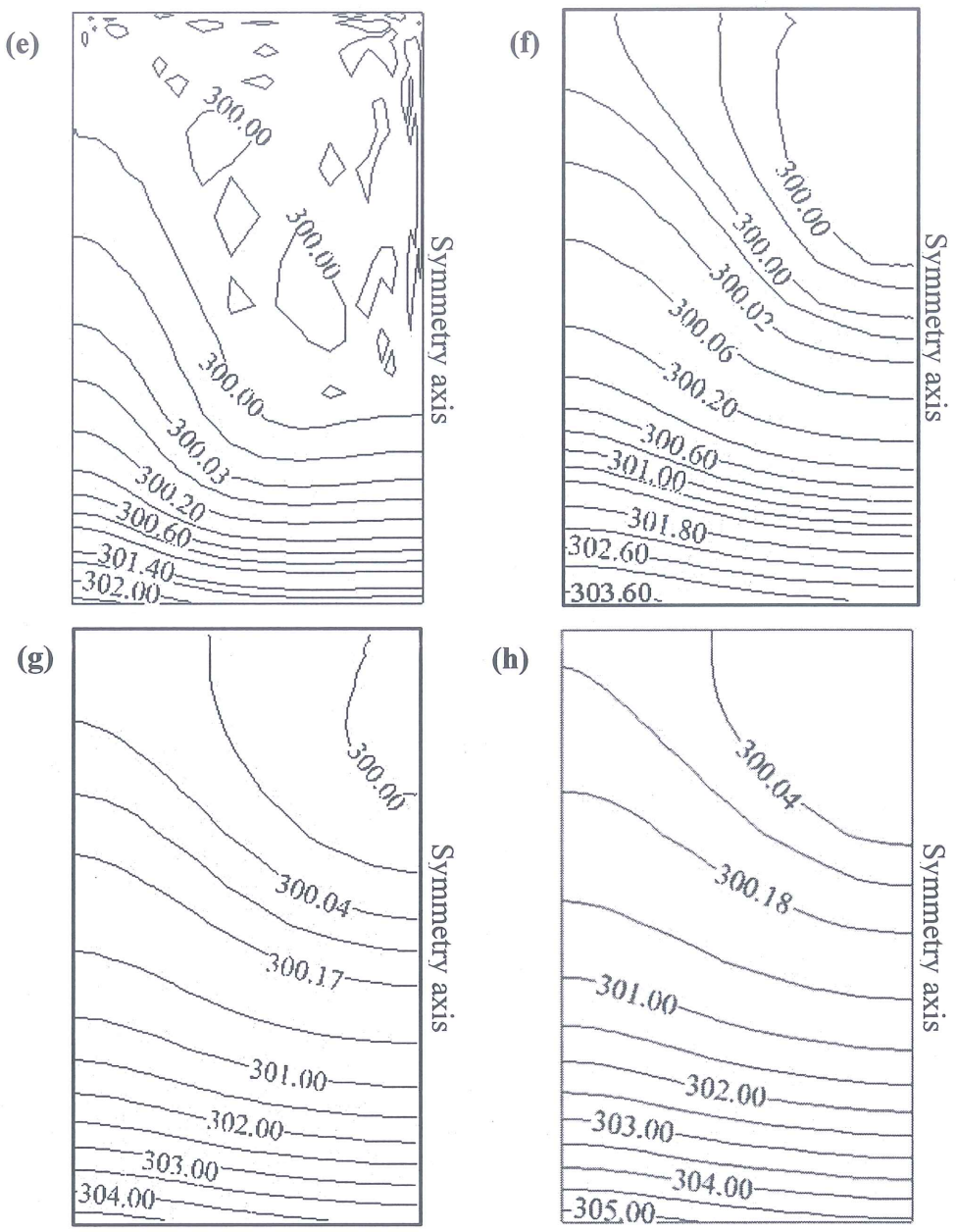

Figure 3.14. (continuing).

Figure 3.15 - Figure 3.18 are presented to show temperature distribution in recirculation zone due to changing of expansion ratio, nanoparticles volume fraction, Reynolds number and types of nanofluids, respectively. It is revealed that temperature distribution in recirculation zone is proportional to expansion ratio but it is inversely proportional to nanoparticle volume fraction and Reynolds number. In addition, Al_2O_3/water nanofluid has lower temperature in recirculation zone.

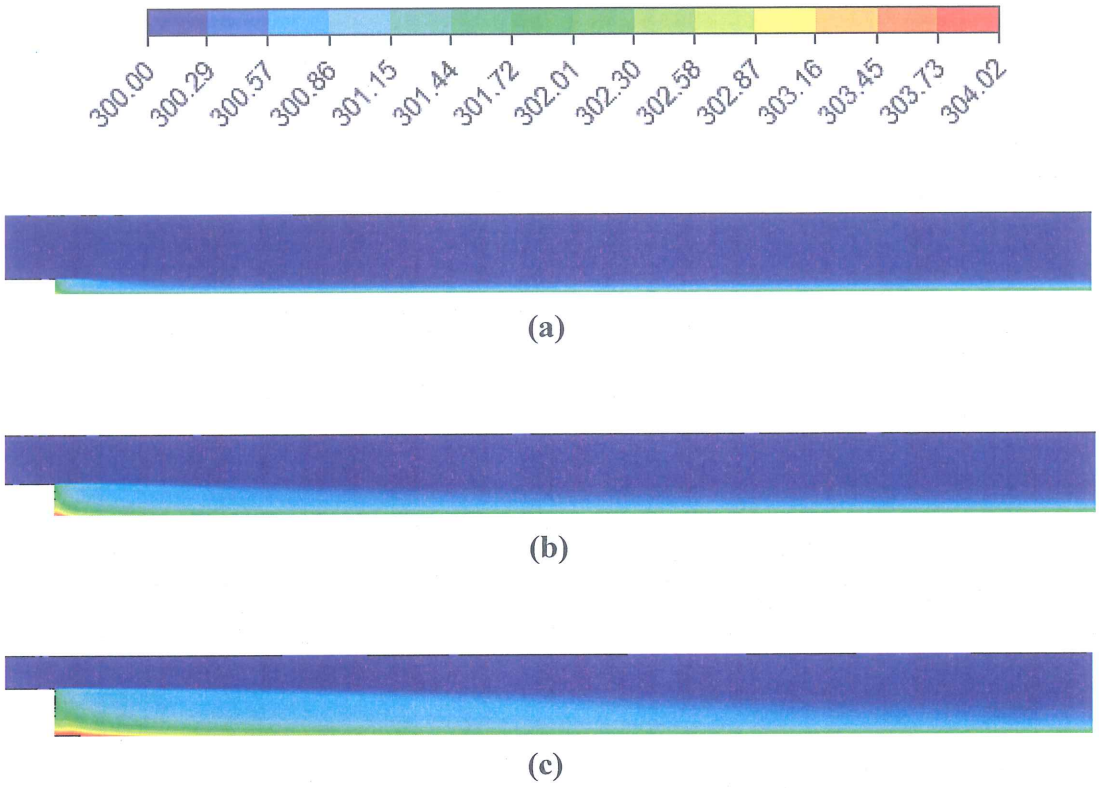

Figure 3.15. Contours of temperature for different expansion ratios using Al_2O_3/water nanofluid with 4.0% volume fraction at Re=500 a) ER=1.25, b) ER=1.67, c) ER=2.50.

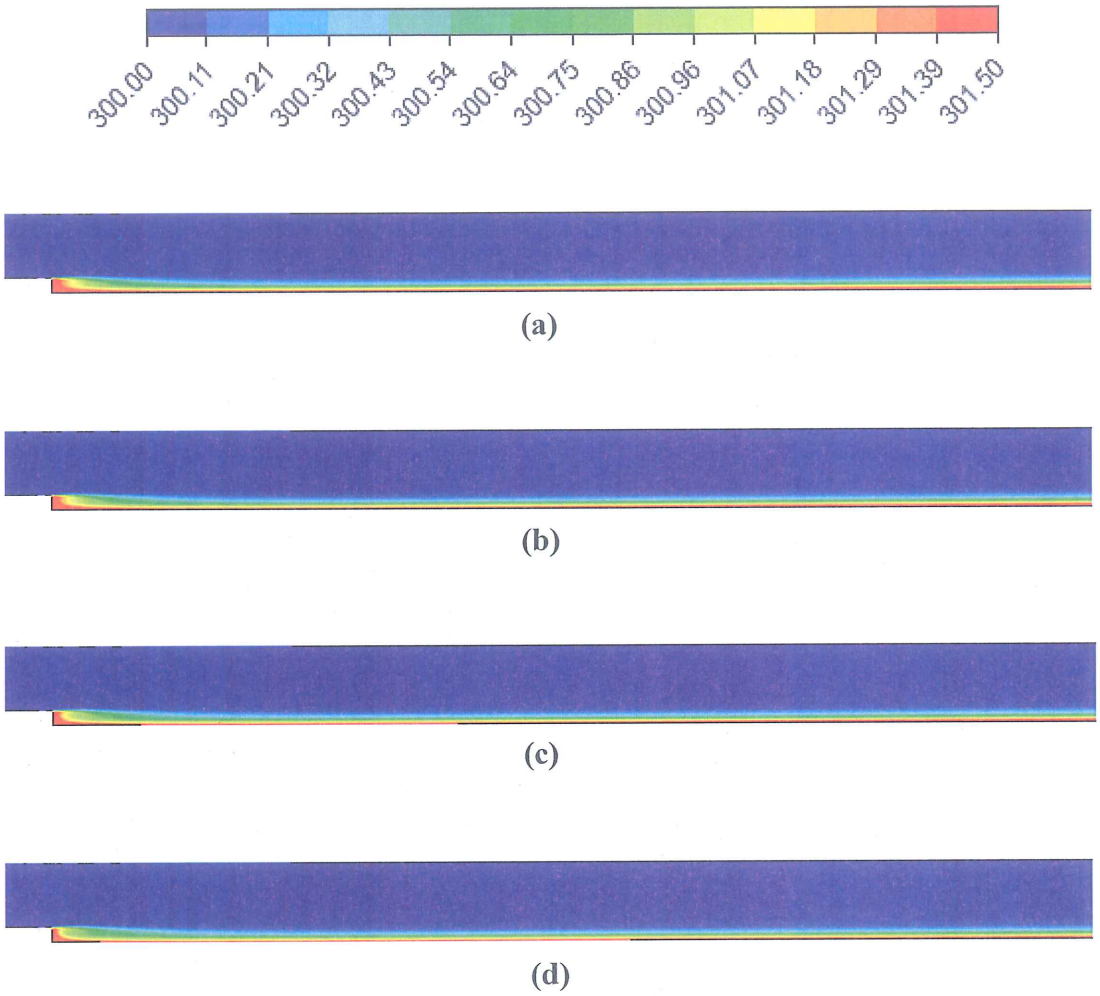

Figure 3.16. Contours of temperature for different nanoparticle volume fractions using Al_2O_3/water nanofluid at ER=1.25 and Re=500 a) 1.0%, b) 2.0%, c) 3.0%, d) 4.0%.

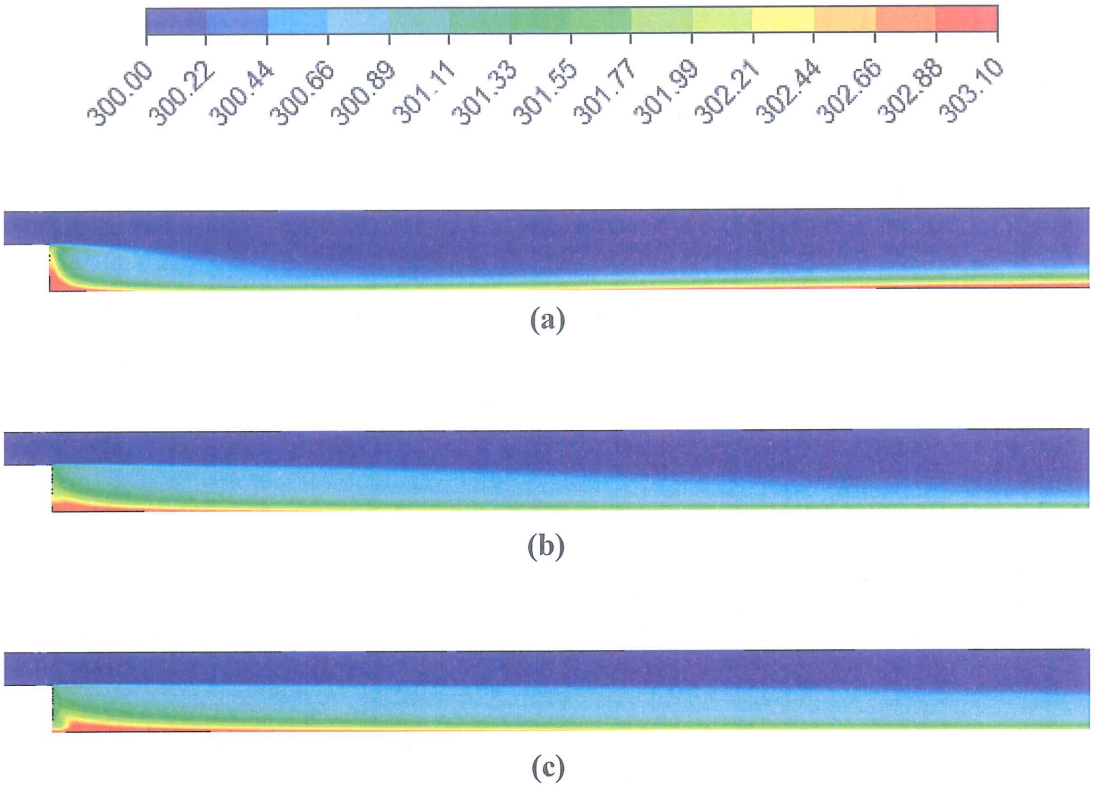

Figure 3.17. Contours of temperature for different Reynolds numbers using Al_2O_3/water nanofluid with 4.0% volume fraction at ER=2.50 a) Re=100, b) Re=500, c) Re=1000.

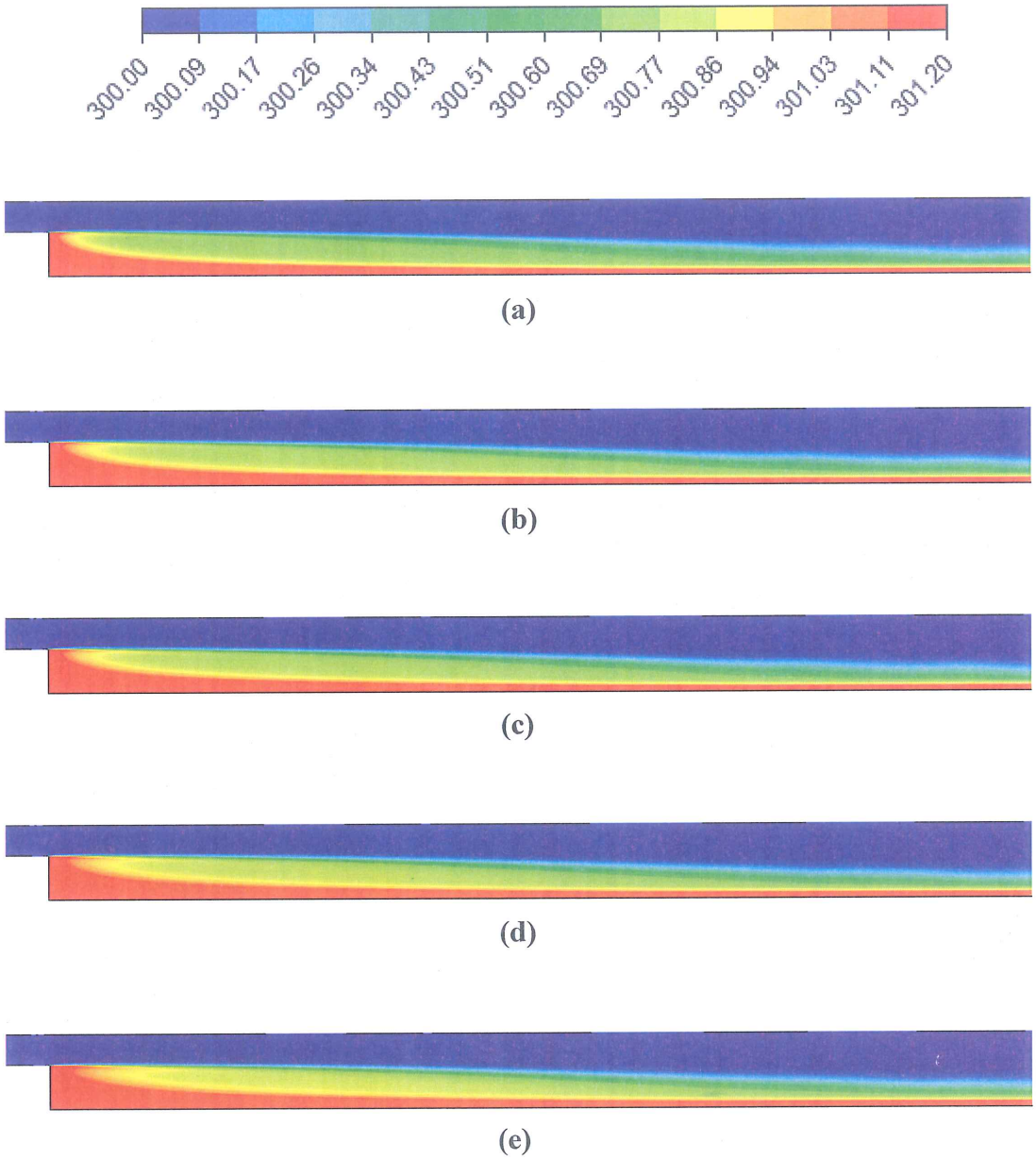

Figure 3.18. Contours of temperature for different nanofluids with 4.0% volume fraction at ER=2.50 and Re=500 a) Al_2O_3/water, b) SiO_2/water, c) TiO_2/water, d) CuO/water, e) ZnO/water.

3.2. FLOW CHARACTERISTICS

In this section, predictions of numerical simulation predictions of the Darcy friction factor are presented for different Reynolds numbers, nanoparticles volume fractions and nanofluids.

Figure 3.19 is presented to obtain effects of different nanoparticles volume fractions and Reynolds numbers on average Darcy friction factor for expansion ratio of 1.25. It is revealed that while the Reynolds number increases the average Darcy friction factor decreases. The graph of average Darcy friction factor of pure water and tdifferent nanofluid types coincides. Namely, the average Darcy friction factor is independent from nanoparticles volume fractions and types of nanofluids.

Figure 3.20 and Figure 3.21 are presented to obtain effects of Reynolds numbers, nanofluid types and volume fractions on average Darcy friction factor for expansion ratio of 1.67 and 2.50. It is noticed that the average Darcy friction factor influences from the changing of expansion ratio. It is observed that the average Darcy friction factor decreases with increasing expansion ratio.

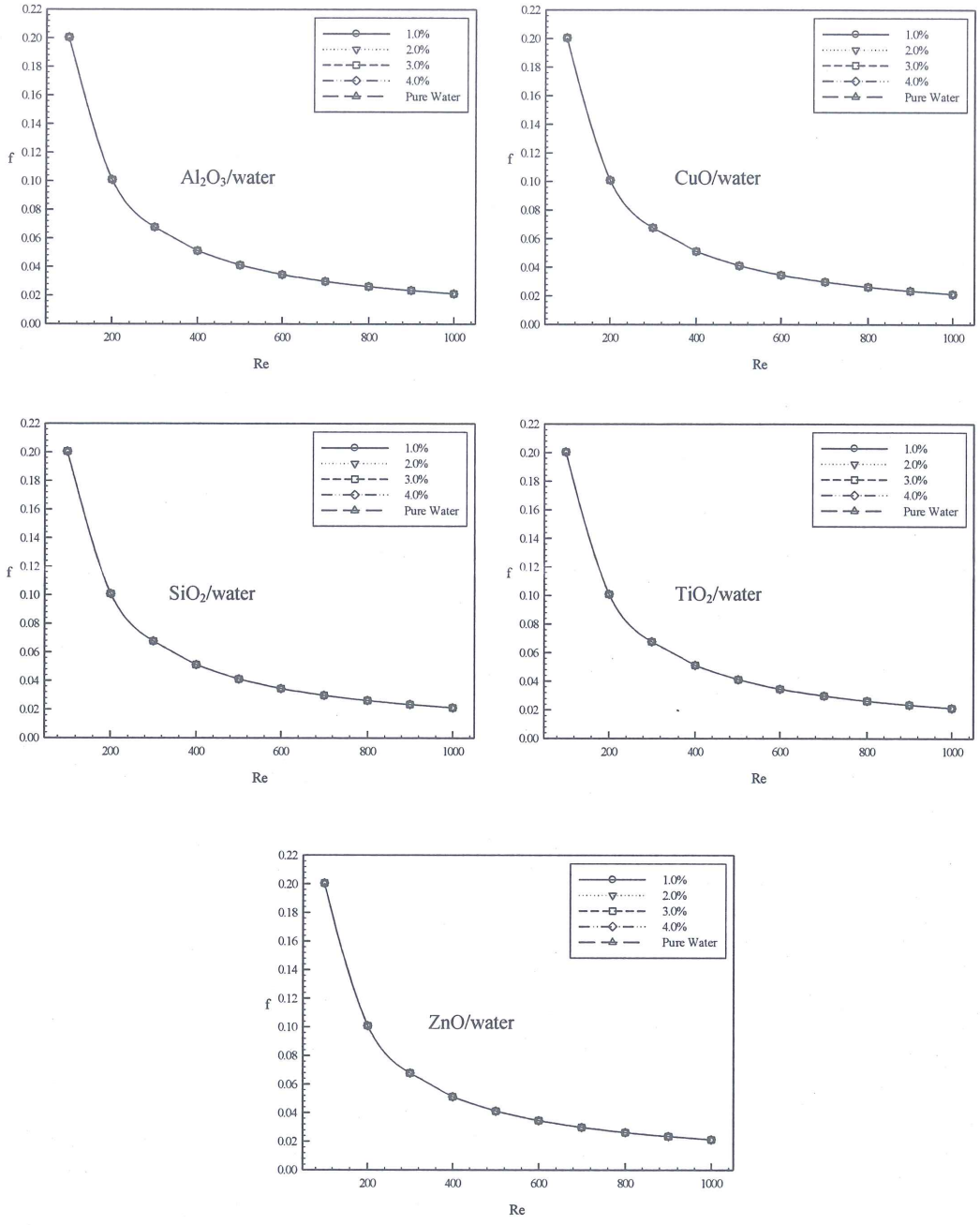

Figure 3.19. Average Darcy friction factor variation with Reynolds number for different nanoparticle volume fractions of different nanofluids at ER=1.25.

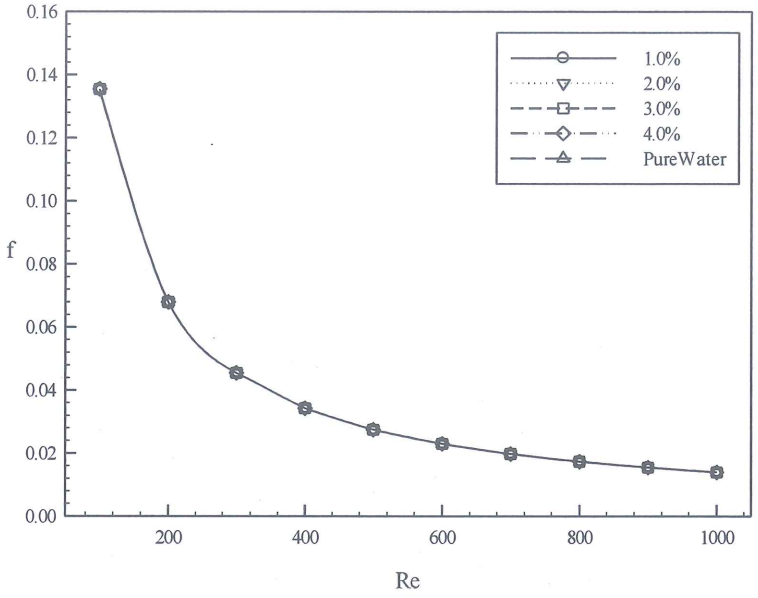

Figure 3.20. Average Darcy friction factor variation with Reynolds number for different types of nanofluids and nanoparticles volume fractions at ER=1.67

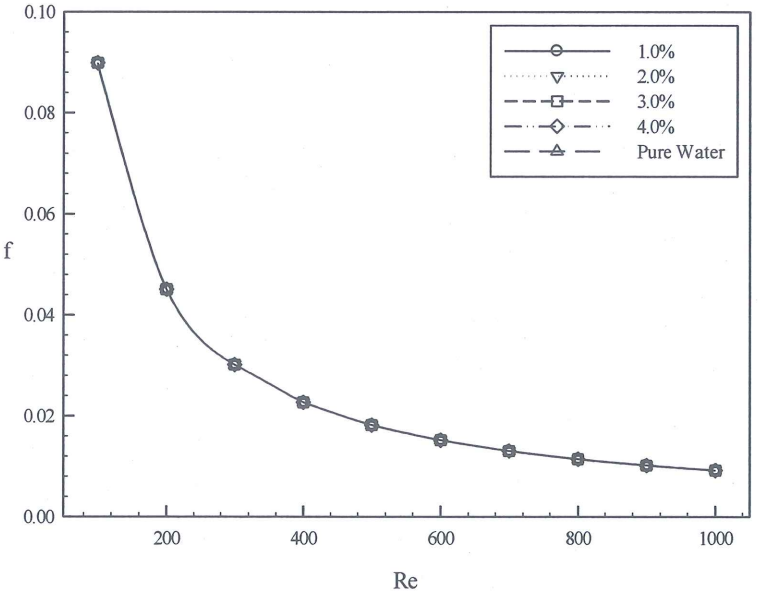

Figure 3.21. Average Darcy friction factor variation with Reynolds number for different types of nanofluids and nanoparticles volume fractions at ER=2.50.

Figure 3.22, Figure 3.23 and Figure 3.24 are presented to verify whether the average Darcy friction factor changes with types of nanofluids or not. Five different nanoparticles with volume fraction of 4.0% are dispersed in pure water at ER=1.25,

1.67 and 2.50. It can be revealed that the effects of types of nanofluids on the average Darcy friction factor are not important.

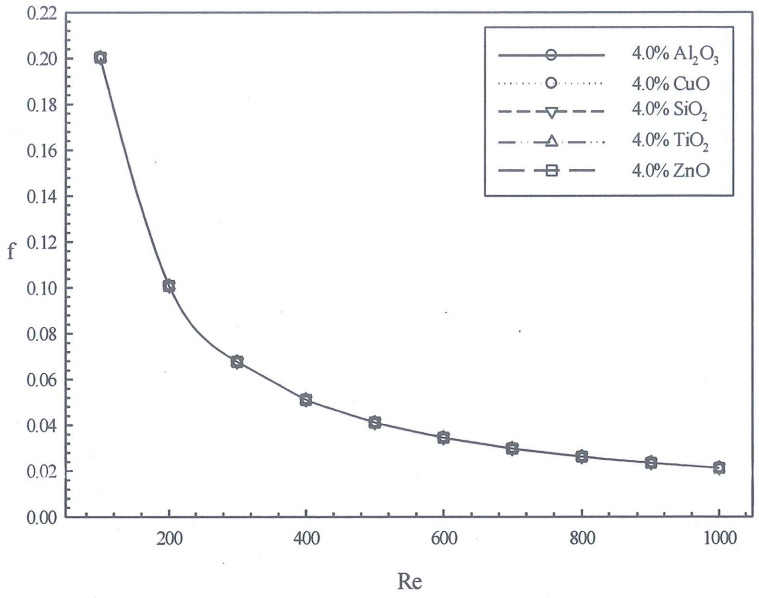

Figure 3.22. Average Darcy friction factor variation with Reynolds number for Al_2O_3/water, SiO_2/water, CuO/water, ZnO/water and TiO_2/water nanofluids having 4.0% nanoparticle volume fractions at ER=1.25.

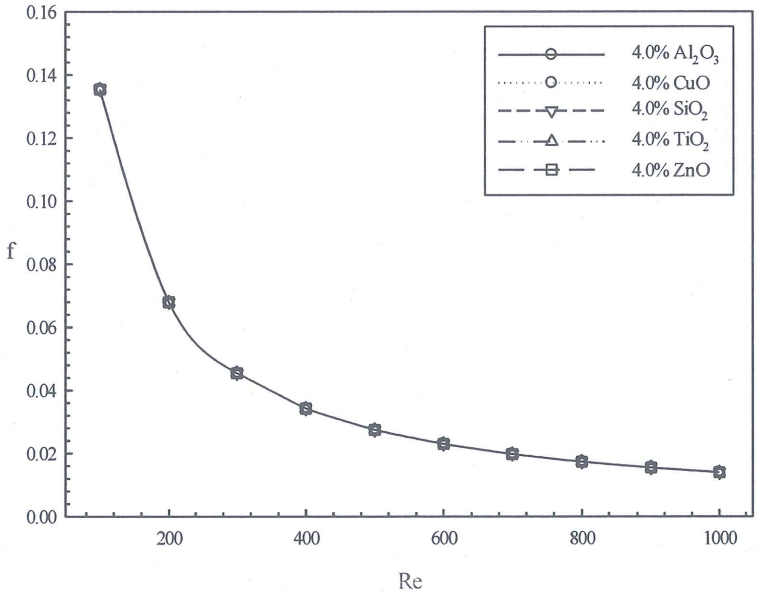

Figure 3.23. Average Darcy friction factor variation with Reynolds number for Al_2O_3/water, SiO_2/water, CuO/water, ZnO/water and TiO_2/water nanofluids having 4.0% nanoparticle volume fractions at ER=1.67.

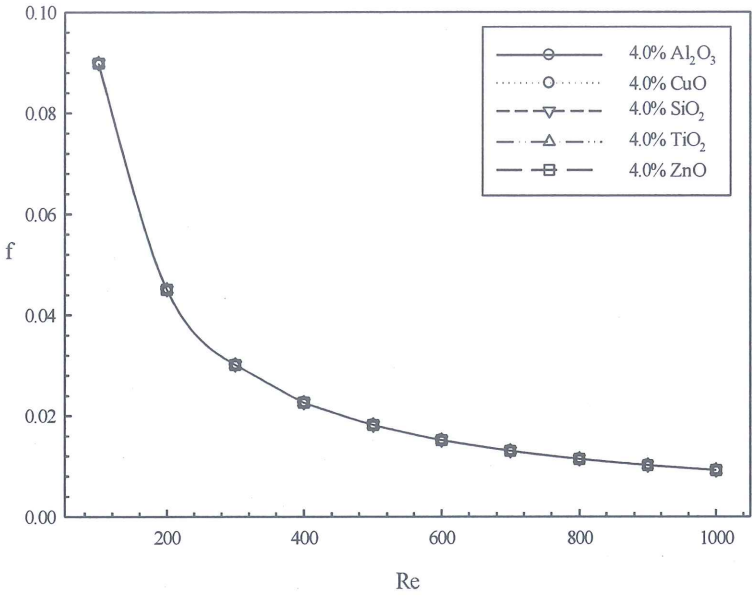

Figure 3.24. Average Darcy friction factor variation with Reynolds number for Al_2O_3/water, SiO_2/water, CuO/water, ZnO/water and TiO_2/water nanofluids having 4.0% nanoparticle volume fractions at ER=2.50.

Figure 3.25 is presented to investigate the effects of expansion ratio on the average Darcy friction factor. It can be noticed that the average Darcy friction factor decreases with increasing expansion ratio and Reynolds number. This is due to increasing velocity of flow.

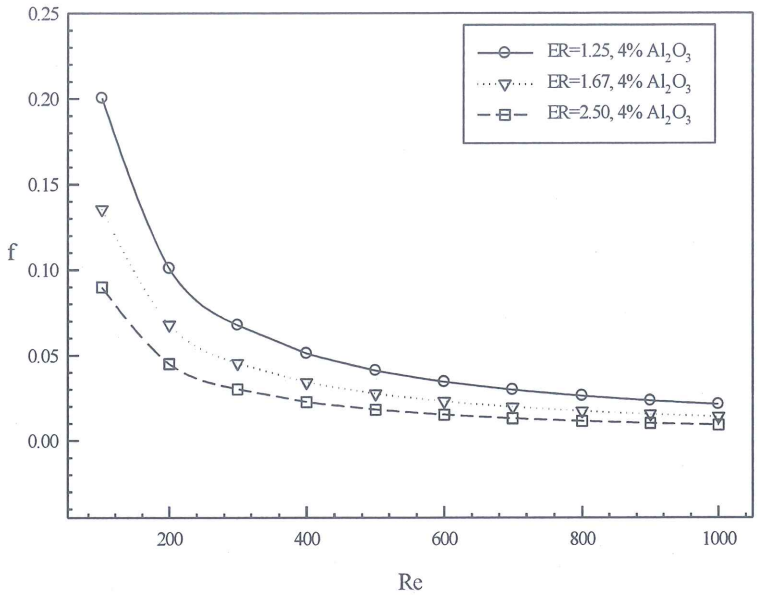

Figure 3.25. Average Darcy friction factor variation with Reynolds number for different expansion ratios using Al_2O_3/water nanofluid having 4.0% nanoparticles volume fractions.

The effects of nanofluids types on the local Darcy friction factor along the downstream stepped wall (heated wall) at constant Re=500 are presented in Figure 3.26. It is revealed that the local Darcy friction factor increases slightly and reaches its maximum summit as the distance downstream from the step increases. Then, it decreases slightly until it goes down the minimum value. This value occurs due to the recirculation flow where there is a change in the velocity distributions and the minimum value occurs due to the reattachment point where the velocity is practically equal to zero. After that, it increases until it reaches a point where the local Darcy friction factor remains constant along the rest of heated wall. This shows that the local Darcy friction factor asymtotically approaches to hydrodynamically fully developed duct flow. Also, it is interpreted that the local Darcy friction factor is independent from nanofluid types.

Figure 3.27 is presented to investigate the effects of expansion ratio on the local Darcy friction factor using Al_2O_3/water nanofluid having 4.0% nanoparticle volume fraction along the downstream stepped wall (heated wall) at constant Re=500. It is noticed that the local Darcy friction factor influences the changing of expansion

ratio. It is obtained that the local Darcy friction factor is inversely proportional to the expansion ratio.

Figure 3.28 is presented to investigate the effects of Reynolds number on the local Darcy friction factor using Al_2O_3/water nanofluid having 4.0% nanoparticle volume fraction along the downstream stepped wall (heated wall) at constant ER=1.25. It can be noticed that the local Darcy friction factor influences the changing of Reynolds number. It is found that the local Darcy friction factor decreases with increasing Reynolds number. This is because the local and average Darcy friction factor are inversely proportional to the flow velocity.

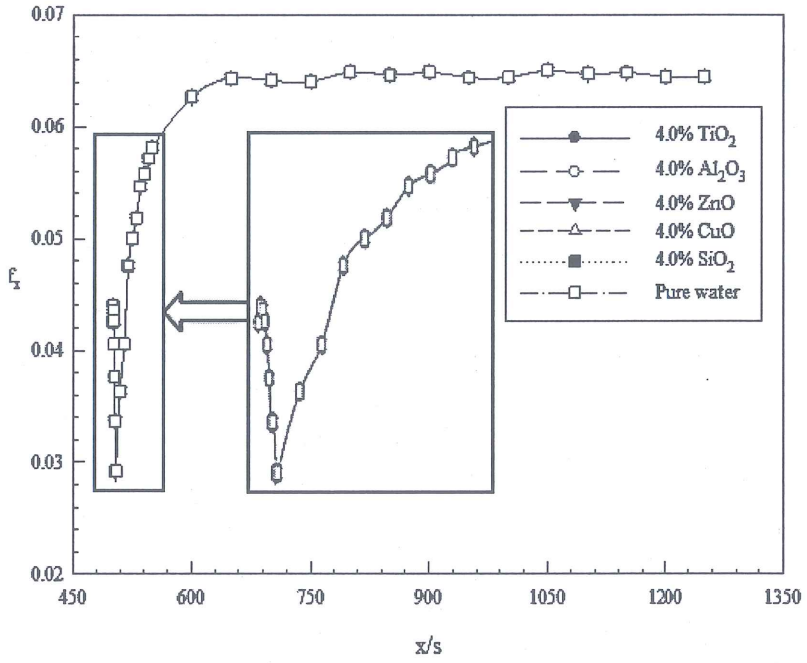

Figure 3.26. Variation of local Darcy friction factor for different Reynolds numbers using Al_2O_3/water, SiO_2/water, CuO/water, ZnO/water and TiO_2/water nanofluids having 4.0% nanoparticle volume fractions and pure water at Re=500.

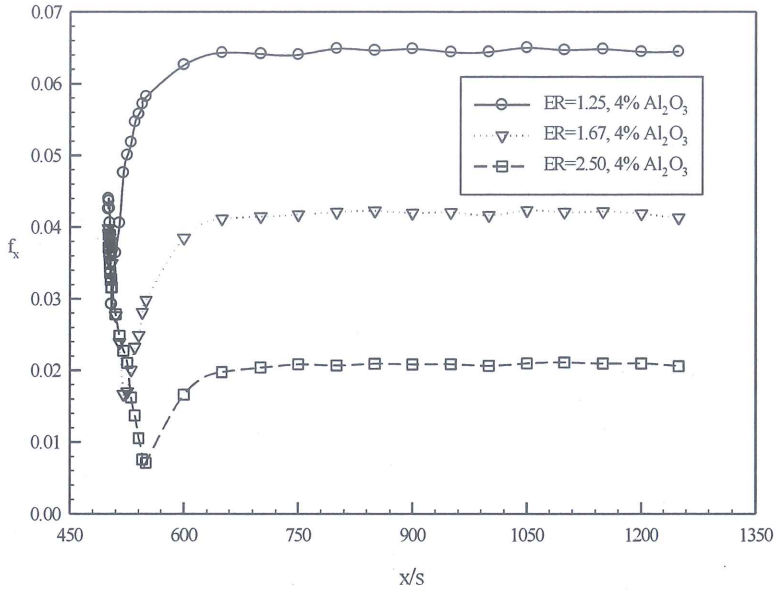

Figure 3.27. Variation of local Darcy friction factor for different expansion ratios using Al_2O_3/water nanofluid having 4.0% nanoparticle volume fractions at Re=500.

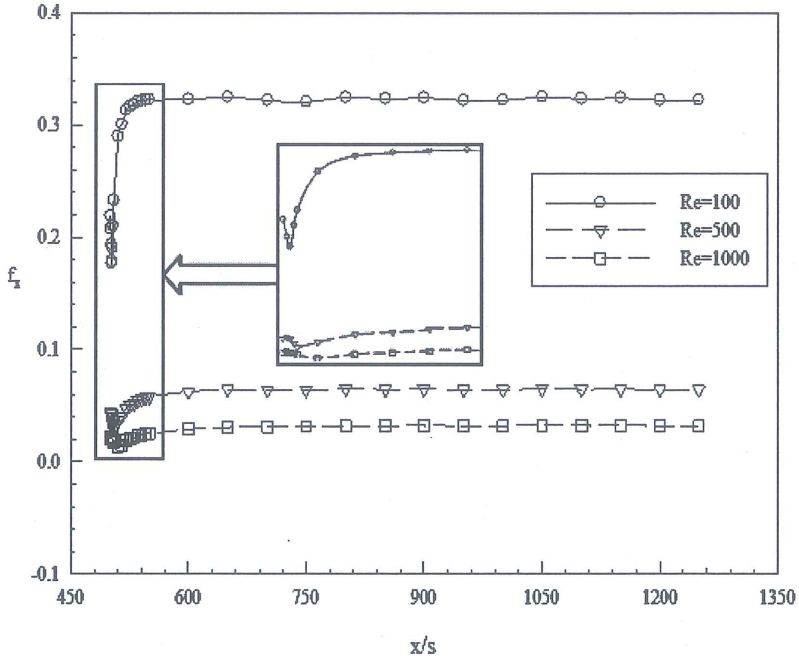

Figure 3.28. Variation of local Darcy friction factor for different Reynolds numbers using Al_2O_3/water nanofluid having 4.0% nanoparticle volume fractions at ER=1.25.

Figure 3.29 is drawn to explain the effects of nanoparticles volume fraction on velocity distribution of duct outlet. With increasing of nanoparticles volume fraction, velocity distribution of duct outlet increases due to increasing viscosity of nanofluid.

Figure 3.30 is shown to explain the effects of Reynolds number on velocity distribution of duct outlet. It can be seen that Reynolds number significantly effects the velocity distributions. As Reynolds number increases, velocity values of duct outlet increases.

Figure 3.31 is shown to understand the effects of expansion ratios on velocity distribution of duct outlet. It can be obtained that with increasing of expansion ratio, velocity distribution of duct outlet decreases.

Figure 3.32 is drawn to show the changing of local velocity distributions from stepped wall to outlet of duct. It was revealed that velocity distributions begin to not change to the duct outlet. This means that the flow reaches hydrodynamically fully developed condition.

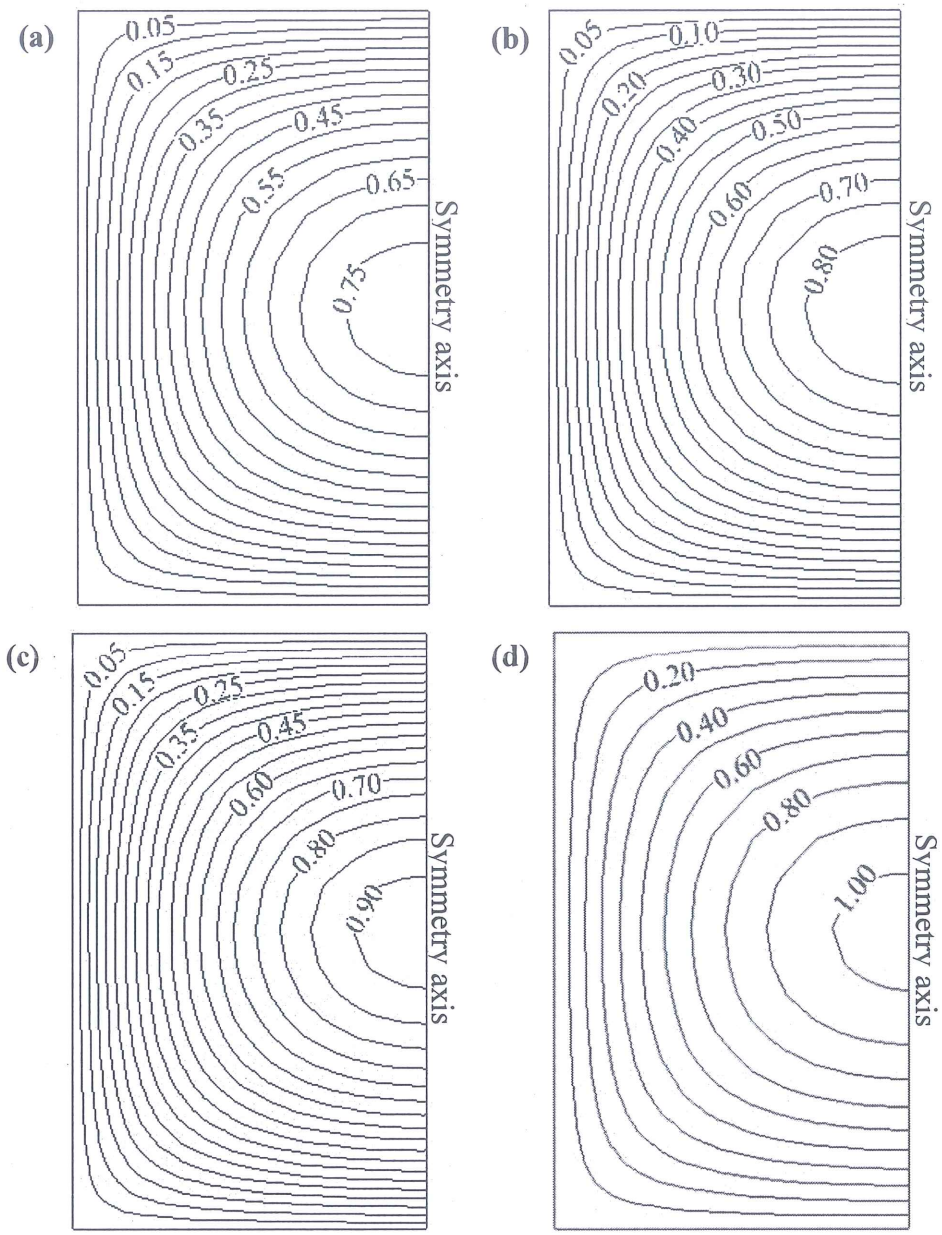

Figure 3.29. Velocity contours at the duct outlet for different nanoparticle volume fraction using Al_2O_3/water nanofluid at ER=1.25 and Re=500 a) 1.0%, b) 2.0%, c) 3.0%, d) 4.0%.

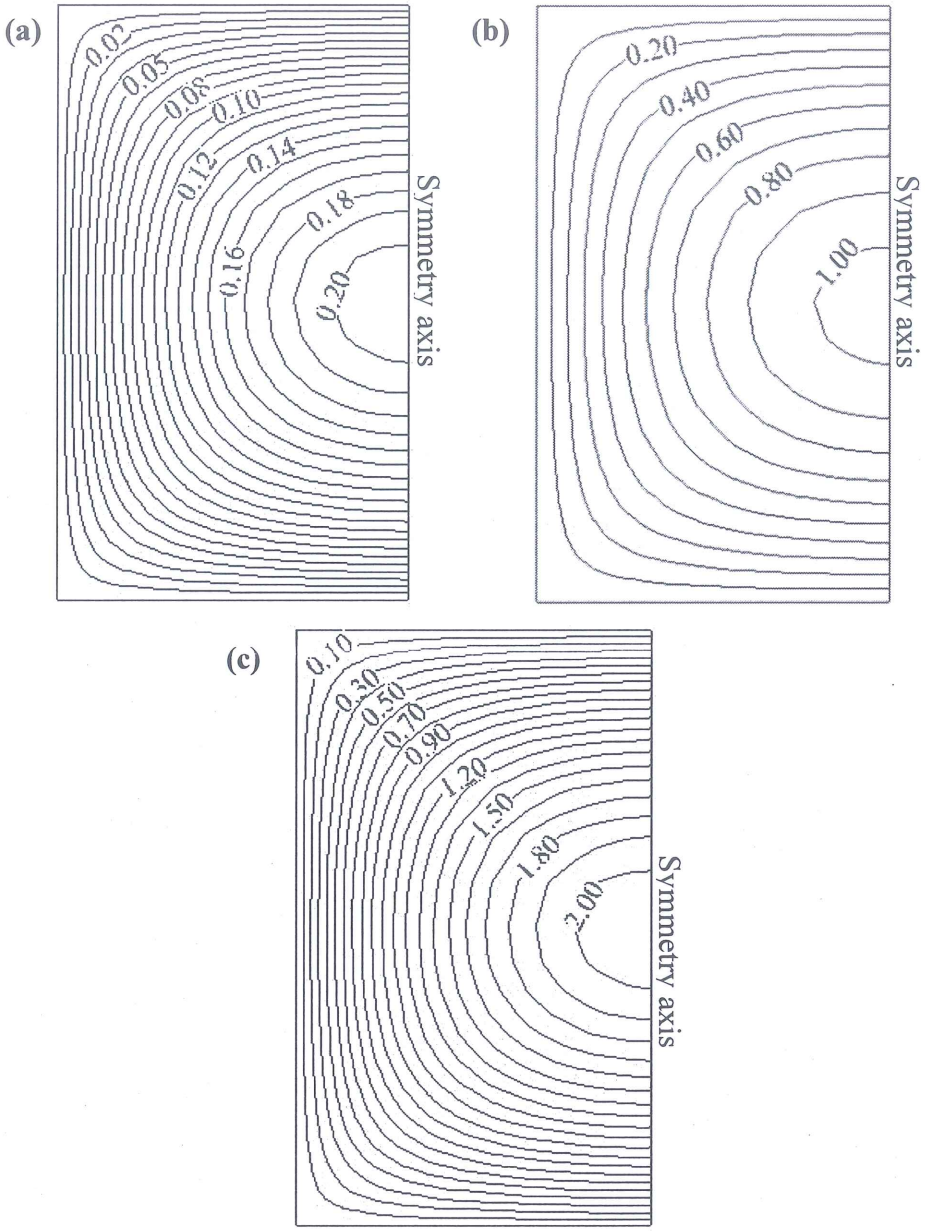

Figure 3.30. Velocity contours at the duct outlet for different Reynols number using Al_2O_3/water nanofluid with 4.0% volume fraction at ER=1.25 a) Re=100, b) Re= 500, c) Re=1000.

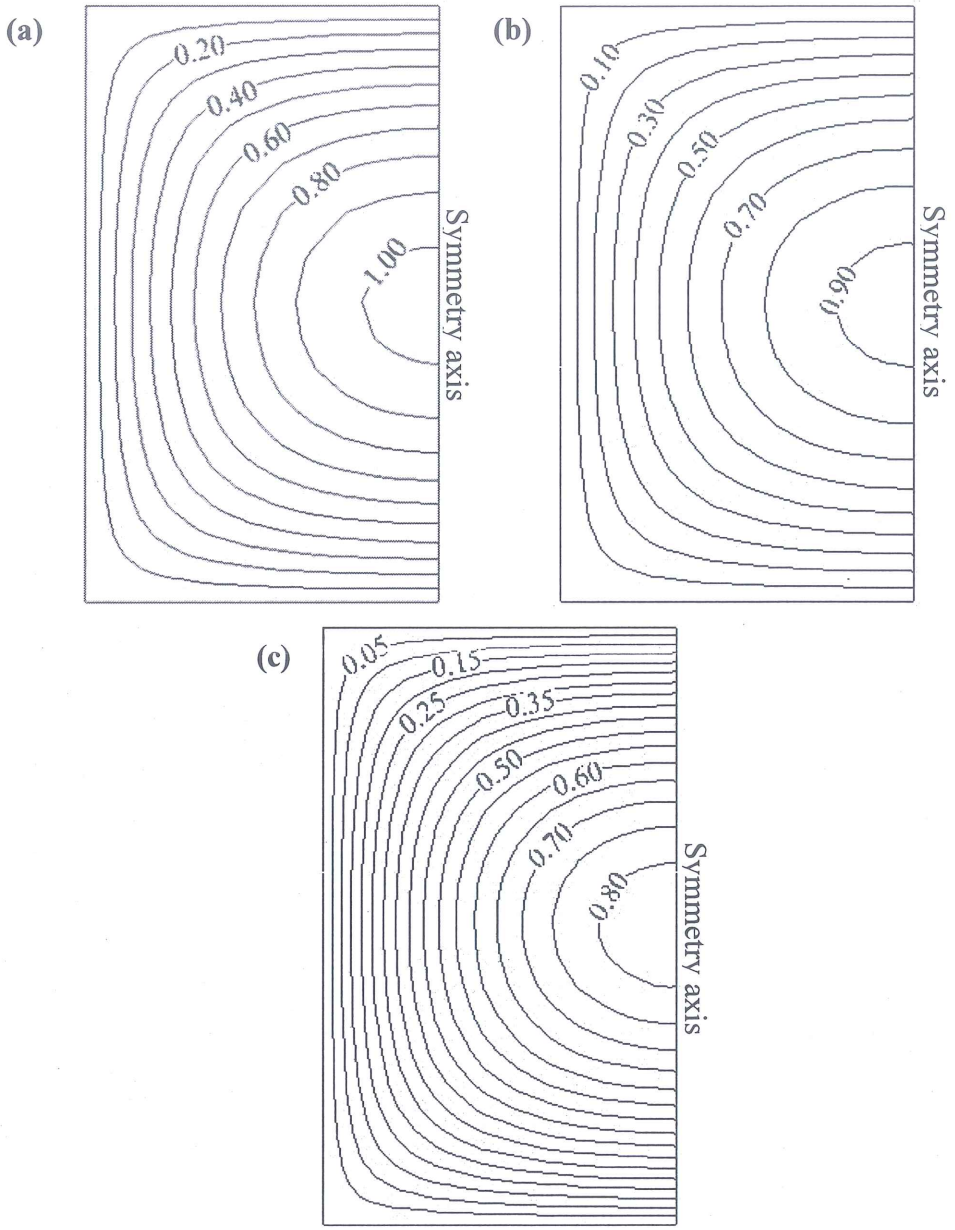

Figure 3.31. Velocity contours at the duct outlet for different expansion ratios using Al_2O_3/water nanofluid with 4.0% volume fraction at Re=500 a) 1.25, b) 1.67, c) 2.50.

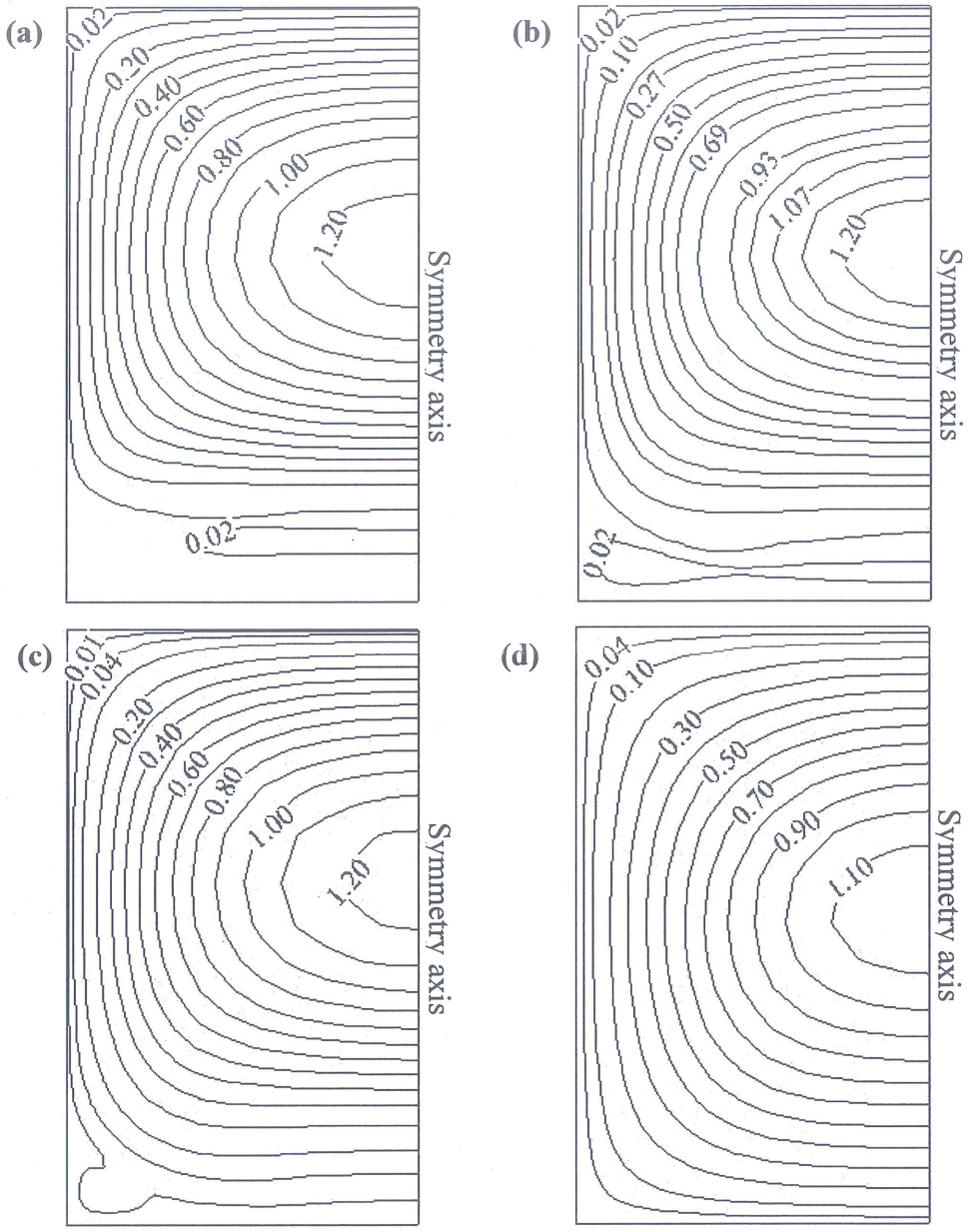

Figure 3.32. Velocity contours at the duct outlet for different distances from the step wall using Al_2O_3/water nanofluid with 4.0% volume fraction at ER=1.25 a) x/s=500.5, b) x/s=502.5, c) x/s=504.5, d) x/s=525, e) x/s=550, f) x/s=750, g) x/s=1000, h) x/s=1250.

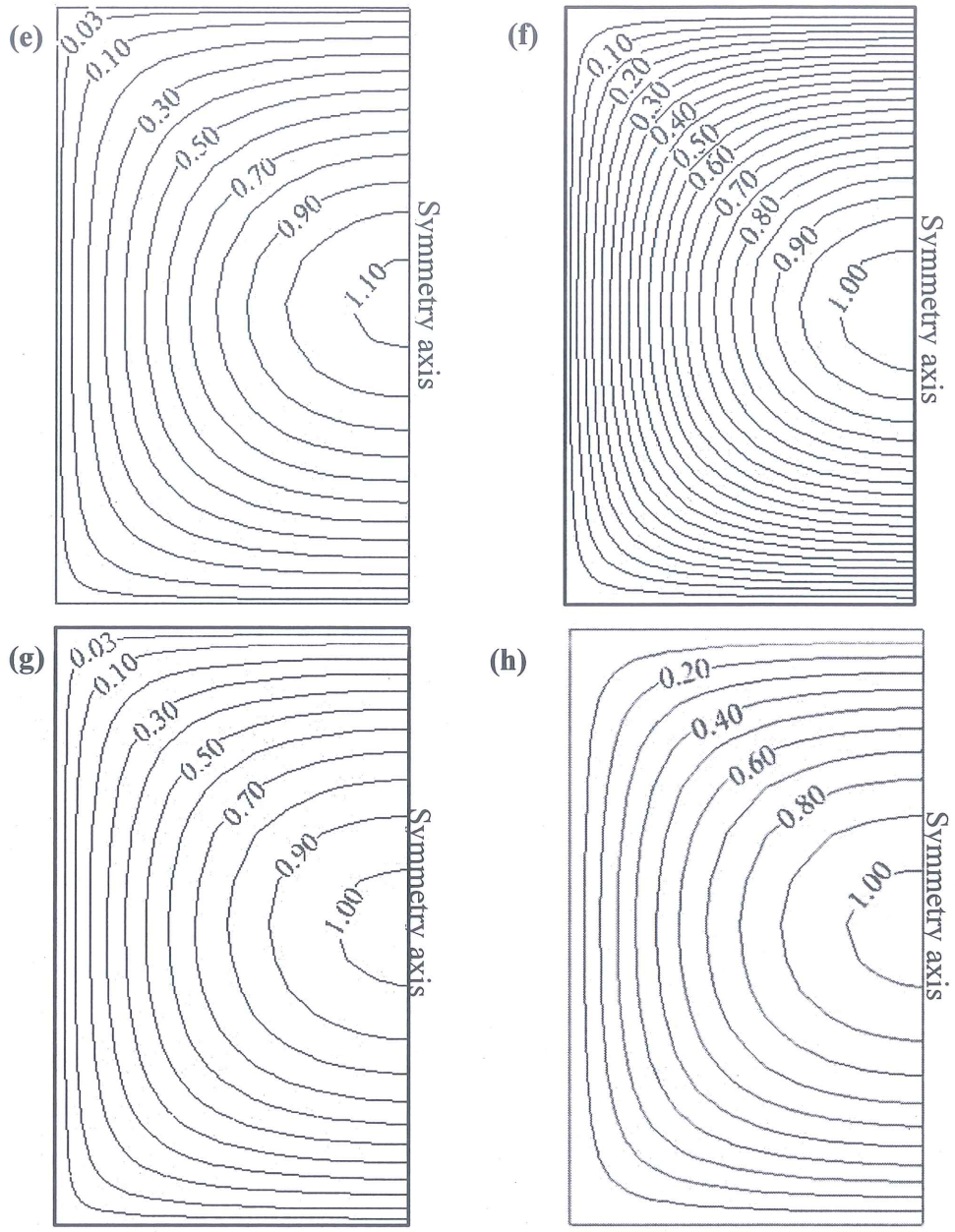

Figure 3.32. (continuing).

Figure 3.33 shows to explain the effects of expansion ratio on the size of the recirculation zones. The size of the recirculation zones increases as expansion ratio increases.

Figure 3.34 is drawn to understand the effects of nanoparticles volume fraction on the size of the recirculation zones. It can be obtained that variation of nanoparticle volume fraction does not affect the size of the recirculation zones. Also, flow

velocity increases with increasing nanoparticles volume fraction because of increasing viscosity of nanofluid.

The effects of Reynolds number on the size of the recirculation zones is presented on Figure 3.35. It can be obtained that changing of Reynolds number markedly affects the size of the recirculation zones. As the Reynolds number increases, the size of the recirculation zone increases, also.

Figure 3.36 is presented to understand the effects of types of nanofluids on the size of the recirculation zones. It can be obtained that changing of nanofluids do not affect the size of the recirculation zones.

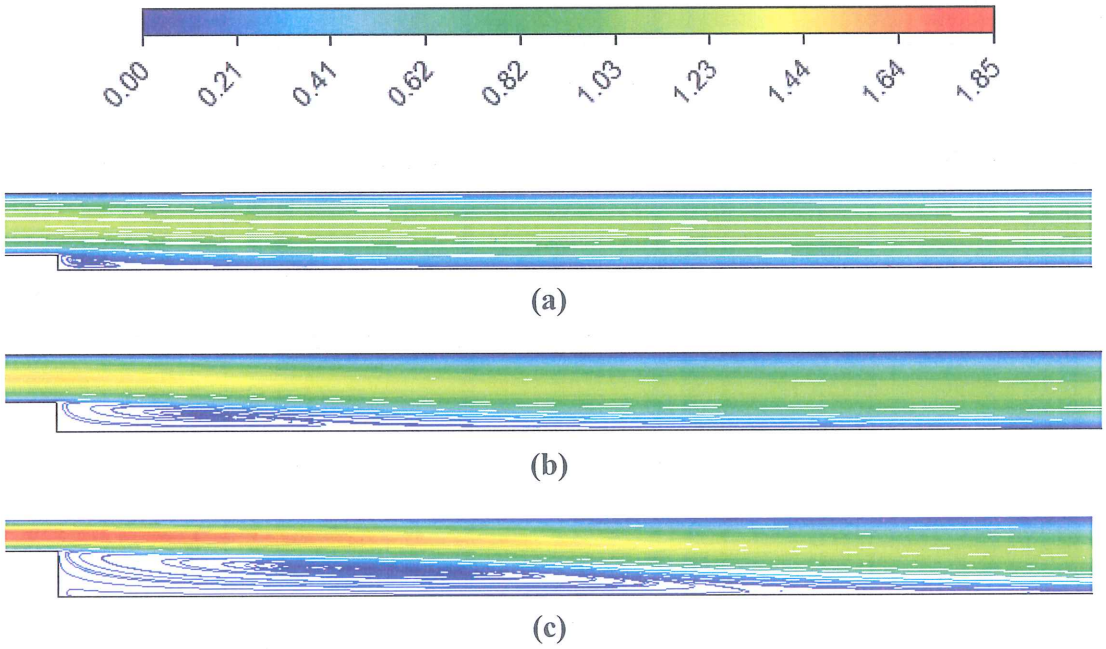

Figure 3.33. Streamlines of velocity for different expansion ratios using Al_2O_3/water nanofluid with 4.0% volume fraction at Re=500 a) ER=1.25, b) ER=1.67, c) ER=2.50.

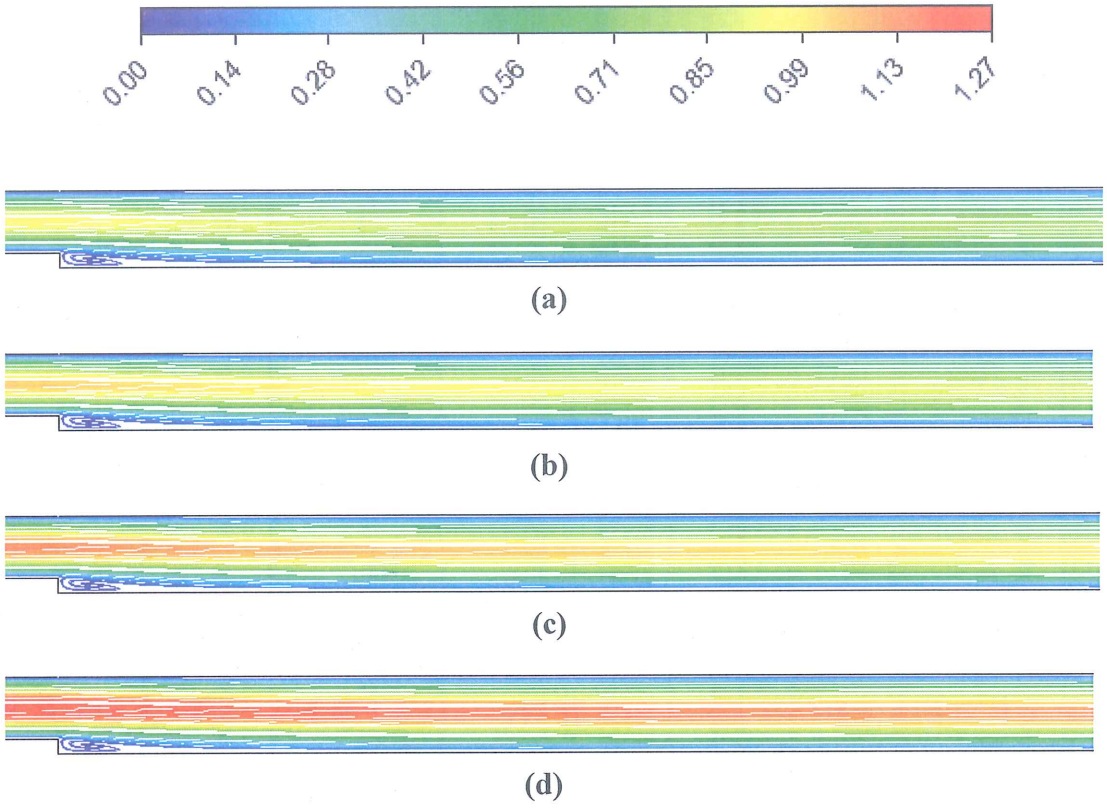

Figure 3.34. Streamlines of velocity for different nanoparticle volume fractions using Al_2O_3/water nanofluid at ER=1.25 and Re=500 a) 1.0%, b) 2.0%, c) 3.0%, d) 4.0%.

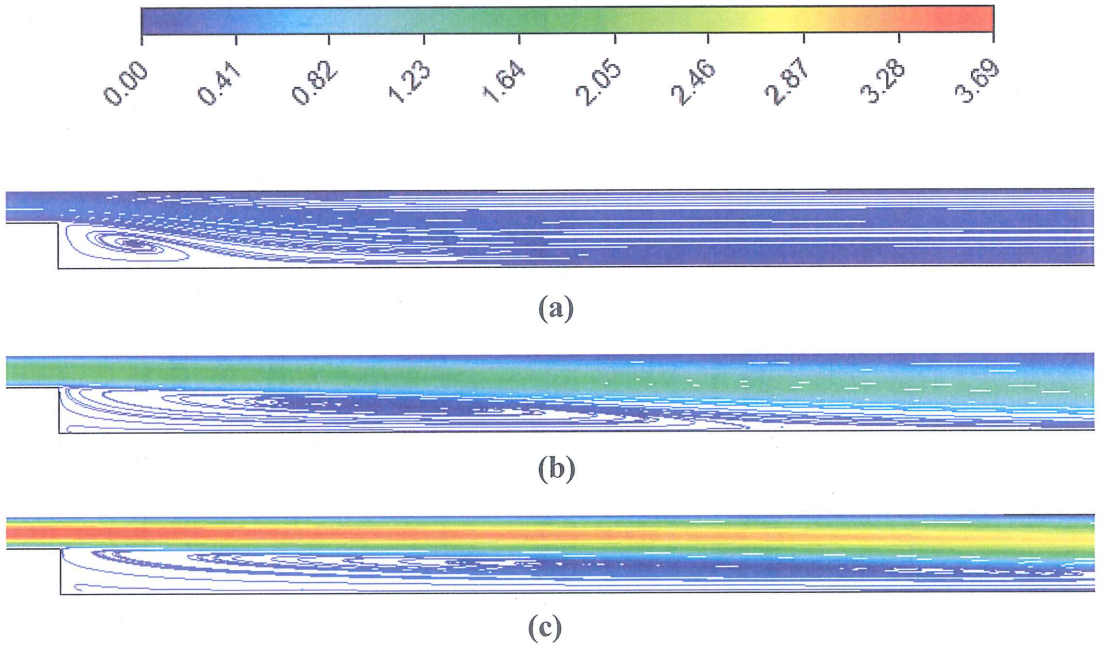

Figure 3.35. Streamlines of velocity for different Reynolds numbers using Al_2O_3/water nanofluid with 4.0% volume fraction at ER=2.50 a) Re=100, b) Re=500, c) Re=1000.

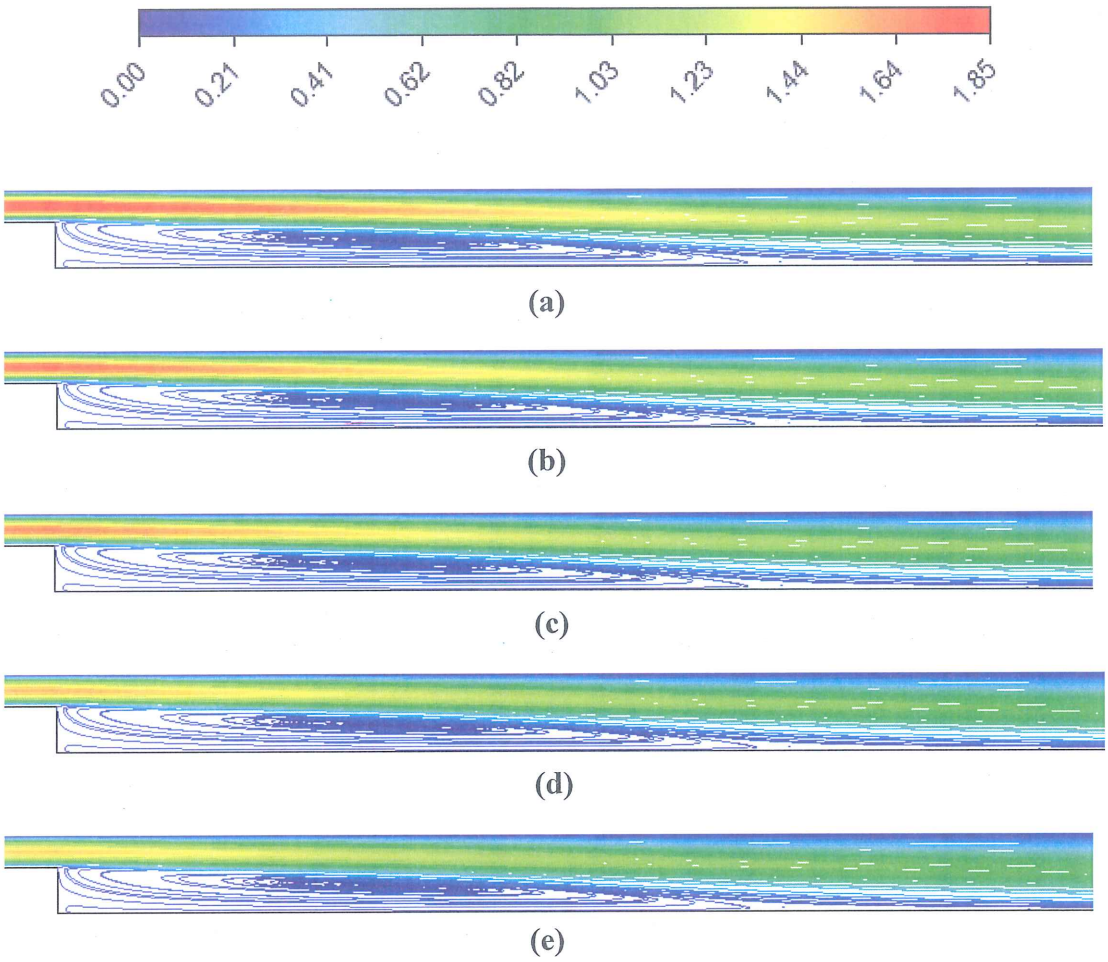

Figure 3.36. Streamlines of velocity for different nanofluids with 4.0% volume fraction at ER=2.50 and Re=500 a) Al_2O_3/water, b) SiO_2/water, c) TiO_2/water, d) CuO/water, e) ZnO/water.

Figure 3.37 - Figure 3.40 are presented to show the counter flow in recirculation zone due to the changing of expansion ratio, nanoparticles volume fraction, Reynolds number and nanofluids, respectively. It is revealed that the flow reaches hydrodynamically fully developed condition as faster as compared to higher Reynolds numbers and expansion ratios. The flow develops at the same condition as compared to changing of nanoparticles volume fractions and types of nanofluids.

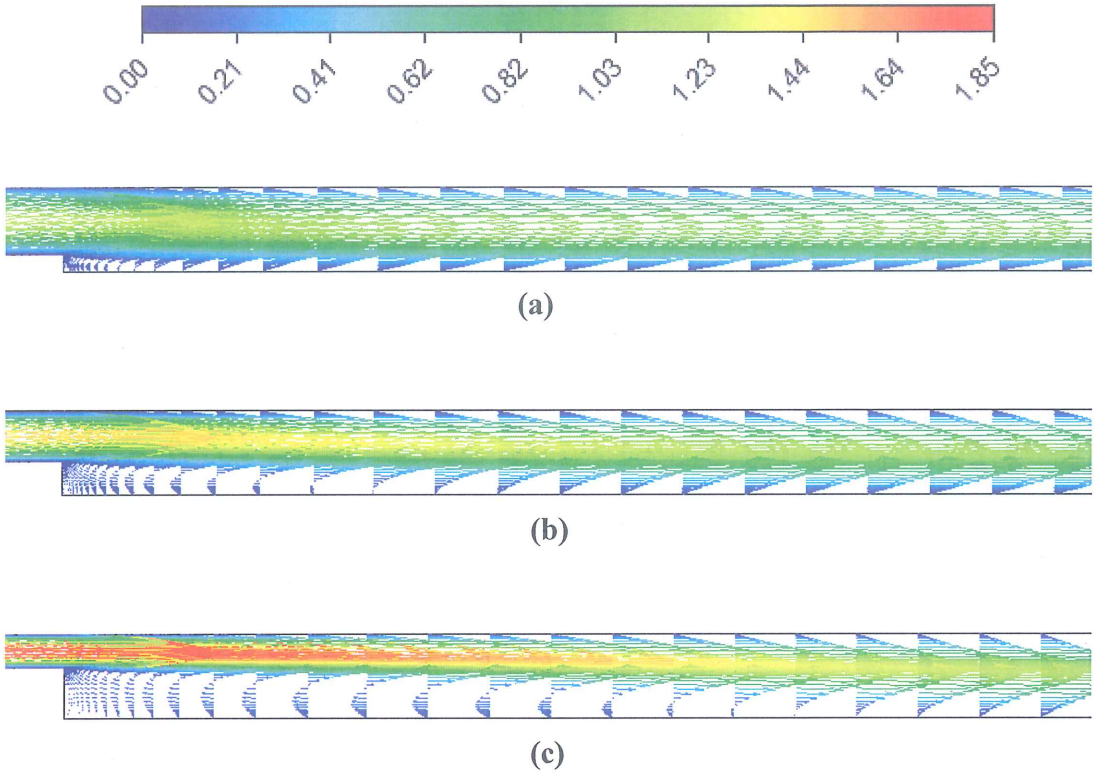

Figure 3.37. Velocity vectors for different expansion ratios using Al_2O_3/water nanofluid with 4.0% volume fraction at Re=500 a) ER=1.25, b) ER=1.67, c) ER=2.50.

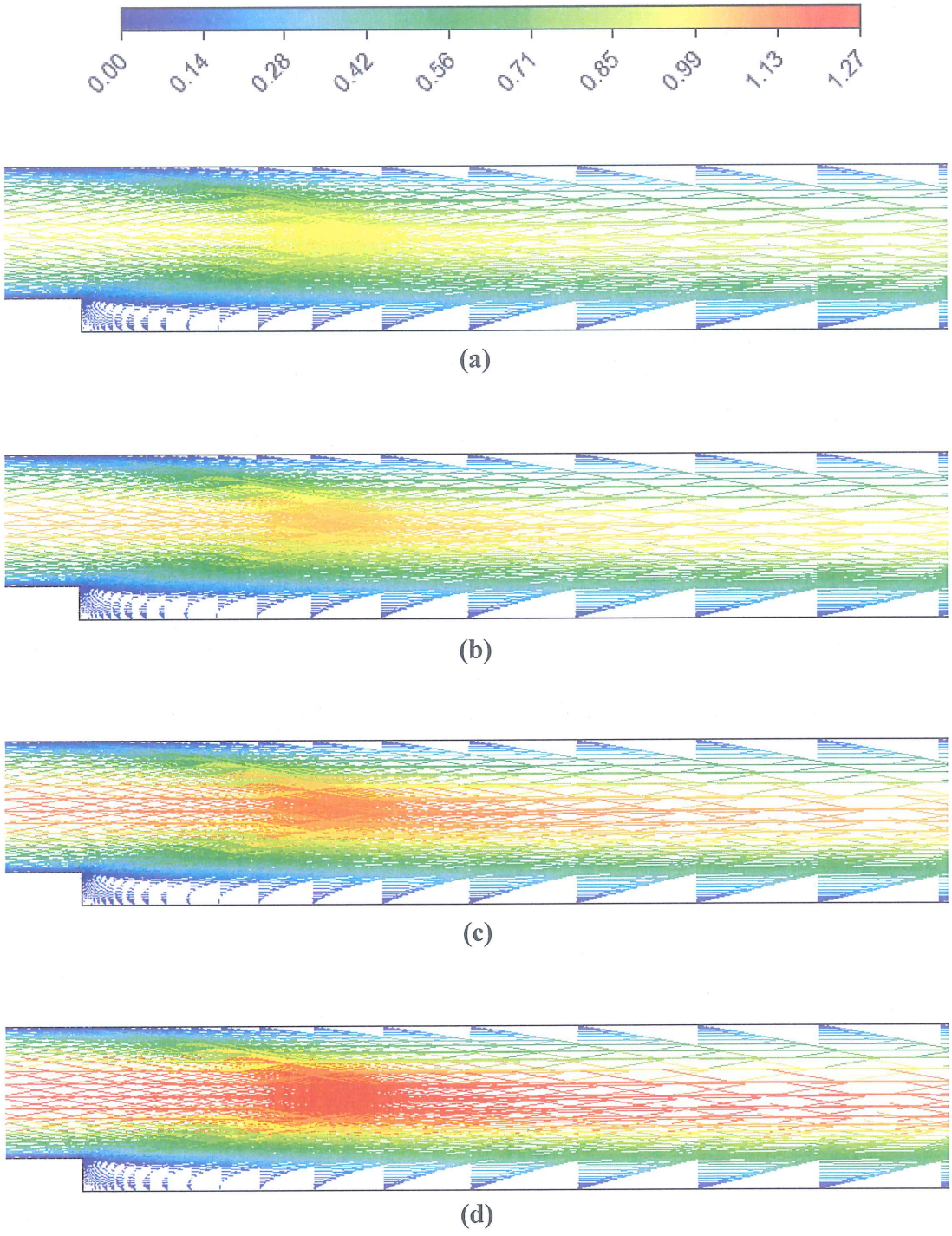

Figure 3.38. Velocity vectors for different nanoparticle volume fractions using Al_2O_3/water nanofluid at ER=1.25 and Re=500 a) 1.0%, b) 2.0%, c) 3.0%, d) 4.0%.

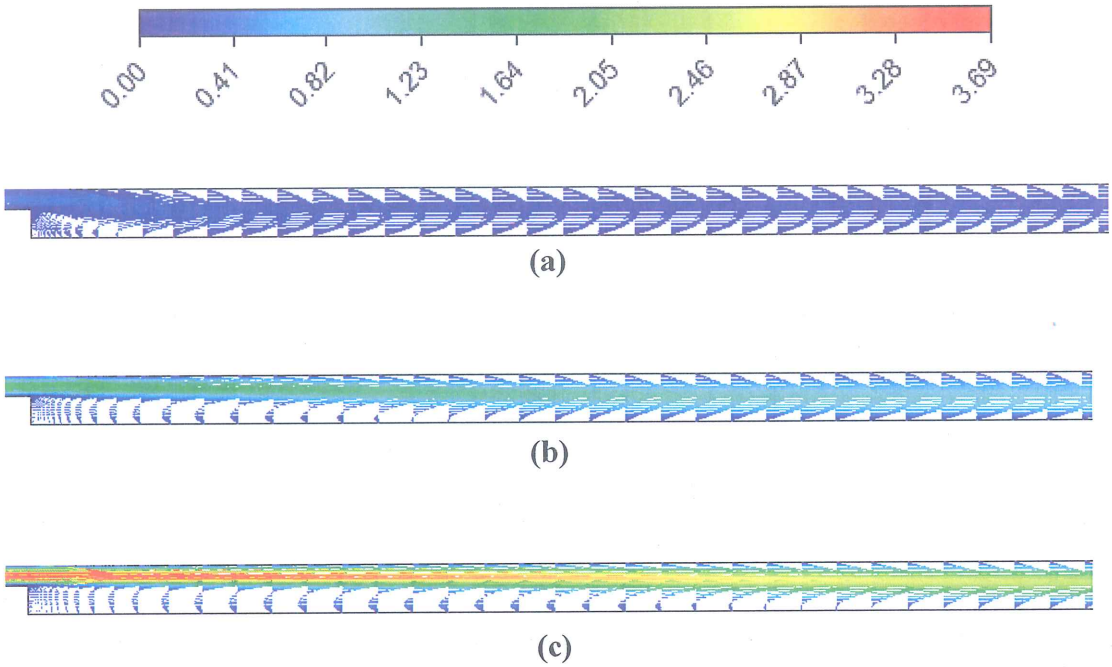

Figure 3.39. Velocity vectors of for different Reynolds numbers using Al_2O_3/water nanofluid with 4.0% volume fraction at ER=2.50 a) Re=100, b) Re=500, c) Re=1000.

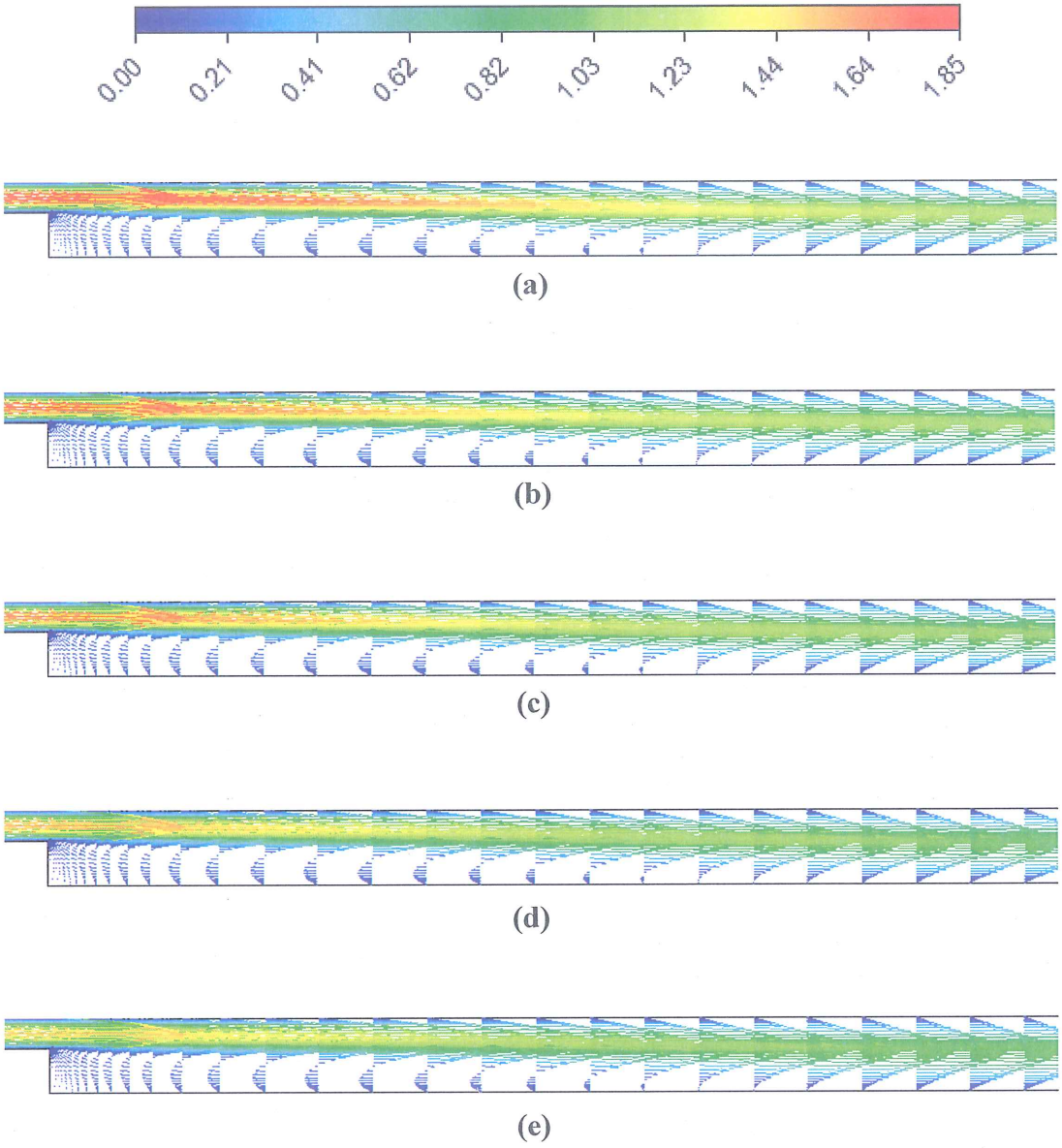

Figure 3.40. Velocity vectors of for different nanofluids with 4.0% volume fraction at ER=2.50 and Re=500 a) Al_2O_3/water, b) SiO_2/water, c) TiO_2/water, d) CuO/water e) ZnO/water.

3.3. COMPARISION OF TYPES OF NANOFLUIDS, NANOPARTICLE VOLUME FRACTIONS AND EXPANSION RATIOS DUE TO HEAT TRANSFER PERFORMANCE

The use of nanofluids associated with MBFS simultaneously in the rectangular duct leads not just to enhance Nusselt number, but also varies Darcy friction factor. In order to compare the thermal and hydraulic performance of the duct with MBFS having different expansion ratios, the Performance Evaluation Criterion (PEC) is

evaluated. The greater value of PEC denotes the better overall performance. For this reason, PEC > 1 denotes that the improvement of heat transfer is greater than the increase in the pressure drop penalty. PEC can be written as follows [48]:

$$PEC = \frac{\left(\frac{Nu_{nf}}{Nu_f}\right)}{\left(\frac{f_{nf}}{f_f}\right)^{1/3}} \tag{3.1}$$

Figure 3.41 is presented to obtain the best nanofluid with the constant expansion ratio and 4.0% nanoparticles volume fraction regarding heat transfer. It is revealed that improvement of heat transfer of all nanofluids are dominant because PEC is bigger than 1. Al_2O_3/water nanofluid has the greatest PEC at all Reynolds number. ZnO/water nanofluid has the lowest PEC, also. Moreover, PEC also increases with increasing the Reynolds number.

Figure 3.42 is presented to obtain the best nanoparticle volume fraction of Al_2O_3/water nanofluid with constant expansion ratio regarding heat transfer. Also, PEC increases with increasing the Reynolds number. It is found that PEC increases by increasing nanoparticle volume fraction.

Figure 3.43 is presented to obtain the best duct expansion ratio of MBFS in duct. It is revealed that improvement of heat transfer of all expansion ratios is superior. Also, PEC increases with increasing the Reynolds number. In addition, with the increasing of Reynolds number to about 700, the duct having expansion ratio of 1.25 displays higher PEC value, which is higher heat transfer enchacement. After Re=700, the PEC value of the duct having ER=2.50 starts to increase and become the greatest.

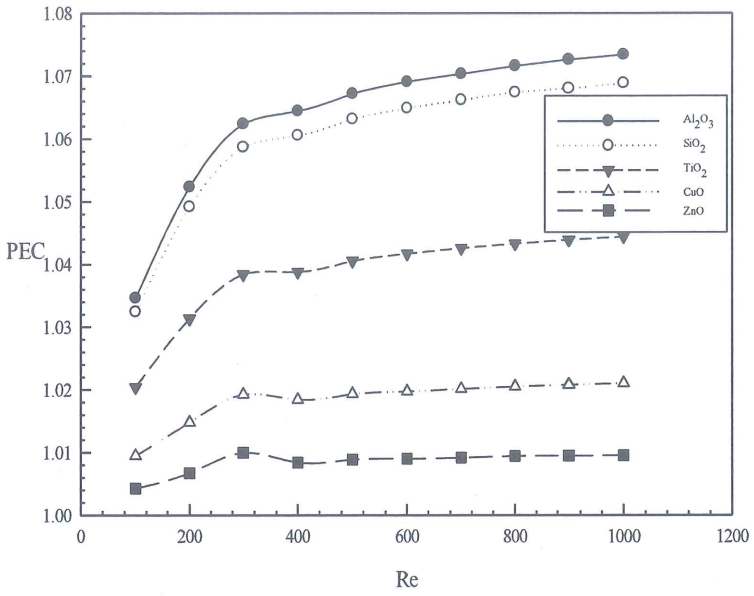

Figure 3.41. Comparision of performance evaluation criterion for different nanofluids at 4.0% nanoparticle volume fraction and ER=1.25.

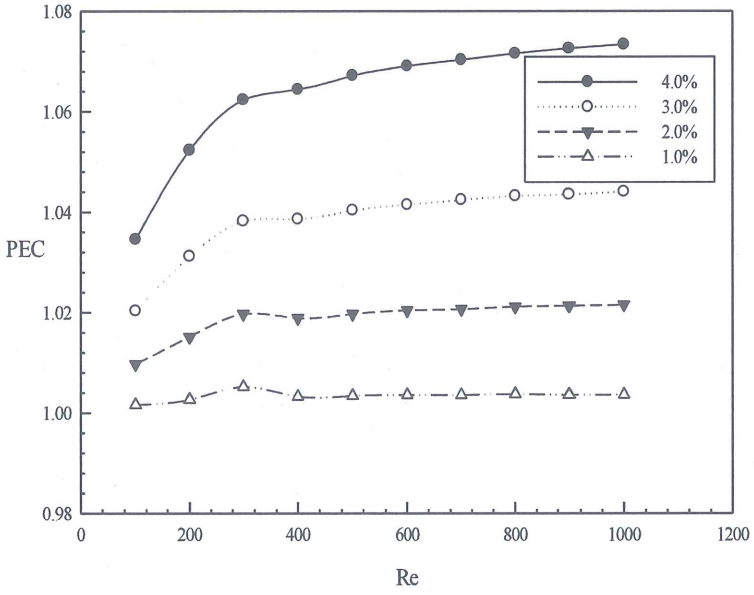

Figure 3.42. Comparision of performance evaluation criterion for different nanoparticles volume fractions of Al_2O_3/water nanofluid at ER=1.25.

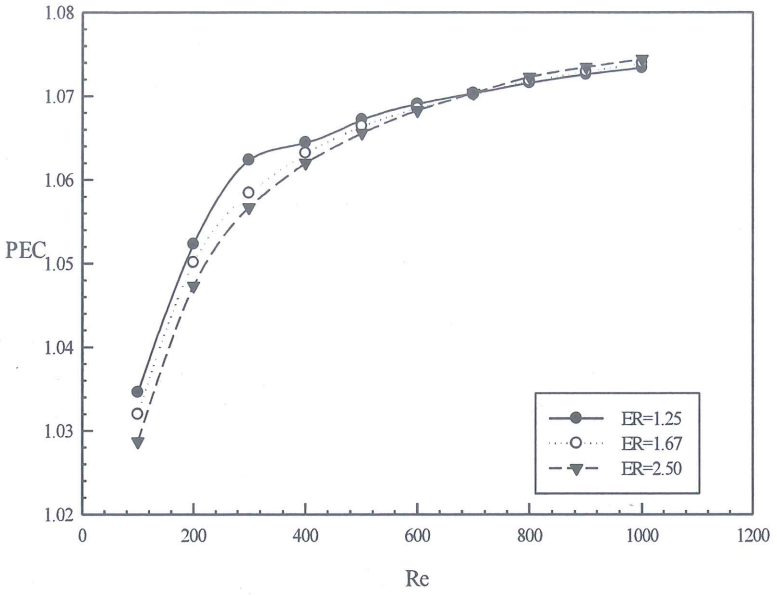

Figure 3.43. Comparision of performance evaluation criterion for the MBFS having different expansion ratios for Al_2O_3/water nanofluid having 4.0% nanoparticle volume fraction.

PART 4

CONCLUSIONS

Nanofluid, nanoparticle volume fraction, duct expansion ratio and the Reynolds number are varied to understand their effects on flow and heat transfer characteristics using MBFS under laminar forced convection. Although the duct expansion ratio and the Reynolds number significantly affect flow and heat transfer characteristics over, types of nanofluids and nanoparticle volume fractions affect the heat transfer characteristics only.

Types of nanofluids have a great effect on heat transfer. It is obtained that Al_2O_3/water nanofluid has the greatest Nusselt number for all expansion ratios and nanoparticle volume fractions. ZnO/water nanofluid has the lowest Nusselt number in the four nanofluids. But, ZnO/water nanofluid has bigger Nusselt number when compared to pure water. It can be said from this investigation that nanofluid increases the heat transfer over MBFS. Darcy friction factor is not significantly affected by the types of nanofluids.

Heat transfer usually increases with increasing nanoparticle volume fraction. It is revealed that Al_2O_3/water nanofluid having 4.0% nanoparticle volume fraction has the biggest Nusselt number for all expansion ratios and Reynolds numbers. ZnO/water and CuO/water nanofluids, which have 1.0% and 2.0% nanoparticle volume fraction, have lower Nusselt number in comparison to pure water. It can be said that the Nusselt number does not always increase with increasing nanoparticles volume fraction. Darcy friction factor is not significantly affected by the types of nanofluids.

Duct expansion ratio has a great effect on the heat transfer and flow characteristics. It is obtained that the maximum Nusselt number is seen at ER=1.25 and the minimum

Nusselt number is seen at ER=2.50. Moreover, Darcy friction factor is inversely proportional to increasing expansion ratio.

The Reynolds number has a great effect on the heat transfer and flow characteristics, too. It is obtained that the Nusselt number, the lenght of reattachment point and PEC increase with increasing the Reynolds number. On the other hand, Darcy friction factor decreases with increasing the Reynolds number.

PART 5

SUGGESTIONS FOR FUTURE WORK

In this section, a number of topics, which may be considered as future work, are given below.

1. In this thesis, the nanofluid flow over MBFS was considered under laminar forced convection flow conditions and using single phase approach. Future work should consist of turbulent, mixed and forced convection conditions. Also, two phase approach can be used for nanofluid flow.
2. Recently, entropy generation, which is important to design a system, is the important topic for researhers. In the literature, there is no investigation about entropy generation of nanofluid flow over MBFS. Future work should take into account entropy generation of nanofluid flow over MBFS.
3. In this thesis, the numerical calculations were performed for four nanoparticle volume fractions. Future work should be performed by increasing number of nanoparticle volume fractions to obtain effects of heat transfer characterictics of nanofluids.
4. In this study, thermophysical properties of nanofluids were assumed independent from temperature changing. Future work should be conducted with temperature depended thermophysical properties of nanofluid in terms of approaching the reality.

REFERENCES

1. Oosthuizen, P. H., and Naylor, D., "Introduction to Convevtive Heat Transfer Analysis", ***McGraw-Hills***, USA, 1-30 (1999).

2. Incropera, F. P. and DeWitt, D. P., "Introduction to Heat Transfer 3rd ed.", ***John Wiley&Sons Inc.***, New York, 75-370 (1993).

3. Çengel, Y. A. and Ghajar, A. J., "Heat and Mass Transfer 5th ed.", ***McGraw-Hills***, NewYork, 379-395 (2015).

4. Choi, S. U. S., "Enhancing thermal conductivity of fluid with nanoparticles", ***ASME FED,*** 231: 99-105 (1995).

5. Maxwell, J. C., "Treatise on Electricity and Magnetism" ***Clarendon Press***, Oxford, (1873).

6. Das, S. K., Putra, N., Thiesen, P., and Roetzel, W., "Temperature dependence of thermal conductivity enhancement for nanofluids", ***Journal of Heat Transfer***, 125: 567-574 (2003).

7. Chandrasekar, M., Suresh, S., and Bose, A. C., "Experimental investigations and theoretical determination of thermal conductivity and viscosity of Al_2O_3/water nanofluid", ***Experimental Thermal and Fluid Science***, 34: 210-216 (2010).

8. Chon, C. H., Kihm, K. D., Lee, S. P., and Choi, S. U. S., "Empirical correlation finding the role of temperature and particle size for nanofluid (Al_2O_3) thermal conductivity enhancement", ***Applied Physics Letters***, 87(15), 153107 (2005).

9. Duangthongsuk, W., and Wongwises, S., "Measurements of temperature-dependent thermal conductivity and viscosity of TiO_2(21 nm)/water nanofluids", ***Experimental Thermal and Fluid Science***, 33: 706-714 (2009).

10. Hong, T. K., Yang, H. S., and Choi, C. J., "Study of the enhanced thermal conductivity of Fe nanofluids", ***Journal of Applied Physics***, 97, 064311 (2005).

11. Park, E. J., Park, S. D., Bang, I. C., Park, Y. B., and Park, H. W., "Critical heat flux characteristics of nanofluids based on exfoliated graphite nanoplatelets (xGnPs)", ***Materials Letters***, 81: 193-197 (2012).

12. Nasiri, A., Niasar, M. S., Rashidi, A. M., and Khodafarin, R., "Effect of CNT structures on thermal conductivity and stability of nanofluid", ***International Journal of Heat and Mass Transfer***, 55: 1529-1535 (2012).

13. Souza, N. S., Rodrigues, A. D., Cardoso, C. A., Pardo, H., Faccio, R., Mombru, A. W., Galzerani, J. C., Lima, O. F., Sergeenkov, S., and Moreira, F. M. A., "Physical properties of nanofluid suspension of ferromagnetic graphite with high Zeta potential", ***Physics Letters A***, 376: 544-546 (2012).

14. Nasiri, A., Niasar, M. S., Rashidi, A., Amrollahi, A., and Khodafarin, R., "Effect of dispersion method on thermal conductivity and stability of nanofluid", ***Experimental Thermal and Fluid Science***, 35: 717-723 (2011).

15. Chen, L., and Xie, H., "Silicon oil based multiwalled carbon nanotubes nanofluid with optimized thermal conductivity enhancement", ***Colloids and Surfaces A: Physicochemical and Engineering Aspects***, 352: 136-140 (2009).

16. Yu, W., Xie, H., Li, Y., Chen, L., and Wang, Q., "Experimental investigation on the thermal transport properties of ethylene glycol based nanofluids containing low volume concentration diamond nanoparticles", ***Colloids and Surfaces A: Physicochemical and Engineering Aspects***, 380: 1-5 (2011).

17. Turgut, A., "Investigation of thermophysical properties of nanofluids", Ph. D. Thesis, ***Dokuz Eylül University Graduate School of Natural and Applied Sciences***, İzmir, 1-2 (2010).

18. Li, Y., Zhou, J., Tung, S., Schneider, E., and Shengqi, X., "A review on development of nanofluid preparation and characterization", ***Powder Technology***, 196: 89-101 (2009).

19. Chang, P. K., "Separation of Flow", ***Pergamon Press***, Oxford, 42 (1970).

20. Anderson John D., Jr., "Fundementals of Aerodynamics 2nd ed.", ***McGraw-Hill Book Co.***, New York, 715-716 (1991).

21. Driver, D. M., Seegmiller, H. L., and Marvin J. G., "Time-dependent behviour of a reattaching shear layer", ***AIAA Journal***, 25 (7): 914-919, (1987).

22. Goldstein, R. J., Ericsen, V. L., Olson, R. M., and Eckert, E. R. G., "Laminar separation reattachment, and transition of the flow over a downstream-facing step", ***J. Basic Eng.***, 92: 732–741 (1970).

23. Denham, M. K., and Patrick, M. A., "Laminar flow over a downstream-facing step in a two-dimensional flow channel", ***Trans. Inst. Chem. Eng.***, 52: 361–7 (1974).

24. Armaly, B. F., Durst, F., Pereira, J. C. F., and Schonung, B., "Experimental and theoretical investigation of backward-facing step flow" ***J. Fluid Mech.***, 127: 473–96 (1983).

25. Chen, Y. T., Nie, J. H., Armaly, B. F., and Hsieh, H. T., "Turbulent separated convection flow adjacent to backward-facing step—effects of step height", ***International Journal of Heat and Mass Transfer***, 49: 3670–3680 (2006).

26. Pulat, E., and Diner, M., "Geri basamak akışının nümerik analizi", ***Mühendislik Bilimleri Dergisi***, 7: 29-34 (2001).

27. Mahdi, A. A., Neema, H. A., and Kadhem, B., "The effecting of a sudden step change on heat transfer coefficient", ***Journal of Thi-Qar University***, 4: 39-64 (2008).

28. Rinoie, K., Shirai, Y., Saitao, Y., and Sunada, Y., "Behaviours of separated and reattaching flow formed over backward-facing step", ***21st ICAS Congress***, Melbourne, Australia 13-18 September, 1998.

29. Iwai, H., Nakabe, K., Suzuki, K., and Matsubara, K., "The effects of duct inclination angle on laminar mixed convective flows over a backward-facing step", ***International Journal of Heat and Mass Transfer***, 43: 473-485 (2000).

30. Nie, J. H., and Armaly, B. F., "Three-dimensional convective flow adjacent to backward-facing step - effects of step height", ***International Journal of Heat and Mass Transfer***, 45: 2431-2438 (2002).

31. Chen, Y. T., Nie, J. H., Hsieh, H. T., and Sun L. J., "Three-dimensional convection flow adjacent to inclined backward-facing step", ***International Journal of Heat and Mass Transfer***, 49: 4795–4803 (2006).

32. Lan, H., Armaly, B. F., and Drallmeier, J. A., "Three-dimensional simulation of turbulent forced convection in a duct with backward-facing step", ***International Journal of Heat and Mass Transfer***, 52: 1690–1700 (2009).

33. Abu-Nada, E., "Application of nanofluids for heat transfer enhancement of separated flows encountered in a backward facing step", ***International Journal of Heat and Fluid Flow***, 29(1): 242–249 (2008).

34. Al-aswadi, A. A., Mohammed, H. A., Shuaib, N. H., and Campo, A., "Laminar forced convection flow over a backward facing step using nanofluids", ***International Communications in Heat and Mass Transfer***, 37: 950–957 (2010).

35. Heshmati, A., Mohammed, H. A., and Darus, A. N., "Mixed convection heat transfer of nanofluids over backward facing step having a slotted baffle", ***Applied Mathematics and Computation***, 240: 368-386 (2014).

36. Togun, H., Safaei, M. R., Sadri, R., Kazi, S. N., Badarudin, A., Hooman, K., and Sadeghinezhad, E., "Numerical simulation of laminar to turbulent nanofluid flow and heat transfer over a backward-facing step", ***Applied Mathematics and Computation***, 239: 153–170 (2014).

37. Kherbeet, A. S., Mohammed, H. A., and Salman, B. H., "The effect of nanofluids flow on mixed convection heat transfer over microscale backward-facing step", ***International Journal of Heat and Mass Transfer***, 55: 5870–5881 (2012).

38. Kherbeet, A. S., Mohammed, H. A., Salman, B. H., Ahmed, H. E., and Alawi, O. A., "Experimental and numerical study of nanofluid flow and heat transfer over microscale backward-facing step", ***International Journal of Heat and Mass Transfer***, 79: 858–867 (2014).

39. Kherbeet, A. S., Mohammed, H. A., Munisamy, K. M., and Salman, B. H., "The effect of step height of microscale backward-facing step on mixed convection nanofluid flow and heat transfer characteristics", ***International Journal of Heat and Mass Transfer***, 68: 554-566 (2014).

40. Vajjha, R. S., and Das D. K., "Experimental determination of thermal conductivity of three nanofluids and development of new correlations", ***Int. J. Heat Mass Transfer,*** 52: 4675–4682 (2009).

41. Ghasemi, B., and Aminossadati, S. M., "Brownian motion of nanoparticles in a triangular enclosure with natural convection", ***Int. J. Therm. Sci.***, 49: 931–940 (2010).

42. Corcione, M., "Heat transfer features of buoyancy-driven nanofluids inside rectangular enclosures differentially heated at the sidewalls", ***Int. J. Therm. Sci.,*** 49: 1536–1546 (2010).

43. Zahmatkesh, I., and Ebrahim, J., "Experimental analysis of thermal expansion of nanofluids", ***Majlesi Journal of Energy Management***, 3: 63-69 (2014).

44. Salman, B. H., Mohammed, H. A., and Kherbeet, A. S., "Heat transfer enhancement of nanofluids flow in microtube with constant heat flux", ***International Communications in Heat and Mass Transfer***, 39: 1195–1204 (2012).

45. Azmi, W. H., Sharma, K. V., Sarma, P. K., Mamat, R., and Najafi, G., "Heat transfer and friction factor of water based TiO_2 and SiO_2 nanofluids under turbulent flow in a tube", ***International Communications in Heat and Mass Transfer***, 59: 30-38 (2014).

46. Kumar, S., Prasad, S. K., and Banerjee, J., "Analysis of flow and thermal field in nanofluid using a single phase thermal dispersion model", ***Appl. Math. Model***, 34: 573–592 (2010).

47. Mohammed, H. A., Al-aswadi, A. A., Yusoff, M. Z., Saidur, R., "Mixed convective flows over backward facing step in a vertical duct using various nanofluids bouyancy-assisting case", ***Thermophys. Aeromech.***, 42(1): 1-30 (2012).

48. Kherbeet, A. S, Mohammed, H. A., Salman, B. H.,. Ahmed, H. E., Alawi, O. A., and Rashidi, M. M., "Experimental study of nanofluid flow and heat transfer over microscale backward- and forward-facing steps", ***Experimental Thermal and Fluid Science***, 65: 13–21 (2015).

APPENDIX A.

SAMPLE CALCULATIONS

A.1. Average Heat Transfer Coefficient and Nusselt Number

In this section, average heat transfer coefficient and Nusselt number are determined for 4.0% volume fraction of Al_2O_3/water nanofluid flow over MBFS having ER=1.25. The Reynolds number is chosen 500. As a result of the numerical study, some variables is obtained from ANSYS 15.0. They are tabulated in the table below.

T_i [K]	T_o [K]	T_w [K]	ΔP [Pa]
300	300.7271	303.6559	2340.885

Firstly, thermopysical properties of Al_2O_3/water nanofluid should be determined. The effective thermal conductivity equations for nanofluid are given below.

$$k_{static} = k_f\left[\frac{(k_s+2k_f)-2\varphi(k_f-k_s)}{(k_s+2k_f)+\varphi(k_f-k_s)}\right] = 0.613\left[\frac{(40+2x0.613)-2x0.04(0.613-40)}{(40+2x0.613)+0.04(0.613-40)}\right]$$

$$k_{static} = 0.666 \quad W/mK$$

$$k_{brownian} = 5x10^4\beta\varphi\rho_f Cp_f\sqrt{\frac{KT}{\rho_s d_p}}f(T,\varphi) = 5x10^4(0.2716)(0.04)(1115.2)(4179)$$
$$\sqrt{\frac{(1.38066x10^{-23})(301)}{(3970)(2.5x10^{-8})}}x(4.5456x10^{-5})$$

where

$$f(T,\varphi) = (2.8217x10^{-2}\varphi + 3.917x10^{-3})\left(\frac{T}{T_0}\right) + (-3.0669x10^{-2}\varphi - 3.91123x10^{-3})$$
$$= (2.8217x10^{-2}x0.04 + 3.917x10^{-3})\left(\frac{301}{293}\right) + (-3.0669x10^{-2}x0.04 - 3.91123x10^{-3})$$

$$f(T,\varphi) = 4.5456x10^{-5}$$

$$k_{eff} = k_{static} + k_{brownian} = 0.666 + 6.65x10^{-4} = 0.667 \quad W/mK$$

The effective viscosity of nanofluid equation for nanofluid is presented

$$\frac{\mu_{eff}}{\mu_f} = \frac{1}{1-34.87(d_p/d_f)^{-0.3}\varphi^{1.03}} = \frac{\mu_{eff}}{0.000855} = \frac{1}{1-34.87(2.5x10^{-8}/3.85467x10^{-10})^{-0.3}(0.04)^{1.03}}$$

$$\mu_{eff} = 0.001340615 \quad Ns/m^2$$

where

$$d_f = \left[\frac{6M}{N\pi\rho_{fo}}\right]^{1/3} = \left[\frac{6(0.01801528)}{(6.02x10^{23})(3.14)(998.4)}\right]^{1/3}$$

$$d_f = 3.85467x10^{-10} \quad m$$

The effective density of nanofluid is defined as follows.

$$\rho_{eff} = (1-\varphi)\rho_f + \varphi\rho_s = (1-0.04)(997) + (0.04)(3970)$$

$$\rho_{eff} = 1115.2 \quad kg/m^3$$

The calculation of the effective specific heat of nanofluid is presented below.

$$(Cp)_{eff} = \frac{(1-\varphi)(\rho Cp)_f + \varphi(\rho Cp)_s}{(1-\varphi)\rho_f + \varphi\rho_s} = \frac{(1-0.04)(997x4179) + (0.04)(3970x765)}{(1-0.04)(997) + (0.04)(3970)}$$

$$(Cp)_{eff} = 3693.173 \quad kJ/kgK$$

The effective thermal expansion of nanofluid is defined as follows.

$$\beta_{eff} = \frac{(1-\varphi)(\rho\beta)_f + \varphi(\rho\beta)_s}{(1-\varphi)\rho_f + \varphi\rho_s} = \frac{(1-0.04)(997x303x10^{-6}) + (0.04)(3970x1.9069)}{(1-0.04)(997) + (0.04)(3970)}$$

$$\beta_{eff} = 0.2716 \quad 1/K$$

After calculations of the thermophysical properties of Al_2O_3/water nanofluid, average heat transfer coefficient and the Nusselt number are then obtained from the below equations.

$$D_h = \frac{4A}{P} = \frac{4x(1200\mu m x 800\mu m)}{2x(1200\mu m + 800\mu m)}$$

$$D_h = 960\mu m = 960x10^{-6} m$$

The inlet velocity of nanofluid is calculated at Re=500 as in the below:

$$Re = \frac{\rho V_m D_h}{\mu} \Rightarrow 500 = \frac{(1115.92)(V_m)(960x10^{-6})}{0.001340615}$$

$$V_m = 0.625$$

$$h = \frac{\dot{m}Cp(T_o - T_i)}{A_s(T_w - T_b)} = \frac{\rho V_m A_c Cp(T_o - T_i)}{A_s(T_w - T_b)}$$
$$= \frac{(1115.2)(0.625)(0.0000012)(3693.173776)(300.7271-300)}{(0.00018)(303.6559-300.3636)}$$

$$h = 3796.6405 \quad W/m^2K$$

$$Nu = \frac{hD_h}{k} = \frac{(3796.6405)(0.00096)}{0.667}$$

$$Nu = 5.431855$$

A.2. Average Darcy Friction Factor

The Darcy friction factor is obtained as follows.

$$f = \frac{2(\Delta P)(D_h)}{\rho V_m^{\,2} L_t} = \frac{2(2340.845)(0.00096)}{(1115.2)(0.6257)^2(0.25)}$$

$$f = 0.041149889$$

A.3. Performance Evaluation Criterion (PEC)

PEC is determined from equation given below.

$$PEC = \frac{\left(\frac{Nu_{nf}}{Nu_f}\right)}{\left(\frac{f_{nf}}{f_f}\right)^{1/3}} = \frac{\left(\frac{5.4319}{5.0899}\right)}{\left(\frac{0.041149889}{0.041149912}\right)^{1/3}}$$

$$PEC = 1.0672$$

RESUME

Recep Ekiciler was born in Ankara, Turkey. He graduated from Karadeniz Technical University Mechanical Engineering Department, in Trabzon, Turkey in 2012. He worked as manufacturing engineer for three months in Ankara. Afterwards, he was assigned as research assistant to Karabük University, Department of Mechanical Engineering in 2014 and he is still working at Karabük University. He has been married since 2014.

CONTACT INFORMATION

Address: Karabük University
Engineering Faculty, Mechanical Engineering Department
Demir Çelik Campus/KARABUK

Email: recepekiciler@karabuk.edu.tr